POLITECNICO
MILANO 1863

SCUOLA DI INGEGNERIA INDUSTRIALE
E DELL'INFORMAZIONE

EXECUTIVE SUMMARY OF THE THESIS

Novel copolymers for enhanced energy transfer in Luminescent Solar Concentrators

TESI MAGISTRALE IN MATERIALS ENGINEERING AND NANOTECHNOLOGY

AUTHOR: LUCA GIACOMETTI TADDEI

ADVISOR: PROF. GIANMARCO GRIFFINI

CO-ADVISOR: FRANCESCA CORSINI

ACADEMIC YEAR: 2020-2021

1. Introduction

As climate change is becoming a theme of utmost importance, the need for new sustainable forms of energy is growing day by day. Fortunately, the growth of renewable energy technologies in recent years has been outstanding, and more researchers are dedicating their resources to this field.
Among the various forms of renewable energy, solar power is one of the most popular and widespread. Photovoltaic technology has become much cheaper and more efficient, while research to develop more innovative panels is striving. More recently, efforts to develop more aesthetically pleasing photovoltaic devices are done, in order to obtain panels that are better integrable in urban environments.
In this context, luminescent solar concentrators (LSC) present themselves as an interesting solution. Their simple architecture, consisting of just a thin slab of a semi-transparent material, allows them to be a promising technology for mass production, even though at the current state they still present various problems related to their efficiency and energy losses [1].
First introduced in 1976, the working principle of an LSC is simple, as shown in Figure 1: the device contains luminescent molecules that can absorb light and exploit total internal refraction to trap photons in the slab, which acts as a waveguide. The photons are then transported to the edges of the device, where photovoltaic cells are placed, converting light into electrical energy [2].

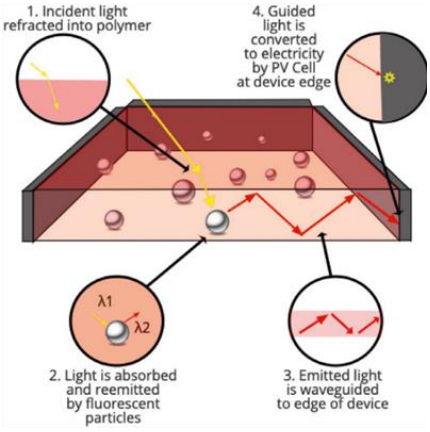

Figure 1 – Typical LSC device schematic.

The devices are usually produced in two configurations, thin-film or bulk: the former is obtained by coating a slab of transparent material, typically glass, with a thin film of luminescent polymer, typically polymethylmethacrylate (PMMA) or polycarbonate (PC), while in the former case the whole device is a host matrix for luminophore molecules.
In typical applications, the luminophores are randomly dispersed in the polymeric matrix. Although this is a simple and cheap way to produce an LSC, the random dispersion can promote aggregation of the luminophores, leading to LSC efficiency losses due to quenching and reabsorption phenomena. Another approach, investigated in this thesis work, is to incorporate luminophores with a monomeric functionality (e.g. methacrylate) in the polymeric chain via direct copolymerization [3].
In this work, the synthesis of a luminescent terpolymer via free-radical random polymerization is described. In particular, the samples were obtained by copolymerizing methylmethacrylate (MMA), coumarin methacrylate (CMA) and perylene methacrylate (PMA) in various concentrations.
The two luminescent molecules were chosen so to promote the occurrence of the energy transfer phenomena between the luminophores. In particular, since the absorption spectrum of the perylene overlaps with the fluorescence spectrum of the coumarin, the former was chosen as an acceptor molecule while the latter as a donor [4].
The donor absorbs light and, instead of emitting a photon by fluorescence, it transfers energy to the acceptor, thus avoiding potential energy losses by reabsorption in the waveguide and broadening the overall absorption spectrum of the LSC.

2. Materials and Methods

The luminescent monomers utilized in this work were synthesized by end-capping the fluorescent dyes, namely coumarin and a custom formulation of perylene diimide synthesized by the University of Milan, with 2-isocyanatoethyl methacrylate (IEM), using dibutyltin dilaurate (DBTDL) as a catalyst. The so-obtained compounds (CMA and PMA) were characterized and stored to be used as monomeric units.
The polymers were produced by copolymerizing MMA with varying concentrations of CMA and PMA. In particular, free-radical random polymerization reactions were carried out by dissolving the monomers in a round-bottom flask containing dioxane, heating it to 83 °C, syringing an appropriate amount of azobisisobutyronitrile (AIBN), which acts as an initiator, and maintaining the system in temperature for 5 hours. Finally, the polymers were precipitated in hexane and left to dry.
First, random copolymers with MMA and CMA were synthesized, respectively with a 5, 10 and 15% molar ratio of CMA to MMA. Then, random copolymers with a 0.025, 0.050 and 0.100% molar ratio of PMA to MMA were produced and finally, terpolymers with 10% of CMA and 0.025, 0.050 and 0.100% of PMA were synthesized as well.
The so-obtained polymeric samples are polymethylmethacrylate chains with luminescent molecules as lateral pendants, as shown in Figure 2. This way, phenomena of luminophore quenching should be reduced because molecules are further spaced from one another, hindering their aggregation.

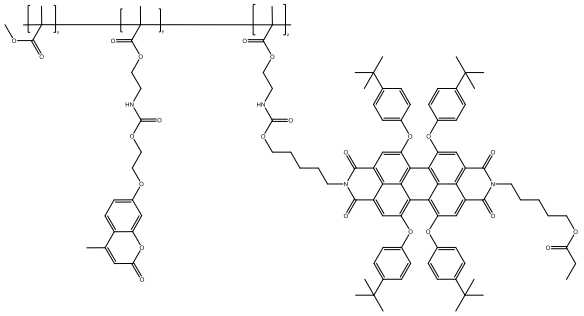

Figure 2 – Chemical structure of the obtained terpolymers.

The polymeric samples were then characterized by means of various techniques and instruments. In particular, optical characterizations were performed using a UV-Vis and a fluorescence spectrometer, physical properties were measured with differential scanning calorimetry (DSC) and gel permeation chromatography (GPC), while the molecular structure of the samples was investigated with nuclear magnetic resonance (H-NMR) and Fourier-transform infrared spectroscopy (FTIR).

3. Results and Discussion

Before synthesizing the copolymers, an in-depth characterization of the novel monomers was performed.

First, their optical properties, namely the absorption and fluorescence spectra, were measured in order to compare them to those of their precursor dyes. The optical spectra were found to be identical, a sign that the functionalization reaction did not affect these characteristics. Subsequently, spectral measurements with NMR and FTIR techniques were carried out and compared to the spectra relative to the precursors to evidence the effectiveness of the functionalization reaction. Finally, DSC analyses were performed to check whether the sample presented a transition temperature. All these analyses evidenced that the end-capping reactions were successful.

The optical spectra of the monomers were then compared to investigate whether they could be suited to exploit the energy transfer mechanism, as shown in Figure 3.

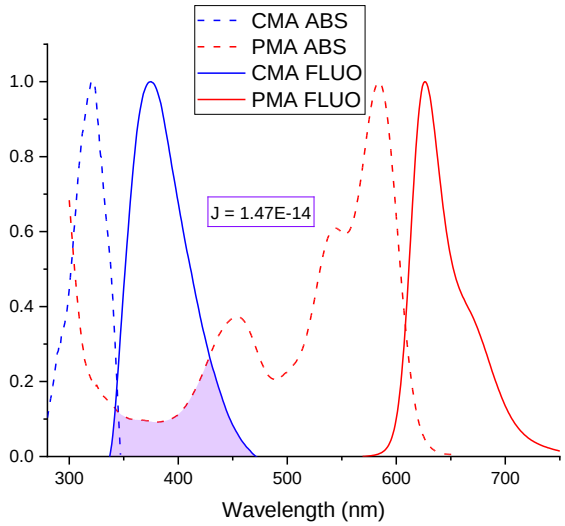

Figure 3 – Overlap of the absorption and fluorescence spectra of CMA and PMA with the value of the overlap integral J.

The fluorescence spectrum of the coumarin overlaps significantly with the absorption spectrum of the perylene, and the calculated value of the overlap integral was found to be in line with those reported in the literature.

After synthesizing the random CMA-MMA and PMA-MMA copolymers, they were also characterized by means of various techniques.

First, the optical properties of the samples were investigated; for both types of copolymers, the absorbance was found to be proportional to the content of luminophore in the polymer. In the case of PMA-MMA polymers, the fluorescence spectra were also stronger as the content of fluorophore increased, while for the polymers with CMA the most intense spectrum was associated with CMA10 MMA90, and increasing concentrations of coumarin resulted in a lower fluorescence intensity. Subsequently, 10% molar was considered to be the optimal concentration of CMA in the polymer to avoid the onset of quenching or efficiency losses phenomena.

Spectral analyses were also carried out by means of NMR and FTIR spectroscopy. In particular, NMR spectra were utilized to calculate the actual quantity of luminophore incorporated in the copolymers. The results highlighted that the real quantity of CMA in the copolymers is higher than the one in the reaction feed, while the quantity of PMA is less controllable, probably due to the higher steric hindrance of the molecule, and also less identifiable since the NMR signals relative to perylene are very weak, given the generally low quantities of luminophore in the sample.

Finally, DSC analyses were performed to infer the glass transition temperature of the polymers, which was found to be around 47°C for the CMA copolymers and around 125 °C for the samples with PMA. Their molecular weight was also investigated with GPC, resulting in an average molecular weight of around 40000 g/mol with an average PDI of 2.15 for the CMA copolymers and 57000 g/mol with a PDI of 1.52 for the samples with PMA.

Afterwards, the terpolymers were synthesized and characterized. The average Tg was found to be around 60 °C, while the average molecular weight was around 45000 g/mol.

FTIR and NMR analyses were also performed, confirming the quantity of incorporated coumarin with respect to the CMA-MMA random copolymer with 10% molar of CMA and reiterating the difficulties found in measuring the real quantity of PMA in the polymers. In particular, the samples named PMA0.050 MMA99.950 and CMA10 PMA0.050 MMA89.950 were found to have a much lower quantity of perylene incorporated than the feed composition, thus explaining why their fluorescence spectra were comparable to that of the sample with 0.025% molar of PMA.

After that, optical characterizations of the terpolymers were performed to assess the occurrence of the energy transfer mechanism [5]. First, as shown in Figure 4, the excitation spectra of the polymers with the highest content of PMA were measured.

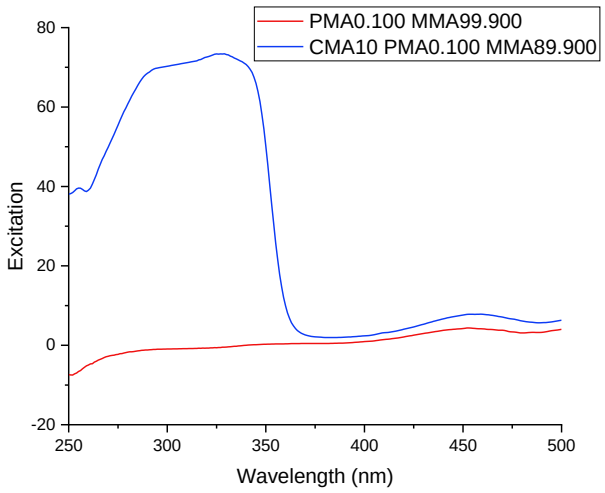

Figure 4 – Excitation spectrum of the CMA10 PMA0.100 MMA89.900 terpolymer (λ_{EM}= 650 nm).

The excitation spectra were obtained by detecting light at 650 nm. As it can be denoted from the graph, the copolymer containing only perylene does not emit by fluorescence when excited around 300 nm, while in the case of the terpolymer containing also CMA the coumarin absorbs photons and the perylene can fluoresce via energy transfer mechanisms.

Further tests were performed to assess the efficiency of the energy transfer process. In particular, calculations on steady-state fluorescence spectra and time-resolved fluorescence decays were performed.

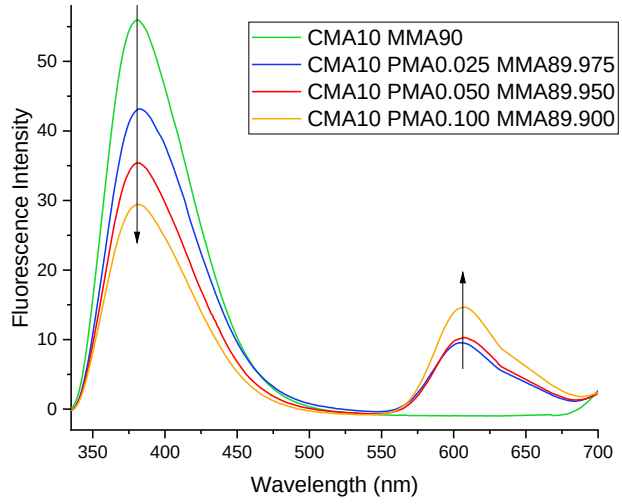

Figure 5 – Comparison of the fluorescence intensity of various copolymers (λ_{EXC}=320 nm).

As shown in Figure 5, the fluorescence spectra of samples with the same optical density (thus the same absorbance) were measured. It can be noted how, even though the quantity of coumarin is the same and they absorb the same amount of photons, the sample with 0.100% molar of PMA has a much weaker fluorescence emission in the 350 – 450 nm range, compared to the counterpart without incorporated perylene. This phenomenon can be explained with the occurrence of the energy transfer phenomenon. The efficiency of the process was calculated with the following equation:

$$E = 1 - \frac{F_{DA}}{F_D}$$

where F_{DA} is the fluorescence intensity (calculated on the peak relative to the donor) of the polymer with both donor and acceptor luminophores, while F_D is the fluorescence intensity of the copolymer with only the donor. The calculated efficiencies were 22.87% for CMA10 PMA0.025 MMA99.975, 36.75% for CMA10 PMA0.050 MMA99.950 and 47.39% for CMA10 PMA0.100 MMA99.900.

Furthermore, the energy transfer efficiency was calculated by means of time-resolved fluorescence spectroscopy. The efficiency was calculated with the following equation:

$$E = 1 - \frac{\tau_{DA}}{\tau_D}$$

where τ_{DA} is the fluorescence time of the donor molecule in a terpolymer with both luminophores and τ_D is the fluorescence time of the donor molecule in a copolymer without the acceptor.

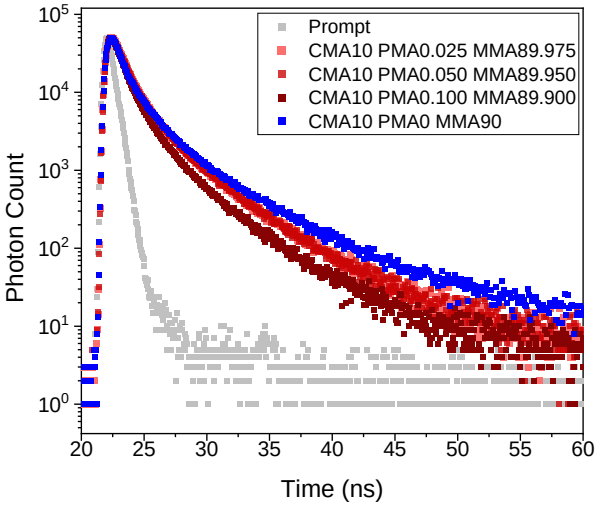

Figure 6 – Time-resolved fluorescence profiles of the terpolymers.

The results are shown in Figure 6 and the calculated efficiencies were 6.5% for CMA10 PMA0.025 MMA99.975, 7.0% for CMA10 PMA0.050 MMA99.950 and 26% for CMA10 PMA0.100 MMA99.900

Finally, luminescent solar concentrators were produced by spin-coating the above-described

polymers on slabs of soda glass. The devices were obtained by dissolving the polymers in chloroform at different weight concentrations. Namely, random CMA-MMA and PMA-MMA copolymers were dissolved to a 3 wt% concentration, while 3, 10 and 20 wt% concentrations were utilized to produce LSCs from the terpolymers.

Measurements of photonic efficiencies were carried out using a spectroradiometer and a solar simulator; the highest external photonic efficiency η_{EXT} was measured to be 2.28%, associated with CMA10 PMA0.100 MMA89.900 20%, while the highest internal photonic efficiency η_{INT} was measured to be 59.42%, associated with CMA10 PMA0.025 MMA89.975 20%. Furthermore, the photovoltaic efficiency of the devices was measured using a multimeter. The highest PCE reported, still associated with CMA10 PMA0.100 MMA89.900 20%, was 0.158% with a black mask covering the edges of the solar cells and avoiding direct irradiance on the panels.

The spectroradiometer was also utilized to measure the chromaticity of the devices. By measuring the irradiance spectrum of a white light lamp bulb and comparing it to the signal received from the light passing through the LSCs, it was possible to calculate the chromaticity values and plot them on a CIE 1931 graph, as shown in Figure 7, where the red square represents the values of the white light of the lamp.

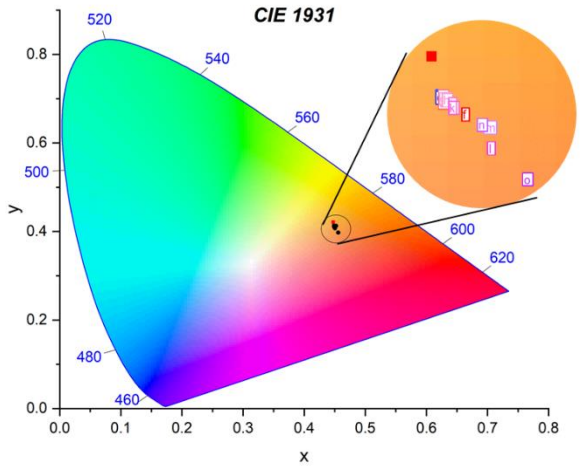

Figure 7 – Chromaticity plot of the LSC devices.

It can be denoted that the chromaticity values are quite similar to each other for all the devices. This is an indication of the fact that the produced LSCs do not significantly distort the colour of the light passing through them.

Further measurements and calculations were performed to calculate the average visible-light transmissivity (AVT) of the devices. The AVT is a figure of merit introduced to mediate the optical transmissivity of a device on the light response of the human eye, and it is calculated using the following formula:

$$AVT\% = \frac{\int T\%(\lambda) \cdot P(\lambda) \cdot S(\lambda)}{\int P(\lambda) \cdot S(\lambda)}$$

where T% is the transmissivity of the device, P is the photopic response of the human eye to light and S is the AM 1.5G solar spectrum expressed as photon flux. A device with an AVT of 100% is fully transparent to the human eye while an AVT of 0% is associated with total light absorbance. For LSCs, a high value of AVT is particularly important for all those applications, such as building integration, where the transparency of the product is a desired quality.

The results of the calculations of AVT values are reported in Figure 8.

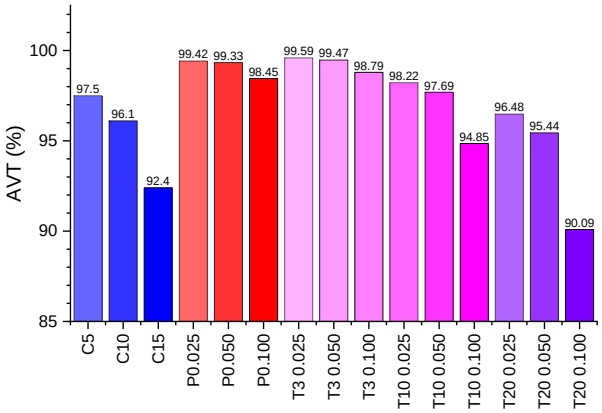

Figure 8 – Average visible-light transmissivity values of the LSCs.

Finally, a figure of merit called light utilization efficiency (LUE) was calculated with the following equation:

$$LUE = PCE \cdot AVT$$

This figure of merit describes how a high transmissivity compensates for the low PV efficiency of an LSC. The values of LUE obtained for the produced devices were similar to those reported in the literature.

4. Conclusions

In this work, the synthesis and characterization of novel luminescent copolymers for applications in thin-film luminescent solar concentrators exploiting energy transfer is presented.

The efficiency of the energy transfer mechanism between the two dyes in the copolymers was

measured with two different techniques and it was found to be 47% and 26% for the best device, respectively calculated with fluorescence and time-resolved fluorescence spectroscopy techniques.
The energy transfer mechanism was found to be beneficial for the efficiency of the LSC devices, as well as the direct incorporation of the luminophores in the polymeric chain compared to their random dispersion in the matrix.
Albeit the efficiency values of the devices, both photonic and photovoltaic, is on average lower than those reported in the literature, the devices were found not to distort the colour of the light passing through them. In fact, their AVT values are significantly high if compared to LSC devices reported in the literature. Moreover, the high LUE values obtained for the LSC devices fabricated with our novel fluorescent materials make the latter promising candidates as active host matrices for highly-transparent, efficient LSCs.

5. Future Developments

A further effort was put into the synthesis of luminescent block copolymers with the RAFT polymerization technique. CMA-MMA and PMA-MMA RAFT copolymers were produced with 2-phenyl-2-propyl benzodithioate acting as a RAFT agent and AIBN acting as an initiator.
The so-obtained samples were characterized and their molecular weight was calculated with GPC. Albeit very small, the GPC analyses confirmed an increase in molecular weight when adding a second block of luminescent polymer to an MMA macromer.
Further studies on this matter could lead to the production of more regular polymers that could increase the efficiency of the energy transfer process and of the LSC devices in general.

6. Bibliography

[1] G. Griffini, "Host Matrix Materials for Luminescent Solar Concentrators: Recent Achievements and Forthcoming Challenges," *Front. Mater.*, vol. 6, p. 29, Mar. 2019, doi: 10.3389/fmats.2019.00029.

[2] I. Papakonstantinou, M. Portnoi, and M. G. Debije, "The Hidden Potential of Luminescent Solar Concentrators," *Adv. Energy Mater.*, vol. 11, no. 3, p. 2002883, Jan. 2021, doi: 10.1002/aenm.202002883.

[3] N. J. L. K. Davis *et al.*, "Energy transfer in pendant perylene diimide copolymers," *J. Mater. Chem. C*, vol. 4, no. 35, pp. 8270–8275, 2016, doi: 10.1039/C6TC02555B.

[4] B. Balaban, S. Doshay, M. Osborn, Y. Rodriguez, and S. A. Carter, "The role of FRET in solar concentrator efficiency and color tunability," *Journal of Luminescence*, vol. 146, pp. 256–262, Feb. 2014, doi: 10.1016/j.jlumin.2013.09.049.

[5] C. Berney and G. Danuser, "FRET or No FRET: A Quantitative Comparison," *Biophysical Journal*, vol. 84, no. 6, pp. 3992–4010, Jun. 2003, doi: 10.1016/S0006-3495(03)75126-1.

Politecnico di Milano

SCHOOL OF INDUSTRIAL AND INFORMATION ENGINEERING

Master of Science – Materials Engineering and Nanotechnology

Department of Chemistry, Materials and Chemical Engineering "Giulio Natta"

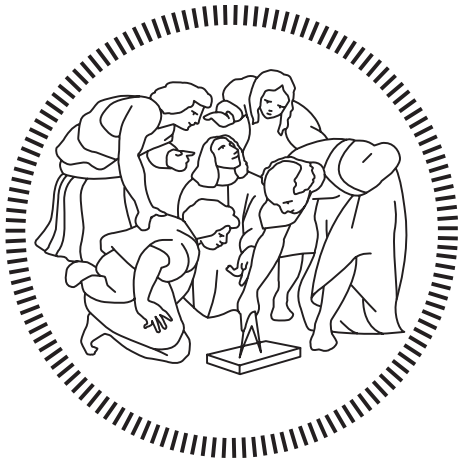

Novel copolymers for enhanced energy transfer in Luminescent Solar Concentrators

Supervisor

Gianmarco Enrico GRIFFINI

Co-Supervisor

Francesca CORSINI

Luca GIACOMETTI TADDEI

ID 939750

Academic Year 2020 - 2021

A *te*

Table of Contents

List of Figures

List of Tables

List of Abbreviations

AIE	Aggregation Induced Emission
AVT	Average Visible-light Transmissivity
CMA	Coumarin Methacrylate
EHP	Electron Hole Pair
FF	Fill Factor
FRET	Förster Resonant Energy Transfer
HOMO	Highest Occupied Molecular Orbital
IEM	2-IsocyanatoEthyl Methacrylate
LSC	Luminescent Solar Concentrator
LUMO	Lowest Unoccupied Molecular Orbital
PC	Polycarbonate
PCE	Power Conversion Efficiency
PEG	Polyethylene Glycol
PMA	Perylene bisimide Methacrylate
PMMA	Poly Methyl Methacrylate
PV	Photovoltaic
RAFT	Reversible Addition-Fragmentation chain-Transfer
TIR	Total Internal Refraction

Abstract

In order to counter the effects of global warming and climate change, the research world has shifted its focus to renewable and sustainable energy. In particular, solar energy technologies have developed exponentially, due to advancements that reduced their cost and increased their efficiency.

A technology that strives to conjugate the harvesting of solar energy and the need for aesthetically pleasing solutions in urban environments is represented by luminescent solar concentrators (LSCs). Being built on a very simple architecture, they can be easily integrated into buildings and facades, and their transparency is a great advantage of this technology.

In this work, novel copolymers based on methyl methacrylate and luminescent monomers with a methacrylate functionality are synthesized and used as host matrices for luminescent solar concentrators. The focus of the thesis is to exploit the energy transfer mechanisms between dyes in order to increase the area of the solar spectrum harvested by the LSC device. In particular, coumarin methacrylate was selected as the donor fluorophore while the acceptor molecule was obtained by adding the methacrylate functionality to a custom perylene diimide molecule synthesized by the University of Milan. The luminescent monomers were end-capped with 2-isocyanatoethylmethacrylate via urethane bond formation reactions and utilized as co-monomers in various concentrations in free-radical random polymerization reactions with methyl methacrylate.

The LSC devices fabricated by spin-coating the copolymers on glass slabs were characterized via various techniques to demonstrate the occurrence of the energy transfer mechanism, to measure their optical and photovoltaic efficiencies, and to assess their colour spectrum and average visible-light transmissivity. It was established that the energy transfer mechanism is beneficial for the efficiency of the devices and that direct polymerization of the luminophores in the polymeric chain is a viable way to reduce luminophore losses by quenching and reabsorption.

Estratto in Italiano

Siccome il cambiamento climatico sta diventando un tema di massima importanza, la necessità di nuove forme di energia sostenibile cresce di giorno in giorno. Fortunatamente, negli ultimi anni la crescita delle tecnologie che sfruttano energie rinnovabili è stata eccezionale e sempre più ricercatori stanno dedicando le loro risorse in questo campo.

Tra le varie forme di energia rinnovabile, quella legata all'energia solare è una delle più apprezzate e diffuse. La tecnologia legata al fotovoltaico diventa sempre più economica ed efficiente, mentre il mondo della ricerca si impegna per sviluppare pannelli più sempre innovativi. Più recentemente sono stati fatti sforzi per sviluppare dispositivi fotovoltaici esteticamente più gradevoli, al fine di ottenere pannelli che siano meglio integrabili negli ambienti urbani.

In questo contesto, i concentratori solari luminescenti (LSC) si presentano come una soluzione interessante. La loro architettura molto semplice, costituita solamente da una sottile lastra di materiale semitrasparente, consente loro di essere una tecnologia promettente per la produzione di massa, anche se allo stato attuale presentano ancora vari problemi legati alla loro efficienza e perdite di energia [1].

Introdotti per la prima volta nel 1976, il principio di funzionamento di un LSC è semplice, come mostrato nella figura sottostante: il dispositivo contiene molecole luminescenti in grado di assorbire la luce e sfruttare il fenomeno di rifrazione interna totale per intrappolare i fotoni nella lastra, che funge da guida d'onda. I fotoni vengono quindi trasportati ai bordi del dispositivo, dove vengono posizionate delle celle fotovoltaiche, in grado di convertire la luce in energia elettrica [2].

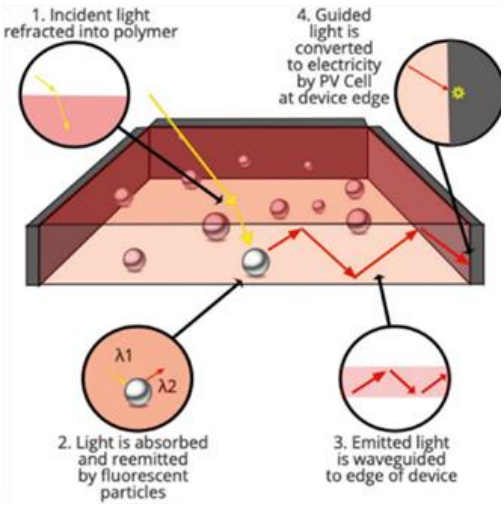

Schema di funzionamento tipico di un LSC.

I dispositivi sono solitamente prodotti in due configurazioni, a film sottile o a bulk: la prima è ottenuta rivestendo una lastra di materiale trasparente, tipicamente vetro, con un film sottile di polimero luminescente, tipicamente polimetilmetacrilato (PMMA) o policarbonato (PC), mentre nel primo caso l'intero dispositivo si comporta da matrice per le molecole di luminoforo.

Nelle applicazioni tipiche, i luminofori sono dispersi casualmente nella matrice polimerica. Sebbene questo sia un modo molto semplice ed economico per produrre un LSC, la dispersione casuale dei luminofori può favorire la loro aggregazione, portando a perdite di energia dovute a fenomeni di quenching e riassorbimento. Un altro approccio, studiato in questo lavoro di tesi, è quello di incorporare luminofori con una funzionalità monomerica (ad esempio metacrilato) nella catena polimerica tramite copolimerizzazione diretta [3].

In questo lavoro viene descritta la sintesi di un terpolimero luminescente tramite polimerizzazione free-radical random. In particolare, i campioni sono stati ottenuti copolimerizzando metilmetacrilato (MMA), cumarina metacrilata (CMA) e perilene metacrilato (PMA) in varie concentrazioni.

Le due molecole luminescenti sono state scelte in modo da favorire il verificarsi dei fenomeni di energy transfer tra i luminofori. In particolare, poiché lo spettro di assorbimento del perilene si sovrappone allo spettro di fluorescenza della cumarina, il primo è stato scelto come molecola accettore mentre la seconda come donatrice [4].

Il donatore assorbe la luce ed, invece di emettere un fotone per fluorescenza, trasferisce energia all'accettore, evitando così potenziali perdite di energia per fenomeni di riassorbimento nella guida d'onda e ampliando lo spettro di assorbimento complessivo dell'LSC.

I monomeri luminescenti utilizzati in questo lavoro sono stati sintetizzati mediante reazioni di end-capping dei luminofori, nello specifico di cumarina e di una formulazione custom di perilene diimmide sintetizzata dall'Università degli Studi di Milano, con 2-isocianatoetil metacrilato (IEM), utilizzando dibutilstagno dilaurato (DBTDL) come catalizzatore. I composti così ottenuti (CMA e PMA) sono stati caratterizzati e conservati per essere utilizzati come unità monomeriche.

I polimeri sono stati prodotti copolimerizzando MMA con concentrazioni variabili di CMA e PMA. In particolare, le reazioni di polimerizzazione free-radical random sono state effettuate sciogliendo i monomeri in un pallone contenente diossano, riscaldandolo a 83°C, siringando un'opportuna quantità di azobisisobutirronitrile (AIBN), che funge da iniziatore, e mantenendo il sistema in temperatura per 5 ore. Infine, i polimeri sono stati precipitati in esano e lasciati essiccare.

In primo luogo, sono stati sintetizzati copolimeri random con MMA e CMA, rispettivamente con un rapporto molare di 5, 10 e 15% tra CMA e MMA. Quindi, sono stati prodotti copolimeri casuali con un rapporto molare di 0,025, 0,050 e 0,100% di

PMA a MMA e, infine, sono stati sintetizzati anche terpolimeri con il 10% di CMA e 0,025, 0,050 e 0,100% di PMA.

I campioni polimerici così ottenuti sono catene di polimetilmetacrilato con molecole luminescenti come pendenti laterali, come mostrato nella figura sottostante. In questo modo, i fenomeni di quenching del luminoforo dovrebbero essere ridotti perché le molecole sono maggiormente distanziate l'una dall'altra, ostacolando la loro aggregazione.

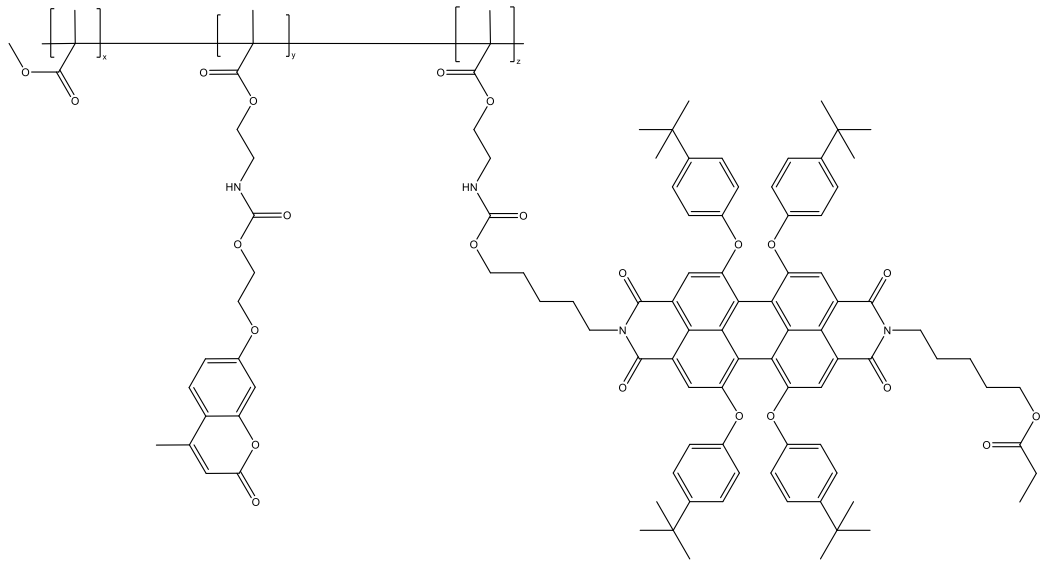

Struttura chimica dei terpolimeri sintetizzati.

I campioni polimerici sono quindi stati caratterizzati mediante varie tecniche e strumenti. In particolare, sono state eseguite caratterizzazioni ottiche utilizzando uno spettrometro UV-Vis e a fluorescenza, le proprietà fisiche sono state misurate con calorimetria differenziale a scansione (DSC) e cromatografia a permeazione di gel (GPC), mentre la struttura molecolare dei campioni è stata studiata con risonanza magnetica nucleare (H-NMR) e spettroscopia a infrarossi a trasformate di Fourier (FTIR).

Prima di sintetizzare i copolimeri, è stata eseguita una caratterizzazione approfondita dei monomeri.

In primo luogo, sono state misurate le loro proprietà ottiche, vale a dire gli spettri di assorbimento e di fluorescenza, per confrontarle con quelle dei loro precursori. Gli spettri ottici sono risultati identici, segno che la reazione di funzionalizzazione non ha influito su queste caratteristiche. Successivamente sono state effettuate misure spettrali con tecniche NMR e FTIR, confrontate con gli spettri relativi ai precursori per evidenziare l'efficacia della reazione di funzionalizzazione. Infine, sono state eseguite analisi DSC per verificare se il campione presentava una temperatura di transizione. Tutte queste analisi hanno evidenziato che le reazioni di end-capping hanno avuto successo.

Gli spettri ottici dei monomeri sono stati quindi confrontati per indagare se potessero essere adatti a sfruttare il meccanismo di energy transfer, come mostrato nella figura sottostante.

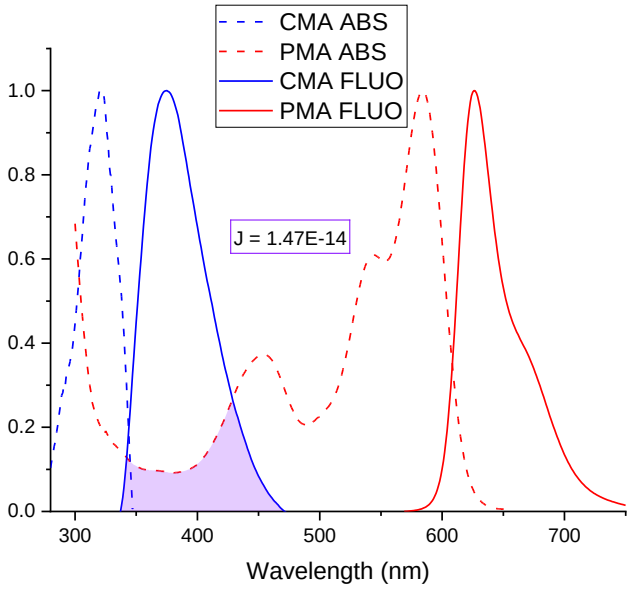

Overlap degli spettri di assorbimento e fluorescenza di CMA e PMA con il valore dell'integrale di overlap J.

Lo spettro di fluorescenza della cumarina si sovrappone in modo significativo allo spettro di assorbimento del perilene, e il valore calcolato dell'integrale di overlap è risultato essere in linea con quanto riportato in letteratura.

Dopo aver sintetizzato i copolimeri random CMA-MMA e PMA-MMA, sono stati caratterizzati mediante varie tecniche.

In primo luogo, sono state studiate le proprietà ottiche dei campioni; per entrambi i tipi di copolimeri, l'assorbanza è risultata essere proporzionale al contenuto di luminoforo nel polimero. Nel caso dei polimeri PMA-MMA, gli spettri di fluorescenza sono risultati più intensi all'aumentare del contenuto di fluoroforo, mentre per i polimeri con CMA lo spettro più intenso era associato a CMA10 MMA90 e l'aumento delle concentrazioni di cumarina determinava una minore intensità di fluorescenza. Per questo motivo, la concentrazione al 10% molare di CMA nel polimero è stata considerata quella ottimale per evitare l'insorgenza di fenomeni di quenching o di perdita di efficienza.

Sono state inoltre effettuate analisi spettrali mediante spettroscopia NMR e FTIR. In particolare, sono stati utilizzati spettri NMR per calcolare la quantità effettiva di luminoforo incorporato nei copolimeri. I risultati hanno evidenziato che la quantità reale di CMA nei copolimeri è superiore a quella nel feed di reazione, mentre la quantità di PMA è meno controllabile, probabilmente a causa del maggiore ingombro sterico della molecola, e anche meno identificabile in quanto i segnali NMR relativi al perilene sono molto deboli, date le quantità generalmente basse di luminoforo nel campione.

Infine, sono state eseguite analisi DSC per dedurre la temperatura di transizione vetrosa dei polimeri, che è risultata essere di circa 47 ° C per i copolimeri CMA e di circa 125 ° C per i campioni con PMA. Il loro peso molecolare è stato studiato anche con GPC, risultando in un peso molecolare medio di circa 40000 g/mol con una PDI media di 2,15 per i copolimeri CMA e 57000 g/mol con una PDI di 1,52 per i campioni con PMA.

Successivamente, i terpolimeri sono stati sintetizzati e caratterizzati. La Tg media è risultata essere di circa 60 °C, mentre il peso molecolare medio di circa 45000 g/mol.

Sono state inoltre eseguite analisi FTIR e NMR, confermando la quantità di cumarina incorporata rispetto al copolimero random CMA-MMA con 10% molare di CMA e ribadendo le difficoltà riscontrate nel misurare la reale quantità di PMA nei polimeri. In particolare, nei campioni denominati PMA0.050 MMA99.950 e CMA10 PMA0.050 MMA89.950 è risultata essere presente una quantità di perilene incorporata molto inferiore, spiegando così perché i loro spettri di fluorescenza fossero paragonabili a quelli del campione con 0,025% molare di PMA.

Successivamente, sono state eseguite caratterizzazioni ottiche dei terpolimeri per valutare l'occorrenza del meccanismo di energy transfer [5]. Innanzitutto, come mostrato nella figura sottostante, sono stati misurati gli spettri di eccitazione dei polimeri con il più alto contenuto di PMA.

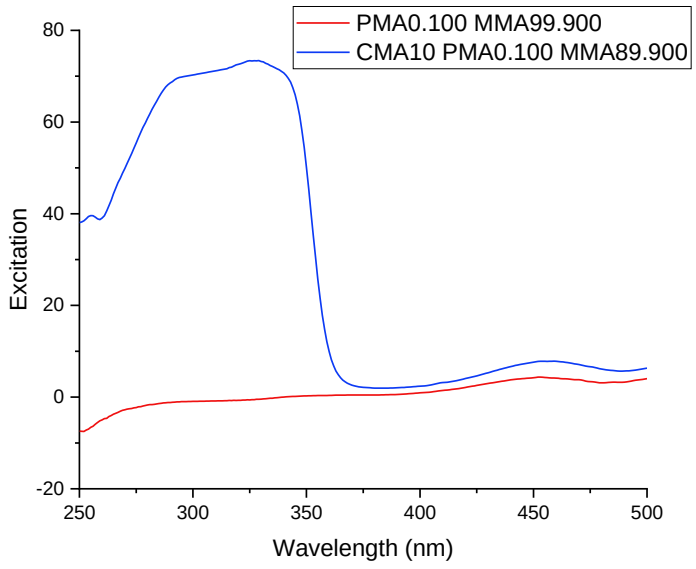

Spettro di eccitazione del terpolimero CMA10 PMA0.100 MMA89.900.

Gli spettri di eccitazione sono stati ottenuti detettando la luce a 650 nm. Come si può denotare dal grafico, il copolimero contenente solo perilene non emette per fluorescenza quando eccitato intorno a 300 nm, mentre nel caso del terpolimero contenente anche CMA la cumarina assorbe fotoni e il perilene può fluorescere tramite meccanismi di energy transfer.

Ulteriori test sono stati eseguiti per valutare l'efficienza del processo di energy transfer. In particolare, sono stati eseguiti calcoli sugli spettri di fluorescenza e fluorescenza time-resolved.

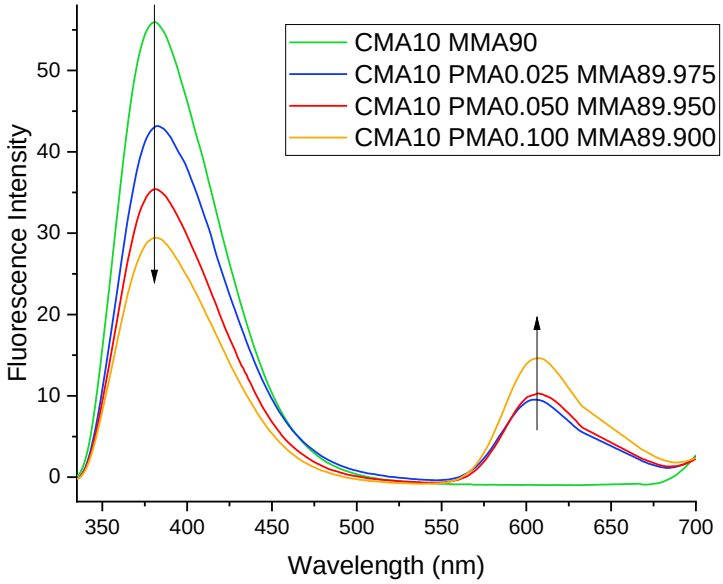

Confronto tra l'intensità di fluorescenza di vari copolimeri.

Come mostrato nella soprastante, sono stati misurati gli spettri di fluorescenza di campioni con la stessa densità ottica (dunque con la stessa assorbanza). Si può notare come, nonostante la quantità di cumarina sia la stessa e i campioni assorbano la stessa quantità di fotoni, il campione con 0,100% molare di PMA ha un'emissione di fluorescenza molto più debole nell'intervallo 350 – 450 nm, rispetto alla controparte senza perilene incorporato. Questo fenomeno può essere spiegato con il verificarsi del fenomeno del energy transfer. L'efficienza del processo è stata calcolata con la seguente equazione:

$$E = 1 - \frac{F_{DA}}{F_D}$$

dove F_{DA} è l'intensità di fluorescenza (calcolata sul picco rispetto al donatore) del polimero con entrambi i luminofori donatore e accettore, mentre F_Dè l'intensità di fluorescenza del copolimero con il solo donatore. Le efficienze calcolate sono 22,87% per CMA10 PMA0.025 MMA99,975, 36,75% per CMA10 PMA0.050 MMA99.950 e 47,39% per CMA10 PMA0.100 MMA99.900.

Inoltre, l'efficienza di energy transfer è stata calcolata mediante spettroscopia di fluorescenza time-resolved. L'efficienza è stata calcolata con la seguente equazione:

$$E = 1 - \frac{\tau_{DA}}{\tau_D}$$

dove τ_{DA} è il tempo di fluorescenza della molecola donatrice in un terpolimero con entrambi i luminofori e τ_D è il tempo di fluorescenza della molecola donatrice in un copolimero senza accettore.

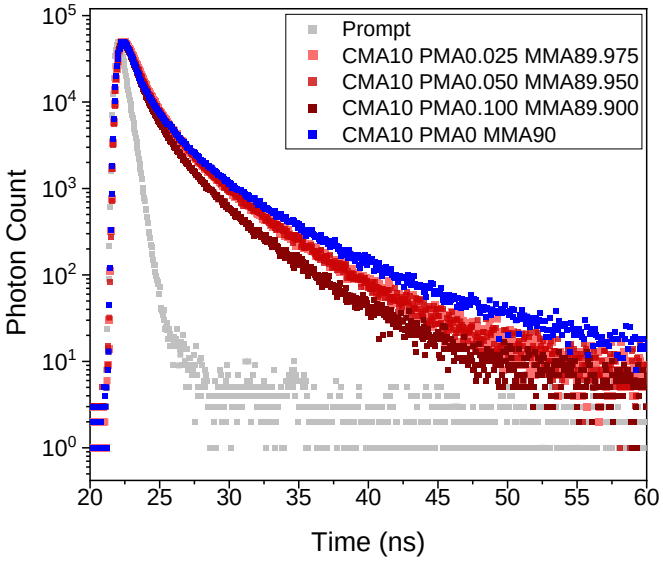

Profili di fluorescenza time-resolved dei terpolimeri.

I risultati sono mostrati nella figura soprastante e le efficienze così calcolate sono 6,5% per CMA10 PMA0.025 MMA99.975, 7,0% per CMA10 PMA0.050 MMA99.950 e 26% per CMA10 PMA0.100 MMA99.900

Infine, sono stati prodotti concentratori solari luminescenti mediante spin-coating dei polimeri sopra descritti su lastre di vetro sodico. I dispositivi sono stati ottenuti sciogliendo i polimeri in cloroformio a diverse concentrazioni in peso. Vale a dire, i copolimeri casuali CMA-MMA e PMA-MMA sono stati sciolti a una concentrazione del 3% in peso, mentre le concentrazioni di 3, 10 e 20% in peso sono state utilizzate per produrre LSC con i terpolimeri.

Misurazioni di efficienza fotonica sono state effettuate utilizzando uno spettroradiometro e un simulatore solare; la più alta efficienza fotonica esterna η_{EXT} misurata è risultata essere pari al 2,28%, associata a CMA10 PMA0.100 MMA89.900 20%, mentre la più alta efficienza fotonica interna η_{INT} misurata è risultata essere pari al 59.42%, associate a CMA10 PMA0.025 MMA89.975 20%. Inoltre, l'efficienza fotovoltaica dei dispositivi è stata misurata utilizzando un multimetro. La PCE più alta riportata, associata ancora a CMA10 PMA0.100 MMA89.900 20%, è stata dello 0,158% con una maschera nera che copre i bordi delle celle solari ed evita l'irradiazione diretta sui pannelli.

Lo spettroradiometro è stato utilizzato anche per misurare la cromaticità dei dispositivi. Misurando lo spettro di irraggiamento di una lampadina a luce bianca e confrontandolo con il segnale ricevuto dalla luce che passa attraverso gli LSC, è stato

possibile calcolare i valori di cromaticità e riportarli su un grafico CIE 1931, come mostrato nella figura sottostante, dove il quadrato rosso rappresenta i valori della luce bianca della lampada.

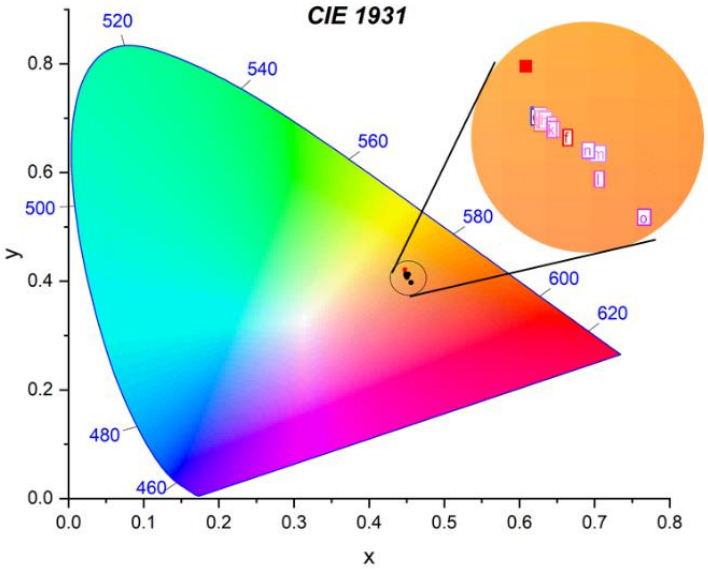

Grafico di cromaticità dei dispositivi LSC.

Si può notare che i valori di cromaticità sono abbastanza simili tra loro per tutti i dispositivi. Questa è un'indicazione del fatto che gli LSC prodotti non distorcono in modo significativo il colore della luce che li attraversa.

Ulteriori misurazioni e calcoli sono stati eseguiti per calcolare la trasmissività media della luce visible (AVT) dei dispositivi. L'AVT è una figura di merito introdotta per mediare la trasmissività ottica di un dispositivo sulla risposta alla luce dell'occhio umano ed è calcolata con la seguente formula:

$$AVT\% = \frac{\int T\%(\lambda) \cdot P(\lambda) \cdot S(\lambda)}{\int P(\lambda) \cdot S(\lambda)}$$

dove T% è la trasmittanza del dispositivo, P è la risposta fotopica dell'occhio umano alla luce e S è lo spettro solare AM 1.5G espresso come flusso di fotoni. Per gli LSC, un alto valore di AVT è particolarmente importante per tutte quelle applicazioni, come l'edilizia abitativa, dove la trasparenza del prodotto è una qualità decisamente apprezzata.

I risultati dei calcoli dei valori AVT sono riportati nella figura sottostante

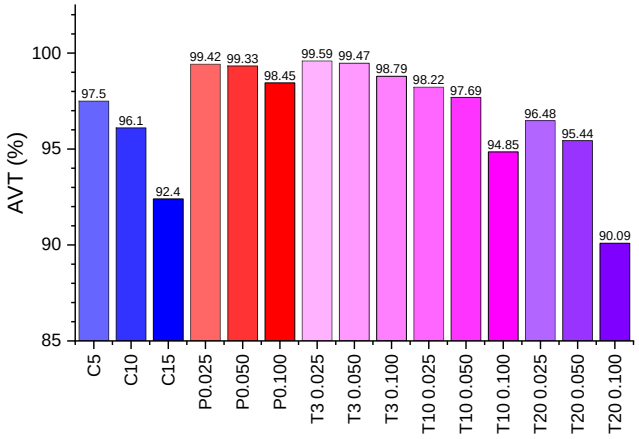

Valori di AVT dei dispositivi LSC.

Infine, è stata calcolata una figura di merito denominata efficienza di utilizzo della luce (LUE) con la seguente equazione:

$$LUE = PCE \cdot AVT$$

Questa figura di merito descrive come un'elevata trasmissività possa compensare la bassa efficienza fotovoltaica di un LSC. I valori di LUE ottenuti per i dispositivi sono risultati essere simili a quelli riportati in letteratura.

In conclusione, in questo lavoro viene presentata la sintesi e la caratterizzazione di nuovi copolimeri luminescenti per applicazioni in concentratori solari luminescenti a film sottile che sfruttano il meccanismo di energy transfer.

Il meccanismo di energy transfer è risultato vantaggioso per l'efficienza dei dispositivi LSC, così come l'incorporazione diretta dei luminofori nella catena polimerica rispetto alla loro dispersione casuale nella matrice.

Nonostante i valori di efficienza dei dispositivi, sia fotonici che fotovoltaici, siano mediamente inferiori a quelli riportati in letteratura, si è riscontrato che i dispositivi non distorcono il colore della luce che li attraversa e i loro valori di AVT sono significativamente elevati. Queste sono entrambe ottime caratteristiche per gli LSC.

Un ulteriore sforzo è stato rivolto alla sintesi di copolimeri luminescenti a blocchi con la tecnica di polimerizzazione RAFT. I copolimeri CMA-MMA e PMA-MMA RAFT sono stati prodotti con 2-fenil-2-propil benzoditioato che agisce come agente RAFT e AIBN che agisce come iniziatore.

I campioni così ottenuti sono stati caratterizzati e il loro peso molecolare è stato calcolato con tecniche GPC. Sebbene molto piccolo, le analisi GPC hanno confermato un aumento del peso molecolare quando si aggiunge un secondo blocco di polimero luminescente a un macromero MMA.

Ulteriori studi su questo argomento potrebbero portare alla produzione di polimeri più regolari che potrebbero aumentare l'efficienza del processo di energy transfer e dei dispositivi LSC in generale.

Foreword

As climate change is becoming a theme of utmost importance, the need for new sustainable forms of energy is growing day by day. Fortunately, the growth of renewable energy technologies in recent years has been outstanding, and more researchers are dedicating their resources to this field.

Among the various forms of renewable energy, solar power is one of the most popular and widespread. Photovoltaic technology has become much cheaper and more efficient, while research to develop more innovative panels is striving; this lead to the adoption of this technology also by developing markets and countries.

In order to avoid the limitations of traditional silicon solar panels, especially aesthetically speaking, thin-film polymeric photovoltaic technologies have been recently developed, although their cost remains too high to be adopted at a large scale. Luminescent solar concentrators come into play as a cheaper solution to provide more aesthetically pleasing solutions of converting light into electrical current. By absorbing a large amount of the solar spectrum, luminophores in the LSCs can spectrally convert photons and redirect them onto photovoltaic panels with a smaller area, allowing for transparency of the photovoltaic device and the harvesting of both direct and diffuse light. Moreover, thin-film LSCs could also be obtained by coating existing panels and windows with thin layers of luminescent polymer, optimizing costs.

At the current state, the technology behind luminescent solar concentrators is still heavily limited by many loss factors; hence, the products are still not efficient or durable enough for their factual commercialization, but the research on this topic is active and new improvements are achieved every year.

Aim and Structure of the Thesis

The aim of this thesis is to develop novel copolymers that rely on the FRET mechanism to optimize the absorption of the solar spectrum of LSC devices prepared with such materials. The polymeric matrix is designed as a copolymer based on polymethyl methacrylate with methacrylate luminophores as co-monomers. The peculiarity of such a host matrix is that the luminophore species are directly incorporated in the polymeric chain of the copolymer instead of being randomly dispersed. Fluorescent host matrices can display different optical properties and provide an advantage in the efficiency of LSC devices.

In order to exploit the energy transfer mechanism, coumarin methacrylate was selected as the donor fluorophore while the acceptor molecule was obtained by adding the methacrylate functionality to a custom perylene diimide molecule synthesized by the University of Milan.

The polymers and the devices obtained were then characterized using various techniques.

The structure of the thesis is as follows:

1. Introduction: an overview of the recent advancements and problems of the energetic sector, focusing on renewable and solar energy, is initially presented. Then, luminescent solar concentrators are introduced, focusing on their working principles and their most important parameters. A more detailed overview of Förster Resonant Energy Transfer is then presented, followed by a description of the materials commonly used in LSCs. Finally, a description of fluorescent polymers and their polymerization method present in the literature is presented.
2. Materials and Methods: a description of all the precursors, reagents and solvents is first made. Then, all the various synthesis methods utilized in the laboratory work are described, followed by the means of fabrication of LSC devices. Last, all the characterization techniques utilized on the polymers and devices are described.
3. Results and Discussion: the chapter describes all the results obtained by characterization tests performed on the samples and devices, together with a discussion of the said results. The first part is dedicated to the synthesized fluorescent monomers while the second focuses on the random copolymers and terpolymers. The third and final part presents the results of various efficiency tests run on the LSC devices.

4. Conclusion: in this chapter, a small summary of the most significant results is presented.
5. Future Developments: in this last chapter, an overview of research lines that were briefly investigated and could be further explored in the future is presented. In particular, the controlled polymerization of fluorescent copolymers with reversible addition-fragmentation chain-transfer (RAFT) polymerization method is described.

Chapter 1
Introduction

Since the industrial revolution, global emissions of greenhouse gases and other pollutants have been increasing alarmingly, leading to climate change and other disastrous environmental effects.

In the most recent years, the rising awareness of environmental issues led markets and governments to increase their focus on researching large-scale affordable methods to produce clean and sustainable energy, in order to reduce the usage of fossil fuels.

1.1 Solar Energy

Worldwide energy demand is constantly rising, reaching a tenfold increase since 1925; energy production and CO_2 emissions increase as a consequence [6].

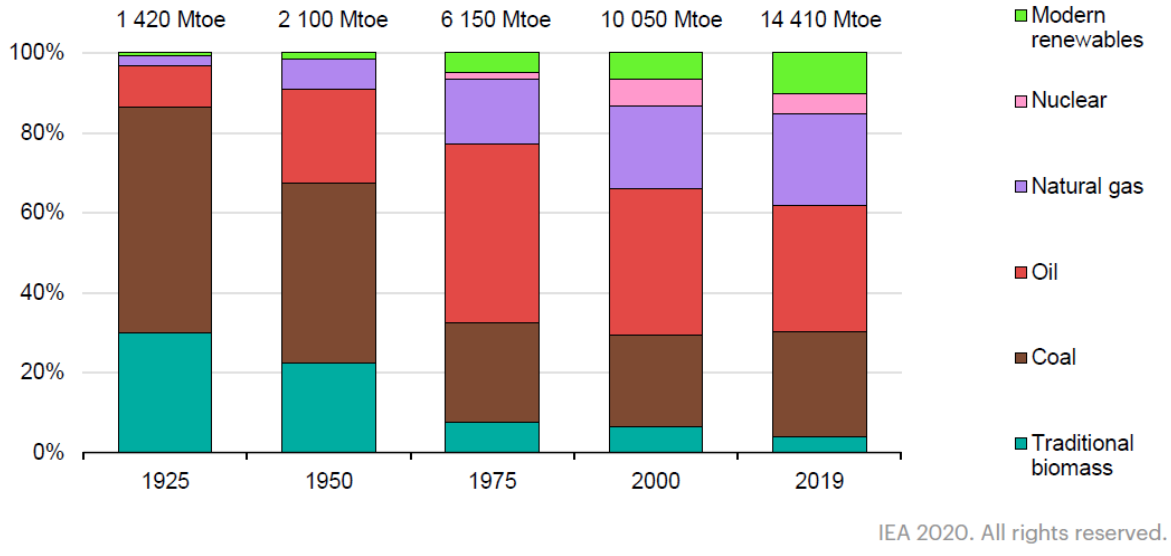

Figure 1.1 - Global primary energy demand by fuel between 1925 and 2019 [6].

Given their low cost and high technological proficiency, coal, natural gas, and oil are still major fuel sources, accounting for over 80% of global energy demand; despite this,

renewable energy is also on the rise, accounting for around 10% of global energy demand in 2019, as reported in Figure 1.1.

Furthermore, despite a 4% contraction in the global energy demand in 2020, given by the consequences of the SARS-CoV-2 pandemic, renewable energy grew by 3% regardless, reaching 29% of the global electrical energy production, and are set to grow by 8% in 2021 [7]. This demonstrates the importance of sustainable sources and the gradual transition of the market towards this kind of technology.

Among renewables, solar photovoltaic seems to be one of the most promising: its growth has been higher than any other technology in the past years, as shown in Figure 1.2, and it accounts for over 60% of additions in renewable power [8].

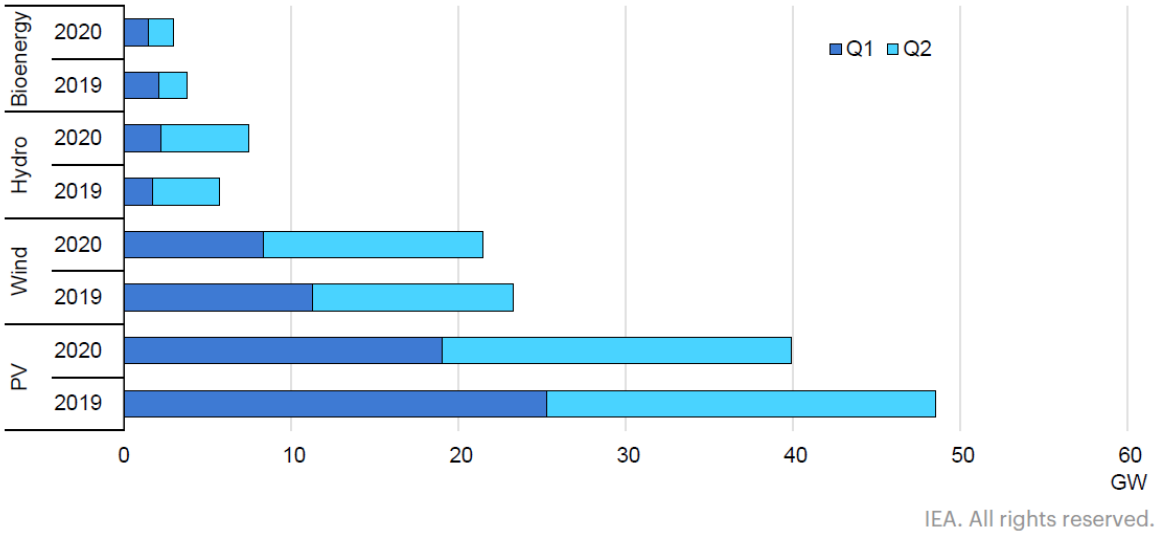

Figure 1.2 – Renewable capacity additions by technology [8].

Its growth is predicted to continue in the next years, and projections show wind and solar PV reaching 33% of global energy production by 2025, surpassing coal and becoming the first production technology worldwide [8].

The sun is an enormous source of energy: the annual effective solar irradiance on our planet varies from 60 to 250 W m^{-2}, and it is estimated that one day's worth of solar power could easily overcome the global annual power demand [9].

Solar radiation consists of 6.6% UV radiation (<380 nm), 44,7% visible radiation, and 48.7% IR radiation (>780 nm), as depicted in Figure 1.3; it corresponds to the black body spectrum of a mass at around 5800K, taking in consideration the effect of the earth atmosphere, in particular of gases such as H_2O or CO_2 [10].

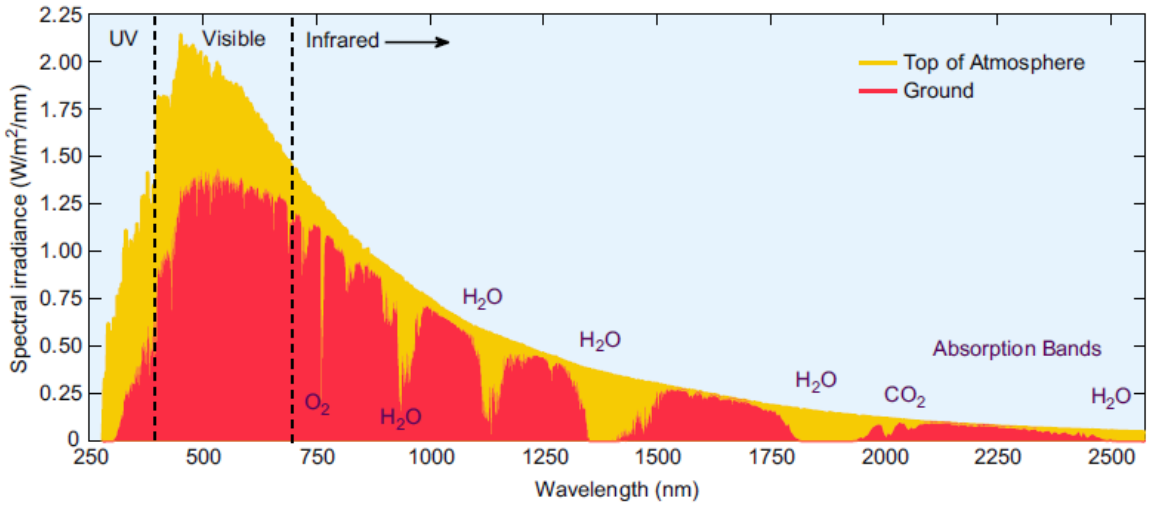

Figure 1.3 – Solar spectrum as a function of wavelength [11].

To evaluate the effect of the atmosphere (among reflection, absorption, and scattering) on the solar spectrum, the air mass standard has been introduced:

$$AM = \frac{1}{\cos \gamma_S}$$

where γ_s is the Zenith angle. The most utilized standard is AM1.5, useful to represent the average at mid-latitudes, with $\gamma_s = 48.2°$. The solar intensity at this angle is 1000 W m^{-2}, resulting in a useful standard to assure a consistent measurement worldwide [12].

1.2 Photovoltaic Cells

A photovoltaic cell is a device that employs the photovoltaic effect to transform photons into electrical current. Multiple PV cells are usually put in series to make a larger PV panel, that can yield a higher power output.

The photovoltaic effect was discovered by Becquerel in 1839, but the first PV devices with higher efficiencies (around 11%) were developed by Bell laboratories in 1954 [13].

A typical semiconductor PV device consists of two regions, one made from a p-doped material and the other from an n-doped material, joint together to form a p-n junction. When the junction is formed, spontaneous charge transfer occurs until equilibrium, creating a depletion zone and an internal "built-in" electric field. Now, when a photon with energy $h\nu > E_g$ (where h is the Planck constant, ν is the frequency of the photon and E_g is the bandgap of the semiconducting material) hits the junction, it can excite an electron from the valence band to the conduction band, leaving a hole in the valence band and creating an electron-hole pair (EHP), as shown in Figure 1.4. The built-in field can separate the EHP, driving the electrons in the n-type material and the holes in the p-type material [12].

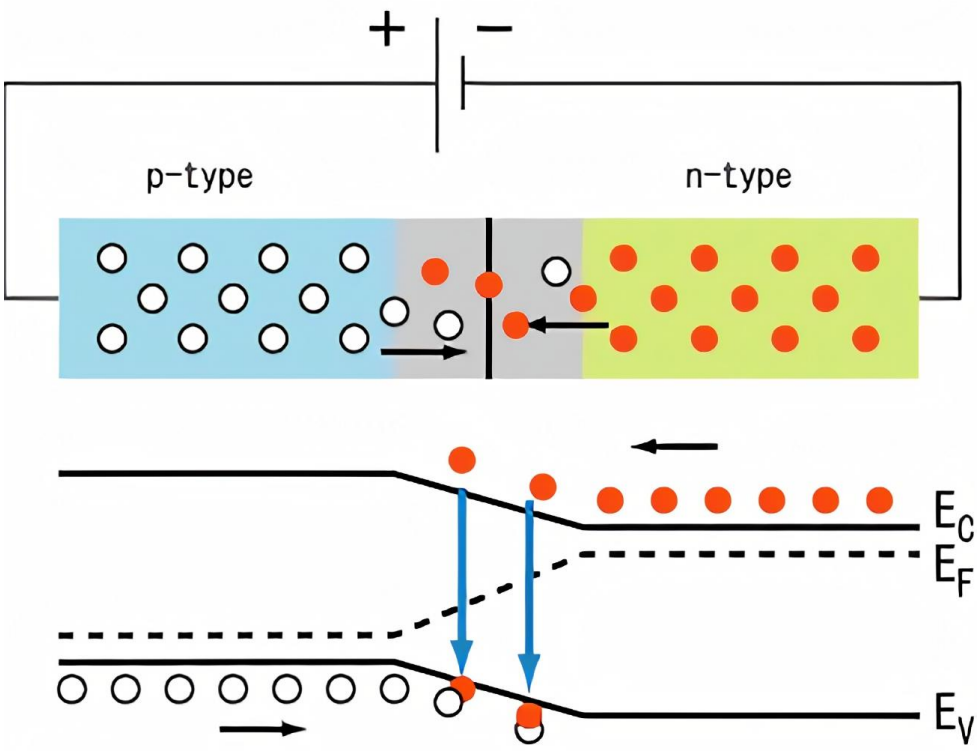

Figure 1.4 – Photovoltaic effect in a semiconductor p-n junction (1), band structure (2) [14].

The drift of charges generates an open-circuit voltage VOC. If we connect a short circuit to the electrodes, the excess electrons will be able to travel and recombine with the excess holes, thus producing a photogenerated current IPH (ISC when in short circuit).

When a load is connected to the PV device, current passes through it and a positive voltage V is established across the p-n junction. The current flows in an opposite verse with respect to the photocurrent, and it can be expressed by the Shockley equation:

$$I_D = I_0 \left(\exp\left(\frac{eV}{nK_B T} \right) - 1 \right)$$

where I_0 is the reverse saturation current, n is an ideality factor and K_B is the Boltzmann constant [12].

As shown in Figure 1.5, we should take into consideration the equivalent resistances, that contribute to deviating the performance of PV devices from ideality. In particular, the series resistance R_S is given by electrons travelling through the n-layer, while the shunt resistance R_{SH} is given by electrons travelling through the edges of the device instead of the external load [15].

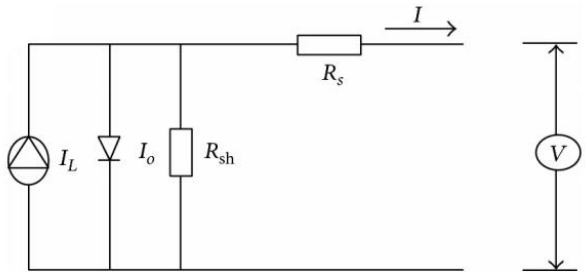

Figure 1.5 – Equivalent electrical circuit of a PV device [15].

We can introduce I_{SH} as:

$$I_{SH} = \frac{V + R_S \cdot I}{R_{SH}}$$

The overall current flowing in the device is then obtained as:

$$I = -I_{PH} + I_D + I_{SH}$$

This equation describes the I-V characteristic of a PV device, and the intersection between the curve and the load line with slope $-1/R$ sets the operating conditions V_{MP} and I_{MP}, with power output $P = V_{MP} \cdot I_{MP}$. These values represent the current and voltage of the PV cell when the output power is the maximum possible, as represented in Figure 1.6 [15].

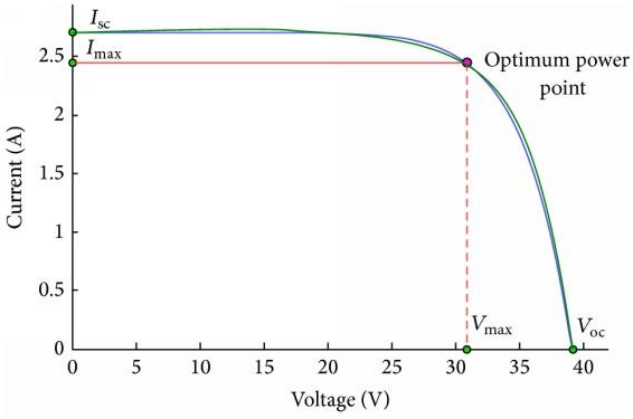

Figure 1.6 – Typical I-V characteristic of a PV device [15].

We can now introduce two important parameters of PV devices: FF (Fill Factor) and PCE (Power Conversion Efficiency).

$$FF = \frac{P_{MAX}}{V_{OC} \cdot I_{SC}} = \frac{V_{MP} \cdot I_{MP}}{V_{OC} \cdot I_{SC}}$$

$$PCE = \frac{P_{MAX}}{P_{IN}} = \frac{V_{OC} \cdot I_{SC} \cdot FF}{P_{IN} \cdot A_{PV}}$$

The fill factor represents the deviation from ideality of a PV device, and its typical value ranges around 70-80%. The PCE represents the efficiency of the cell, and its typical value can range between 0.1% and 30% [12].

1.2.1 Concentrating Systems

Despite efficiencies growing and technology improving, PV cells still require a high surface area to yield large quantities of electrical energy. This is especially a problem in residential and metropolitan contexts, where there may not be lots of surface area to exploit.

The goal of CPV (Concentrator Photovoltaics) is thus to harvest a large number of photons and concentrate them on PV devices with a much smaller area.

There are two main categories of solar concentrators: imaging and non-imaging. Imaging concentrators are usually Fresnel lenses or mirrors with various geometries, which deviate the photons to make them converge on a smaller area; they usually work better with direct perpendicular light. Instead, non-imaging concentrators can also work with indirect diffused light, allowing to harvest a higher quantity of photons [16].

1.3 Luminescent Solar Concentrators

First introduced in 1976 [17], a Luminescent Solar Concentrator (LSC) is a non-imaging concentrator, usually consisting of a thin slab of a transparent material (glass or plastic) that can trap incident light by TIR (Total Internal Refraction) and waveguide it to the edges of the devices, where PV devices can be mounted.

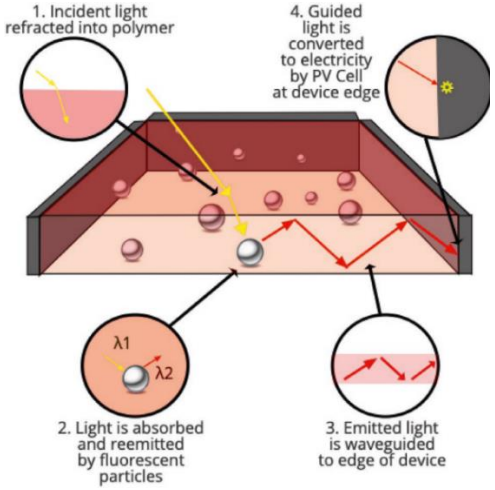

Figure 1.7 – Typical LSC device schematic [2].

Inside the concentrator, there usually are luminescent molecules that absorb incident light and re-emit it while downshifting its wavelength and energy, as shown in Figure 1.7.

The interest in LSCs comes from the concentrating capabilities, spectral conversion, and device transparency. These three characteristics are unique and allow to employ this technology in various contexts. For example, as shown in Figure 1.8, they can be employed in greenhouses, since they have the triple advantage of collecting and converting solar energy that would otherwise be lost, filtering out some wavelengths that are damaging to plants, and spectral converting to wavelengths that are instead more beneficial [2].

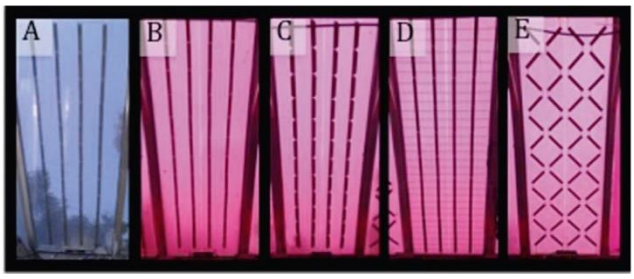

Figure 1.8 – LSC design in a greenhouse [2].

Another important advantage of LSCs is that, since they are non-imaging concentrators, they can also harvest diffused light, making it an interesting application for buildings that do not have much exposure to direct sun. The application that has

been explored the most in research is, in fact, the development of semi-transparent windows with PV cells on their frames, resulting in a window that can produce electrical energy with “passive” solar energy that would be lost otherwise [2].

1.3.1 Working Principles

Going into more detail, we can describe the working principle of an LSC. As shown in Figure 1.9, we can have two different configurations: bulk and thin-film. In the former, a thin plate of transparent material (like PMMA) is doped with luminescent molecules, while in the latter a thin film of doped material is deposited (by spin coating or other techniques) onto a transparent material (usually glass). The thin-film configuration is usually much easier and cheaper to produce [17].

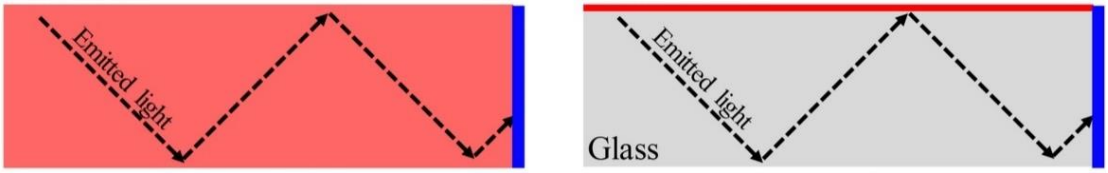

Figure 1.9 – Bulk configuration LSC (left) and thin-film configuration LSC (right) [17].

Despite these differences, the optical behaviour is the same for both LSC configurations; the incoming photons are absorbed by luminescent particles inside the matrix, exciting an electron from the ground state to an upper state. Then, as shown in Figure 1.10, the electron undergoes vibrational deactivations through non-radiative transitions, loses some energy, and finally decays to the ground state level by fluorescence, emitting a photon with lower energy than the one originally absorbed. The process is usually very quick, in the range of nanoseconds. The emitted photon then undergoes TIR between the walls of the matrix (bulk configuration) or the glass (thin-film configuration) and is waveguided to the edges of the device [2].

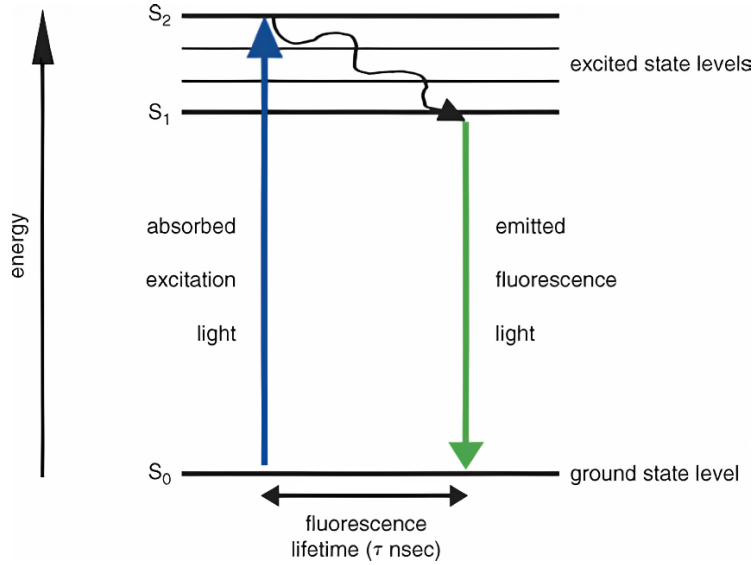

Figure 1.10 – Jablonski diagram of fluorescence [18].

Throughout the process, there are many possible losses and non-efficient mechanisms that end up lowering the efficiency of the LSC device. Some of them are shown in Figure 1.11, and others are listed below [19].

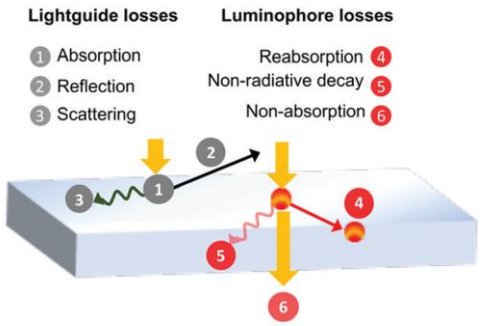

Figure 1.11 – Possible loss mechanisms in LSCs [20].

- Absorption or scattering of photons by the transparent matrix and consequent energy dissipation (represented by η_{HOST}).
- The absorption of photons by the luminophore is not perfectly efficient. This factor depends on the concentration of luminophores in the matrix, the spectral breath and molar absorption coefficient of the luminophores, as well as the maximum path length of the incident photons. In the ideal case, the luminophores should have a broad emission spectrum and emit in the range of maximum spectral response of the PV cells (represented by η_{ABS}).
- Reflection of photons by the transparent matrix (represented by R).
- Transmission of photons from one side of the transparent matrix to the other (represented by $1 - R$).
- Loss of a photon from an escape cone formed at an angle that cannot provide TIR (represented by P_{TIR}).
- Intrinsic inefficiency of the TIR process, given by imperfections and defects (represented by η_{TIR}).
- Reabsorption of a photon emitted by a luminophore from another luminophore. This can be caused by a narrow Stokes shift of the luminophore. Every reabsorption and re-emission increase the probability of losing primary emitted photons due to all the previous mechanisms (represented by η_{SELF}).
- Non-radiative decay of the luminophore and consequent energy dissipation. This term is also called *photoluminescent quantum yield* (represented by η_{PLQY}).
- Intrinsic loss of energy of photons due to the fluorescence process (represented by η_{STOKES})

These numerous loss mechanisms, together with low PV cells efficiencies, contribute to drastically decreasing the LSCs efficiency. The terms that contribute the most to

energy losses and inefficiencies are $P_{TIR}, \eta_{STOKES}, \eta_{SELF}, \eta_{ABS}$; between these, only the last two terms can be effectively improved, as will be shown later on [21].

1.3.2 Device Parameters

To better characterize the LSCs, a series of device parameters are introduced:

- The geometrical gain G is introduced to indicate the influence of the LSC dimensions on the optical efficiency. It is defined as:

$$G = \frac{A_{LSC}}{A_{PV}}$$

where A_{LSC} is the top surface area of the LSC and A_{PV} is the lateral area occupied by PV cells.

- Sometimes also referred to as optical quantum efficiency, internal quantum efficiency, or external quantum efficiency, the internal photon efficiency η_{INT} indicates the overall efficiency of the photon transport process in the LSC, taking into account some of the losses mechanisms and inefficiencies mentioned earlier. It is especially useful to report experimental results since it does not depend on the illumination source, as long as the measurements conditions are kept the same (all edges uncovered, white or solar light). It is defined as:

$$\eta_{INT} = \frac{no.of\ edge - emitted\ photons}{no.of\ total\ absorbed\ photons}$$

- In order to consider losses during the absorption process, we can introduce the external photon efficiency η_{EXT}. It is important that, when reporting this quantity, an accurate description of the illumination source is also given. The quantity is defined as:

$$\eta_{EXT} = \frac{no.of\ edge - emitted\ photons}{no.of\ total\ incident\ photons}$$

- The concentration factor C is defined as:

$$C = G\eta_{EXT}$$

- In order to evaluate the efficiency of an LSC device coupled to PV cells, the device efficiency η_{DEV} is introduced. It is defined as:

$$\eta_{DEV} = \frac{power\ from\ edge - coupled\ PV\ cells}{incident\ optical\ power\ on\ LSC\ surface}$$

- Finally, the absorption efficiency is introduced, defined as:

$$\eta_{ABS} = \frac{fraction\ of\ light\ absorbed\ by\ the\ LSC}{spectral\ irradiance\ input}$$

When reporting values of η_{DEV}, it is also extremely important to report the characteristics and performances of the bare PV cells, since they influence the output power [20], [21].

1.3.3 Förster Resonant Energy Transfer

As mentioned earlier, η_{ABS} and η_{SELF} are two of the factors that most undermine the LSCs' efficiency. One way to try and improve these factors is to exploit an effect called Förster Resonant Energy Transfer (FRET).

First introduced in LSCs by Swartz in 1977 [22], it is a mechanism describing non-radiative energy transfer between two luminophores, as shown in the Jablonski diagram in Figure 1.12. When two different luminophores, called donor and acceptor, meet certain conditions, the donor can transfer the energy of an excited electron (that would otherwise be spent by emitting a photon) to an electron in the ground state of the acceptor molecule, which can now emit a photon. One important condition is that the emission spectrum of the donor and the absorption spectrum of the acceptor must be overlapping, at least partly [23].

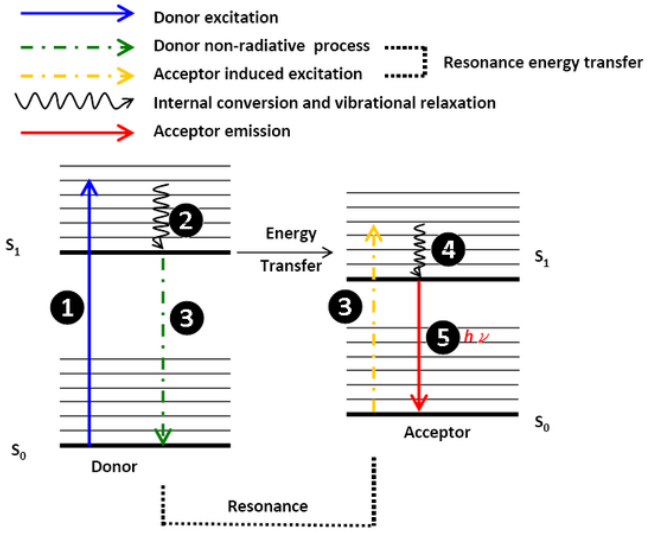

Figure 1.12 – Jablonski diagram of FRET [24].

The mechanism at the base of FRET is dipole-dipole coupling, and the process is highly distance-dependent: the distance between the acceptor and donor molecule needs to be between 1 and 10 nm since the energy transfer efficiency can be written as

$$E = \frac{R_0^6}{R_0^6 + r^6}$$

where R_0 is the Förster radius, the distance at which $E = 50\%$. R_0 is defined as

$$R_0^6 = \frac{9\kappa^2 q}{128\pi^5} \int_0^\infty \frac{F_D(\lambda)\varepsilon_A(\lambda)\lambda^4}{n(\lambda)^4} d\lambda$$

where κ is the distance between the two molecules, q is the quantum yield of the donor, F_D the donor fluorescence probability, ε_A the acceptor extinction coefficient and n the refractive index of the matrix [25], [26].

Other methods usually utilized to calculate FRET efficiency are based on emission and absorption spectra of dyes dispersed in a polymeric matrix. One first method consists of exciting the matrix (with light of wavelength equal to the maximum absorption peak of the donor luminophore) and measuring the fluorescence intensity of the donor both when it is the only dye in the matrix and when dispersed together with an acceptor molecule: when both species are present, the fluorescence intensity of the donor should decrease with respect to the other case, since some of the energy is transferred non-radiatively to the acceptor molecule. The efficiency of the process can thus be calculated as:

$$E = 1 - \frac{F_{DA}}{F_D}$$

where F_{DA} is the fluorescence intensity of the donor in solution with the acceptor and F_D that of the donor alone. With this method, it is straightforward to obtain an approximate value of the FRET efficiency in the polymer, but it overlooks some effects such as fluorescence quenching by other means than FRET, such as aggregation of molecules due to an increased concentration; for this reason, it is preferable to use other approaches to obtain a more precise result [27].

Another method is that of measuring the fluorescence spectrum of the matrix when excited with light of wavelength equal to the maximum absorption peak of the donor molecule. Differently from the previous method, the emission peak of the acceptor molecule is measured: if FRET is sufficiently efficient, the emission peak should increase noticeably, and its ratio with the emission peak of a matrix with the acceptor alone should indicate the efficiency of the FRET system [5], [27], [28].

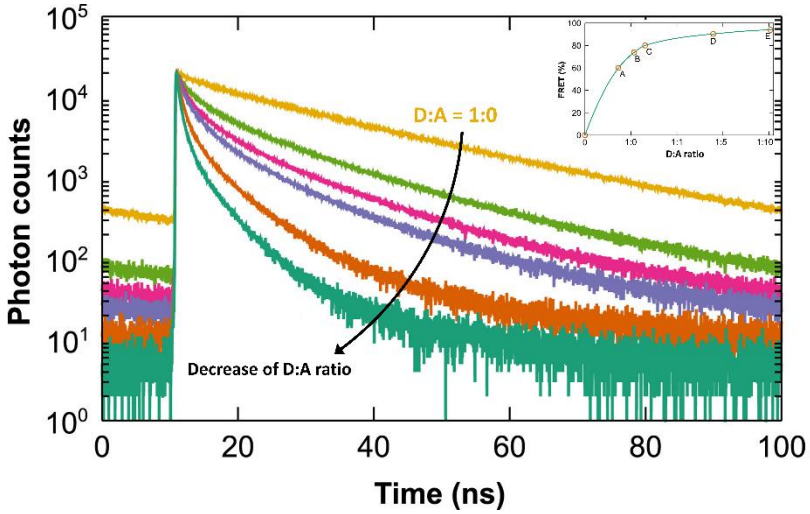

Figure 1.13 – An example of a time-resolved fluorescence measurement [23].

Another method utilized to quantify the FRET mechanism efficiency is to use time-resolved fluorimetry measurements: if energy transfer is happening between dyes in the matrix, the fluorescence time of the donor luminophore should decrease, indicating that less time is needed for the fluorescence process to take place, since the process of

transferring energy to the acceptor molecule takes a shorter time. An example of a time-resolved fluorescence measurement is shown in Figure 1.13 [29], [30].

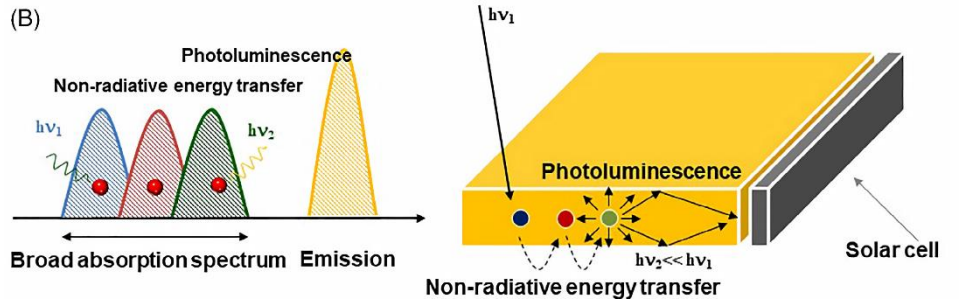

Figure 1.14 – Schematic diagram of FRET mechanism showing absorption spectrum broadening [31]

The advantage gained by LSCs that exploit this mechanism is that the absorption spectrum of the device can be effectively broadened; as shown in Figure 1.14, multiple fluorophores (carefully selected so that absorption and emission spectra overlap conveniently) can be used to promote a FRET cascade effect, so that the largest possible number of photons is absorbed while maintaining a narrow emission peak, usually corresponding with the emission spectrum of the lowest-energy absorbing luminophore. A further advantage is given by the fact that, by selecting the appropriate fluorophores, it is possible to match the emission of the dyes with the absorption of the PV cells while absorbing photons with much higher energy, artificially "stretching" the Stokes shift of the dyes [31].

The FRET mechanism can be exploited with multiple dyes, as long as the spectra overlap conveniently. As shown in Figure 1.15, Delgado-Sanchez et al. demonstrated a FRET system with six dyes in cascade, with good absorbance between 350 and 600 nm [31].

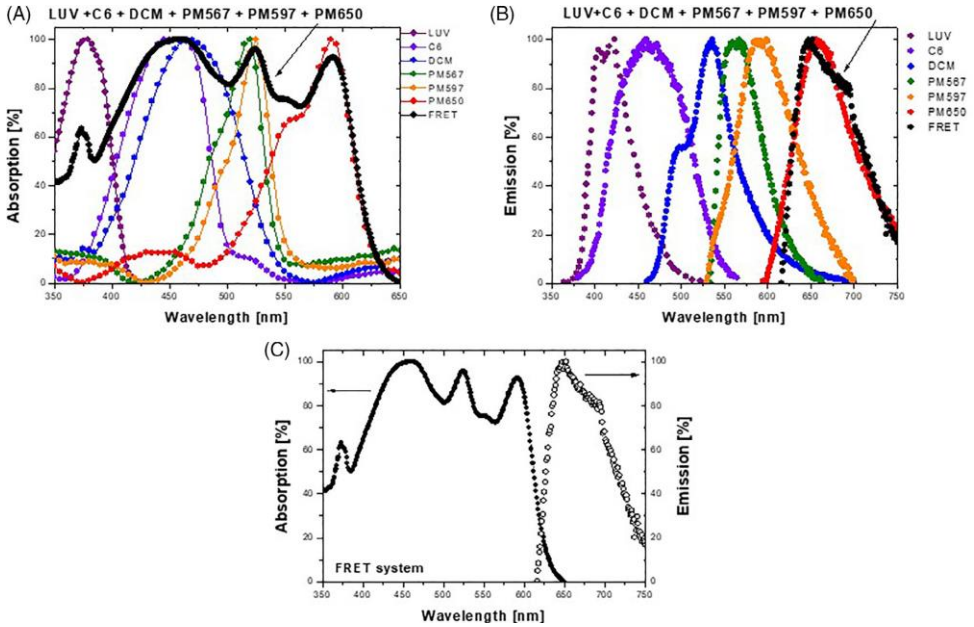

Figure 1.15 – Absorption spectra of individual dyes (A), emission spectra of individual dyes (B), absorption and emission spectra of the so-obtained FRET system (C) [31].

1.4 LSC Materials

LSCs are devices built with two main components: a host matrix and a luminophore. Both components have a fundamental role in device efficiency and a careful selection of them is required in order to maximize the performance of the LSC. What follows is an overview of the characteristics of the two components.

1.4.1 Host Matrices

Research in the field of LSCs has been traditionally focused on optimizing the device assembly and the emission efficiency of luminophores. Despite this, another important aspect to take into consideration is the optimization of the host matrix.

Host matrices are associated with a large percentage of losses in LSCs, such as absorption, scattering, reflection, or transmission of photons, poor optical features for TIR, poor characteristics for luminophore solubility [1].

A good host matrix for an LSC must also satisfy certain requirements [32]:

- Suitable refractive index n in order to optimize the TIR probability P_{TIR}, avoid reflection of photons at the surface and enhance the light-trapping efficiency. A low n is needed to avoid reflection, while a higher index is required for TIR and light-trapping efficiency. A compromise is found for $n \approx 1.5 - 2$, which has been demonstrated to be the optimum value. Many glasses and polymers have refractive indexes around these values [32].
- High optical transmittance (in UV, VIS, and NIR), in order to lower η_{HOST} and avoid absorption and scattering losses.
- High solubility parameter for the luminophore, in order to reduce quenching phenomena caused by aggregates.
- A suitable glass transition temperature T_g, in order to avoid the flowing of the material during operation. The T_g needs to be higher than the highest temperature reached during exposure to sunlight.
- Photostability, weatherability, mechanical and chemical resistance, long term outdoor durability.
- Easy optical coupling to PV cells.

Glass was considered a good material choice, since it satisfies most of the requirements mentioned above, including excellent optical transparency, mechanical properties, and stability, but its processing temperatures are usually too high to be sustained by organic luminophores. Furthermore, its weight could be a disadvantage in practical applications and be counterproductive to the LSCs' goal of ease of handling [32].

For this reason, organic and hybrid matrices have been recently researched and developed.

Polymeric Matrices

The most used polymeric material is by far polymethyl methacrylate (PMMA). It has excellent transparency to visible light and a refractive index $n \approx 1.5$. Together with polycarbonate (PC), it displays the highest output irradiance from the device edges (compared to polymers like polystyrene or styrene-acrylonitrile), because of its high internal transmittance [1].

The main problem with PMMA is its limited photostability, especially against high-energy UV light, which gives rise to the formation of photon trap sites by photo and thermal oxidation [32]. Furthermore, some among the most efficient luminophores have poor solubility in PMMA, which increases the probability of quenching and decreases the fluorescence yield [1].

Polylactic acid (PLA) has been investigated as a potential material for host matrices, with the added advantage of being environmentally friendly. PLA is characterized by excellent processability, photostability, and good photoluminescence quantum yield, but its low refractive index $n \approx 1.45$ makes it less efficient regarding TIR and light-trapping efficiency [32].

Thermally crosslinked systems based on partially fluorinated polymers were also investigated. By crosslinking a functional chloro-trifluoro-ethylenevinyl-ether copolymer with different types of aliphatic polyisocyanates, LSC devices with superior long-term operational stability (up to 500h) were obtained [33].

Organic-Inorganic Hybrid Matrices

In this class of materials, the high refractive index and good stability of inorganic materials are combined with the good processability and accessible chemical functionality of polymers [1].

An example is a hybrid polysiloxane-rubber doped with lumogen red LR305. It was demonstrated that at low dye concentrations the efficiency is comparable to the ones obtained with PC, but increasing the concentration rapidly promotes luminophore quenching, since the LR305 solubility is low in apolar environments [34].

Glassy hybrids have also been investigated: bridged silsesquioxanes containing Eu^{3+} salts and 2-thenoyltrifluoroacetone were proposed. Due to the peculiar optical properties of this combination, high values of optical efficiency η_{OPT} could be reached [35].

One last important class is that of ureasil systems. A reaction between a polyetheramine and an organo-silica precursor, followed by hydrolysis and condensation of the silica network, forms an ureasil matrix. These compounds can be used to fabricate cylindrical LSCs, as shown in Figure 1.16. In a recent study, a PMMA optical fibre was coated with an ureasil layer doped with a Eu^{3+} luminescent species; the fibre displays enhanced UV transparency and good optical efficiency [36].

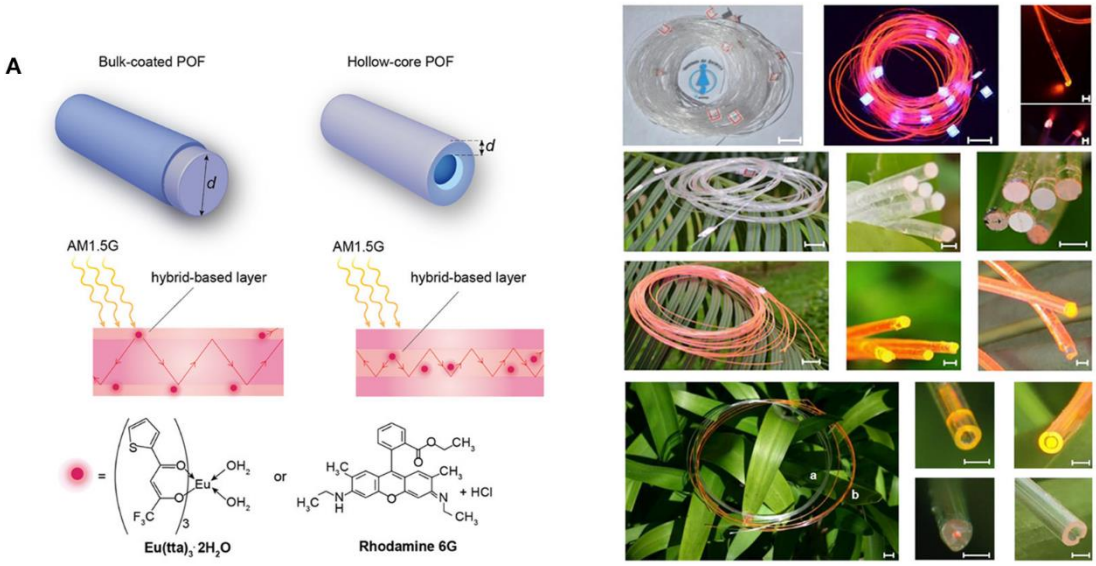

Figure 1.16 – Schematic representation of optical fibres LSCs and corresponding photographs [36].

Multifunctional matrices

The most recent advancements in the research of LSC matrices include the development of multifunctional systems, which provide additional functionalities besides luminophore hosting. Some examples include hydrophobic matrices for better outdoor durability, thermo-responsivity for absorption and emission colour tuning, or electro-responsivity [1].

A hydrophobic matrix was developed from a blend of three different fluorinated polymers and a perylene-based luminophore with lateral C=C bonds. When illuminated with UV light, the blend is crosslinked and a solid thin film is produced, with good hydro- and oleophobic characteristics [37]. Very high contact angles could also be obtained by undergoing a soft-lithographic and a stereolithographic process; a UV-cross-linkable microstructured surface was developed in order to obtain superhydrophobicity [38].

Regarding thermo-responsivity, it can be achieved by employing a matrix with two luminophores, one of which aggregates at low temperatures. As the temperature increases, the solubility of the dyes increases, and fluorescence phenomena become more efficient. Moreover, if the characteristics of the dyes are compatible, FRET mechanisms can take place and the emission colour can shift as the temperature changes, as shown in Figure 1.17 [39].

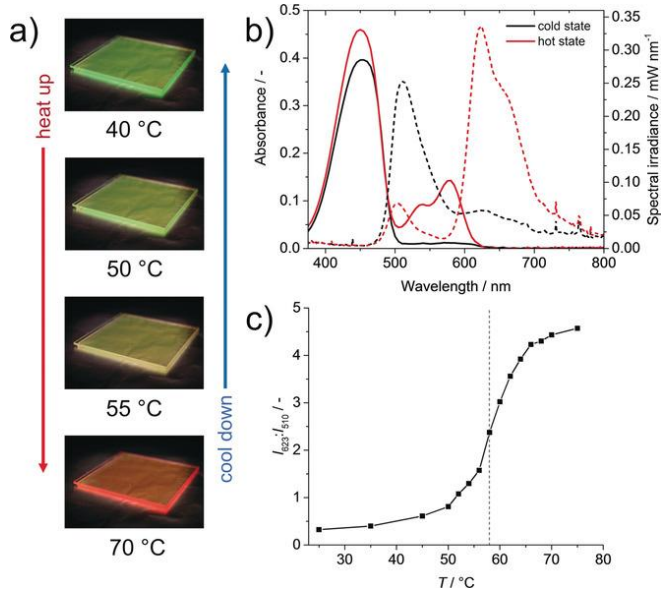

Figure 1.17 – Photographs of an LSC modifying its emission colour with increasing temperature (a), absorbance (solid) and emission (dotted) spectra of the LSC (b), ratio between the emission of the two dyes increasing with temperature, demonstrating FRET efficiency strongly increases above 58 °C (c) [39].

Furthermore, recent papers explored the possibility of developing a thermo-responsive host matrix with self-healing capabilities. By employing the Diels-Alder reaction between a furan-functionalized acrylic copolymer and an aliphatic bismaleimide, an optically clear material is obtained, suited to develop an LSC matrix able to self-repair scratches upon heat treatment [40].

1.4.2 Luminophores

Luminophores are the core components of LSCs. As already depicted in Figure 1.10, a luminophore molecule absorbs a photon, an electron is excited from the ground state to an upper state (S_2), it loses some energy through non-radiative vibrational decay (going to S_1) and finally decays to the ground state (S_0) emitting a photon [2].

Luminescent molecules are subject to many losses, which researchers are constantly seeking to minimize in order to optimize device efficiency. Like host matrices, luminophores also have a list of requirements to satisfy [41]:

- A broad absorption spectrum in order to utilize the solar spectrum most efficiently.
- A high fluorescence quantum yield so as to minimize the energy lost in non-radiative transitions.
- A large Stokes shift in order to minimize overlap of absorption and emission spectra and reabsorption losses.

- Long-term stability and durability of the molecules, which can become less efficient over time.
- Good solubility in the host matrix.
- Good match with the absorption spectra of the PV cells attached to the LSC device.

There are three main categories of luminescent molecules used in LSCs; what follows is an overview of these categories.

Organic dyes

Organic dyes have traditionally been the most used materials in LSCs. They present large absorption coefficients and high photoluminescence quantum yields (over 90%), together with good photostability and solubility in polymeric matrices like PMMA or PC [19].

The typical organic luminophore is a highly π-conjugated molecule with a planar core; this implies that the HOMO (highest occupied molecular orbital) of the molecule is a π orbital and the LUMO (lowest unoccupied molecular orbital) a π*. The difference between the energy of these orbitals determines the energy gap E_g and thus the wavelength of absorbed radiation [42].

The main classes of organic dyes typically used in LSCs are rhodamines, coumarins, and perylenes, shown in Figure 1.18.

Rhodamines have very high quantum yields but narrow Stokes shifts, leading to high reabsorption losses. Rhodamines also display poor photostability, making them unsuitable for long-term LSCs application. Furthermore, the most utilized dye, rhodamine 6G, also displays a decreased luminescence when dissolved in a PMMA matrix.

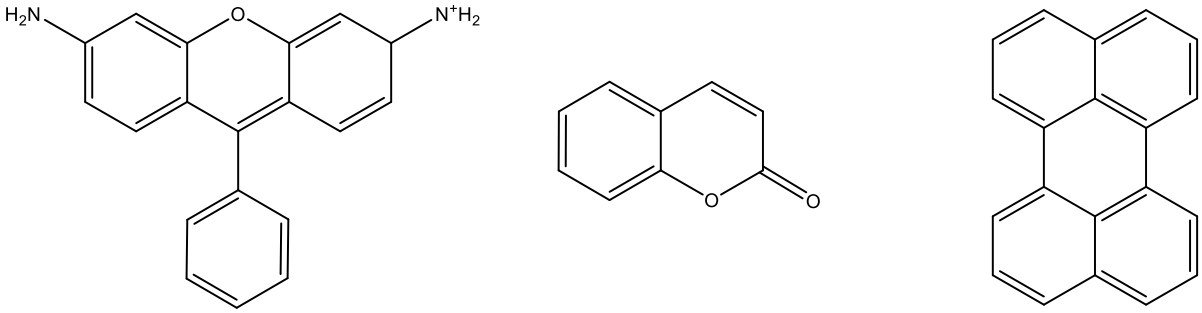

Figure 1.18 – Basic structure of organic luminophores: rhodamine (left), coumarin (centre), and perylene (right).

Coumarins are aromatic molecules, the basic structure of which can be described as a benzene fused with a pyrone ring. They have a much larger Stokes shift compared to rhodamines and they display a high quantum yield (reaching almost unity for compounds like coumarin 540A). They have higher stability compared to rhodamines,

while also displaying good compatibility with polymeric matrices, but they usually absorb in the UV (they are white or transparent) and emit in the blue-green, making them unsuitable to be used as emitters in LSCs. Recently, their usage as donor molecules in FRET systems has been explored in literature.

Overall, the best performing organic dyes are perylenes, aromatic molecules the basic structure of which can be described as two pairs of fused benzene rings joint by another benzene in the middle. The perylene molecule itself displays low photostability, but many perylene derivatives have been developed; the most promising molecules are perylene bisimides: compared to the other luminophores, they display the highest photostability, quantum yield, and absorption coefficient. The most utilized commercial dye is Lumogen Red 305 (shown in Figure 1.19): its quantum yield averaging around 97%, its broad absorption range, its great solubility in PMMA and its strong emission in the red region of the spectrum make it a suitable choice both for LSCs devices and the solar cells matched to them. Due to its structure, LR305 can be dissolved in high concentrations without displaying significant quenching; this effect is mainly explained by the fact that the imide groups are functionalized with bulky substituents to decrease the probability of π-π stacking between molecules. The main downside of LR305 is that it displays a very narrow Stokes shift increasing the probability of reabsorption losses [32], [43], [44].

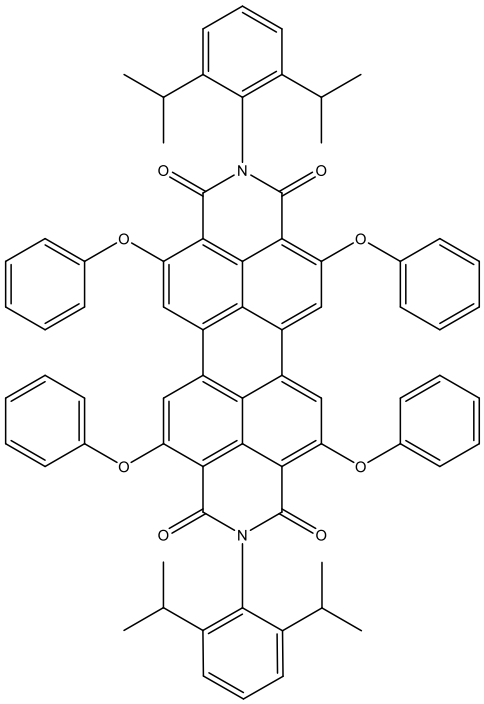

Figure 1.19 – Structure of the commercial perylene bisimide Lumogen Red 305 [45].

Since organic luminophores are generally subject to fluorescence emission quenching when they aggregate, numerous recent studies focused on AIE (Aggregation Induced Emission) dyes, molecules with a particular structure such that they emit light only when in their aggregate form.

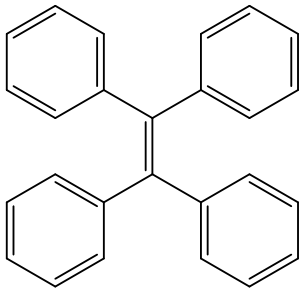

Figure 1.20 – Tetraphenylene, one of the most studied AIE dyes [46].

One of the most studied AIE dyes, tetraphenylene, is shown in Figure 1.20; the particularity of these molecules is that when they aggregate, the external aromatic rings are twisted with respect to the plane, due to steric hindrance, creating a sort of propeller helix shape. This can restrict the intermolecular motion, in particular rotational and vibrational movement, triggering a strong excimer fluorescence due to the opening of a new radiative decay path. The interest in these molecules for LSCs applications comes from the fact that they can be utilized and dissolved in matrices even in high concentrations, without displaying fluorescence quenching [46]. In a recent research work, tetraphenylene has been used as a donor molecule for a single molecule FRET copolymer system: when aggregated, the AIE dye fluoresces and acts as a luminophore, while when not aggregated it transfers its energy to an acceptor dye with almost 100% efficiency. Thus, the luminescence properties of the copolymer can be tuned just by choosing a good or bad solvent for the tetraphenylene [47].

In order to increase the photostability and the durability of organic luminophores, recent studies proposed the encapsulation of luminophores in inorganic or polymeric shells. A possible way is to produce silica-based shells with a sol-gel process, using a hydrophilic and a hydrophobic silica precursor. The silica shells effectively prevent luminophore aggregation and quenching, increasing efficiency, and increase photostability by shielding luminophores from UV light [48].

Quantum dots

In recent works, quantum dots have been utilized as luminophores in LSCs. Quantum dots are crystalline particles with dimensions in the order of a few nanometers; given that their size is comparable to the De Broglie wavelength of electrons, it typically results in quantum confinement effects, where excited electrons are confined in the crystalline structure. The confinement gives rise to particular electronic and optical properties: the most important one for LSC applications is that the absorption and emission wavelength of the dots strictly depends on their radius. Indeed, the smaller the dot the stronger the quantum confinement and the higher the bandgap. Exploiting this property, the emission, the absorption, and the Stokes shift of the quantum dot luminophores can be finely tuned in order to optimize the efficiency of the LSC and the spectral matching with the solar cells [23], [42].

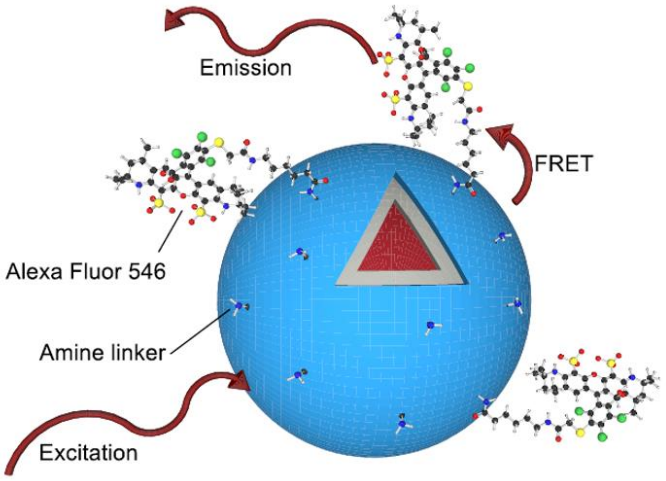

Figure 1.21 – CdSe quantum dot with a ZnS shell, a polymeric coating, and dye molecules attached via amine linkers [23].

Quantum dots have been utilized in LSCs as donor molecules in a FRET system; their emission wavelength can be finely tuned so that it matches with the absorption peak of the acceptor luminophore, enhancing the efficiency of the system. The dots can also increase the photostability of the luminophores: since the most damaging wavelengths for fluorophores are in the UV, the quantum dots can be tuned in order to absorb UV light, shielding the other molecules. Moreover, the Stokes shift of the quantum dots can be optimized in order to reduce reabsorption effects [49].

Despite all these advantages, the usage of quantum dots in LSC applications is still limited, mostly due to their poor stability and resistance to oxidation outside the polymeric matrix, owing to the high scattering losses produced along the waveguide, and because the actual emission wavelength of a dot also depends on the characteristics of the matrix, often leading to unpredictable experimental results. Moreover, the presence of toxic elements such as lead or cadmium is a cause of environmental and health concerns [42].

Rare-earth ions

In order to solve the problem related to reabsorption losses caused by a small Stokes shift, rare earth ions luminophores have been investigated for LSC applications. They usually display high photostability and durability under working conditions. Ions such as europium, yttrium, erbium, samarium, or neodymium are frequently used to dope matrices in order to induce luminescence. Their electronic configuration, represented by $[Xe]4f^n5s^25p^6$, is responsible for the particular absorption and emission spectra, characterized by numerous narrow peaks, as shown in Figure 1.22.

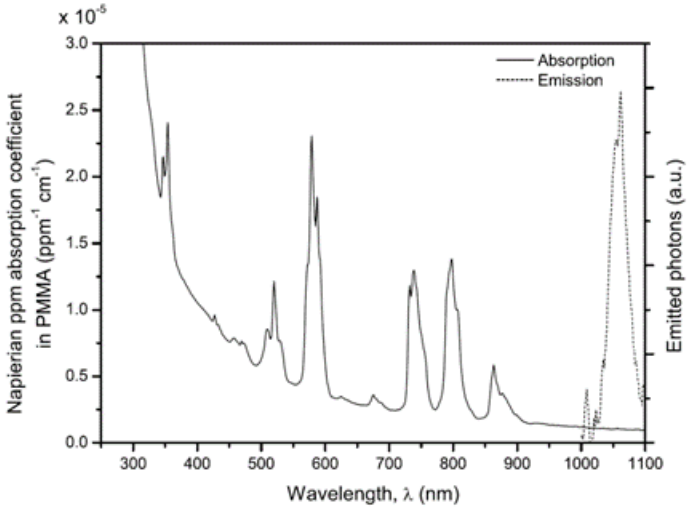

Figure 1.22 – Absorption (solid) and emission (dashed) spectrum of NdF_3 [50].

The emission of such ions is usually shifted towards low energies (i.e., in the IR part of the spectrum) providing a good material choice for solar cells that have absorption peaks in the infrared. On the contrary, narrow absorption peaks are a disadvantage because most of the incident light is not absorbed and the energy is lost [32], [50].

In order to improve their absorption characteristics, rare-earth ions are frequently complexed with organic ligands with a large absorption coefficient. The resulting complex acts like a FRET system: the organic ligand acts as a donor, absorbing energy and transferring it to the ion. The process, however, is more complex than in classic FRET: once an electron is excited from ground to state S_1, intersystem crossing takes place, transferring energy to the triplet state T_1. Just then, energy transfer occurs between T_1 of the organic ligand and the excited state of the rare earth ion, which in turn emits a photon while the electron decays to ground state. Since the energy transfer process is complex, a lot of energy is lost and the Stokes shift is particularly large; however, the presence of the organic ligand can effectively decrease the stability and durability of the rare earth ion [41], [43].

1.5 Fluorescent Polymers

The traditional approach when developing a thin-film LSC is to disperse the luminophores in the polymeric matrix, for example by dissolution in a solvent, and then spin-coat it on a glass substrate. This method, despite being convenient and cheap, has several problems: the luminophore may be poorly distributed in the solution, creating areas with a higher or lower concentration and luminescence; in addition, dyes can easily aggregate and quench, therefore reducing the luminescence quantum yield. In order to try and reduce these negative effects, another approach has been recently explored in literature; instead of dispersing luminophore molecules randomly in solution, polymers with dyes directly incorporated in the polymeric chain have been synthesized [3].

1.5.1 Polymerization Methods

As shown in Figure 1.23, several types of copolymers can be synthesized; they can be divided into two main categories: linear and branched copolymers. A linear copolymer is obtained by alternating two or more monomers on the same polymeric chain, and the type of copolymer depends on the way monomers alternate on the chain [51], [52]:

- A statistical or random copolymer is obtained without any control on the disposition of the monomers in the chain. It is the most straightforward reaction to perform and the easiest copolymer to obtain, but there is low control on those properties determined by the regularity and disposition of repeating units.
- A gradient copolymer is one where the chain displays a gradual change in composition, shifting from mostly monomer A to mostly monomer B. One possible way to obtain a gradient polymer is to slowly add monomer B to a reaction vessel where monomer A is polymerizing.
- An alternating copolymer is one where the monomer units are repeating one after the other with extreme regularity. This class of polymers is quite hard to synthesize and it can only be obtained with certain types of monomers.
- A block copolymer is a macromolecule made by two or more distinct blocks of homopolymers one after the other in the same polymeric chain. It can be obtained with particular reactions such as RAFT (Reversible Addition-Fragmentation chain-Transfer).
- A graft copolymer is a homopolymeric chain with branches of a different polymer (or oligomer, depending on the length) throughout the molecule.

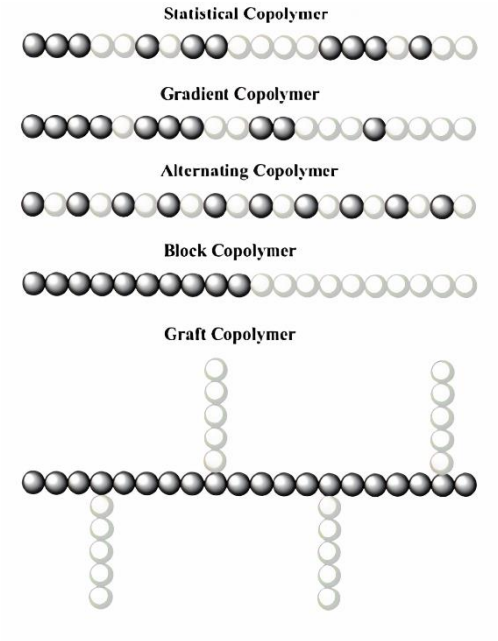

Figure 1.23 – Various types of copolymers that can be synthesized [53].

What follows is a short review of some of the most common polymerization reactions and examples of fluorescent polymers from literature.

Random Polymerization

Random polymerization is a type of reaction in which monomers are mixed to form a statistical copolymer with no control over the disposition of the chain. One of the most common processes is free radical polymerization: monomers are mixed with a solvent and an initiator molecule (e.g., azobisisobutyronitrile - AIBN) which provides the radicals necessary to promote chain growth [54].

Some examples of fluorescent polymers have been recently studied in the literature. One approach is that of synthesizing luminophores with a reactive functionality (acrylate, methacrylate, carboxylic, hydroxylic, etc...), in order to use them as monomers in a reaction and incorporate them in the polymeric chain. For instance, a reaction between tert-butyl acrylate and two different perylene methacrylate monomers has been proposed by N. J. L. K. Davis *et al.* Copolymers with different ratios of monomers have been synthesized, obtaining a polyacrylate with pendant perylene molecules and tert-butyl acrylate acting as a spacer between them, as shown in Figure 1.24. The advantage of such a polymer for LSCs is that luminophore quenching is greatly reduced, since the movement of molecules is hindered and consequently aggregation of molecules is prevented. Furthermore, FRET is established between the two luminophores, increasing the photonic efficiency of the polymer; FRET efficiency is also enhanced due to decreased and controlled average distance between luminophore molecules. The limitations of this work are represented by the narrow stokes shifts of the luminophores, which can give rise to reabsorption losses phenomena, and the small

spectral range of the device, since the absorption peak of the sensitizer is around 525 nm while the one associated with the emitter is around 560 nm, as highlighted in Figure 1.24. Furthermore, no efficiency analyses are performed on LSC devices produced with these polymers [3].

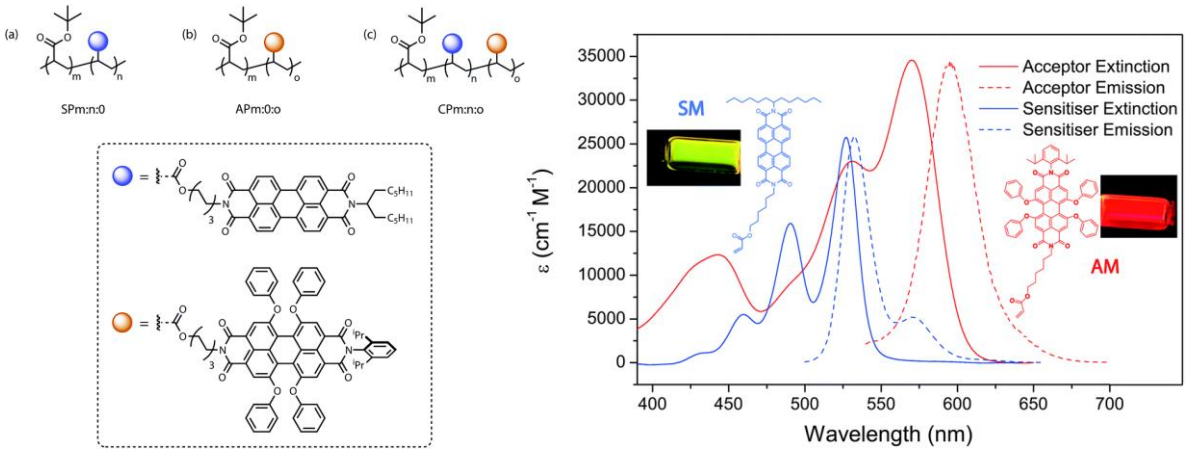

Figure 1.24 – Structure of the synthesized polymers: copolymer with tert-butyl acrylate and the sensitizer molecule (a), copolymer with tert-butyl acrylate and the acceptor molecule (b), terpolymer with all three monomers (c) [3].

In another paper, two other perylene methacrylate molecules act as monomers in a terpolymerization reaction with tert-butyl acrylate, and the resulting molecule is mixed with PMMA to form a polymer blend; this way, tert-butyl acrylate acts as an intramolecular spacer and PMMA acts as an intermolecular spacer. The results of this paper are similar to the previous one, but it highlights the importance of choosing the right ratio between monomers to obtain an optimal FRET efficiency (as shown in Figure 1.25): if spacers are in a too low concentration, luminophores are too closely packed and quenching phenomena such as excimer formation or H-aggregation can occur; on the other hand, if spacers are in a too high concentration, the FRET phenomenon has low efficiency and self-absorption can take place [55].

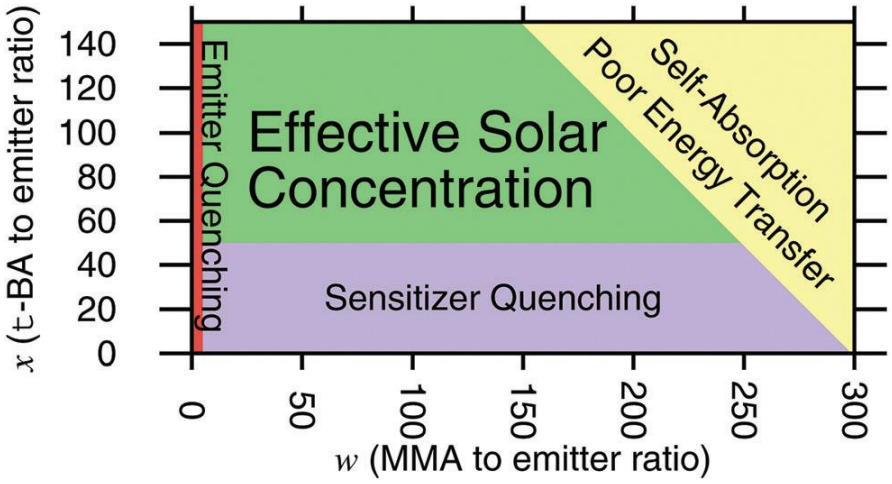

Figure 1.25 – Effect of molar ratios of spacers on photonic efficiency of the polymer blend [55].

An alternative approach to the synthesis of fluorescent random copolymers is to employ a luminophore with two hydroxylic (-OH) terminations, together with polyethylene glycol (PEG) and an isocyanate such as hexamethylene diisocyanate (HDI). In this type of polyaddition reaction, catalyzed by dibutyltin dilaurate (DBTDL), -OH groups react with -NCO groups to form a polyurethane; since both PEG and the perylene have -OH terminations, they can react with the HDI and effectively create a perylene polyurethane with PEG acting as a spacer between luminophore molecules in the chain, as shown in Figure 1.26. Advantages of this polymer are a high quantum yield of fluorescence, low fluorescence quenching, good solubility in water, and low toxicity. Similarly to the previous approach, multiple dyes with two -OH terminations could be employed to create a FRET system [56].

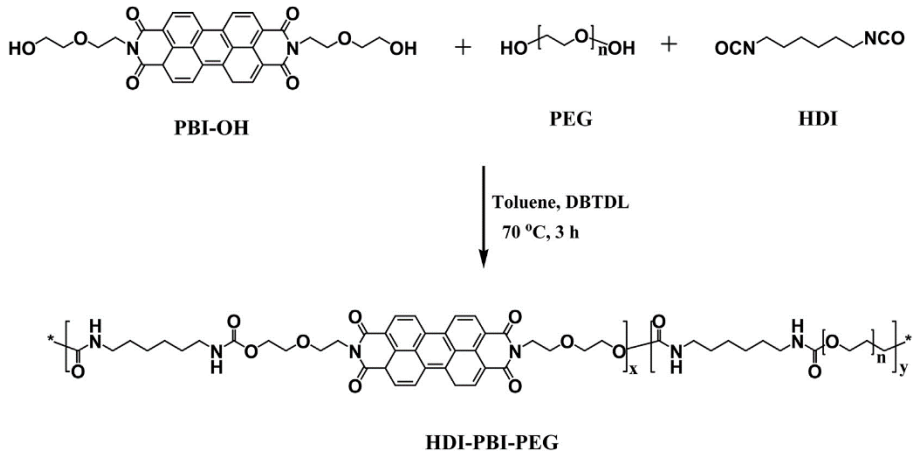

Figure 1.26 – Reaction scheme for HDI-perylene-PEG polyurethane [56].

RAFT Polymerization

Reversible addition-fragmentation chain-transfer is a type of polymerization that employs a particular set of molecules, called RAFT agents, that provide the site of insertion for monomers. The most common general structure for a RAFT agent is a thiocarbonylthio, as shown in Figure 1.27. The main objective of RAFT polymerization is to control the molecular weight and the disposition of monomers in the chain in order to lower the polydispersity index, and to increase the incorporation of monomers in the polymeric chain. It can be employed to synthesize polymers with various and particular structures, such as block copolymers, graft or star-like polymers, or cross-linked networks [57], [58].

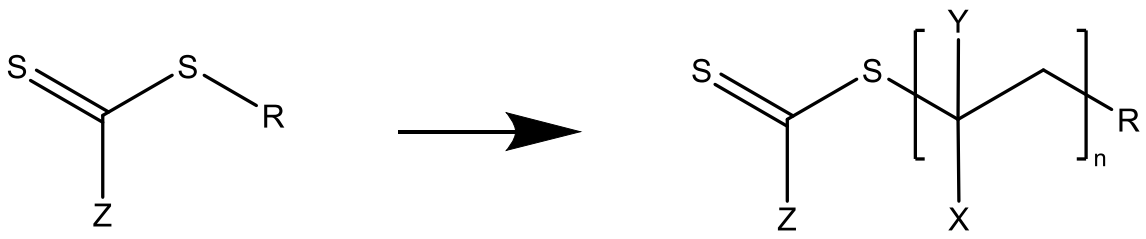

Figure 1.27 – Structure of a thiocarbonylthio molecule and RAFT polymerization mechanism [58].

Even though their main application is not luminescent solar concentrators, examples of fluorescent polymers are present in literature, such as polymeric fluorescent chemosensors that detect fluoride ions [59] and fluorescent AIE polymeric nanoparticles [60]; the main advantage given by RAFT is that the molecular weight is well-controlled and the polydispersity index is quite narrow, around 1.2-1.3 [61].

The main problem of using RAFT polymerization for fluorescent polymers is that luminophores in the chain easily undergo fluorescence quenching. This happens for two main reasons: first of all, the distance between molecules in the chain in a block copolymer is greatly decreased, promoting aggregation; furthermore, some chain-transfer agents used in RAFT act as good quenchers due to the formation of excimers. In conclusion, fluorescent polymers obtained via RAFT represent an interesting route for LSCs due to their controlled structure and properties, but further research needs to be done on quenching [62].

Chapter 2
Materials and Methods

This chapter will be divided into five parts.

The first one will describe materials and precursors utilized to synthesize new molecules and polymers.

The second will describe the synthesis processes utilized to synthesize new molecules and polymers.

The third will describe the machinery and instruments utilized.

The fourth will describe the methods utilized to fabricate LSC devices.

The fifth and final one will describe the characterization techniques and equipment utilized to characterize the materials and the LSC devices.

2.1 Materials

In order to synthesize new molecules and polymers, many precursor materials have been utilized; they will be described in the following pages.

2.1.1 Precursors and Reagents

The first molecules that were synthesized are coumarin methacrylate and perylene bisimide methacrylate; their precursors are listed below.

4-Methylumbelliferone

4-methylumbelliferone (also known as hymecromone), shown in Figure 2.1, is a derivative of coumarin with a methyl group on the 4th carbon and a hydroxyl group on the 7th. It is a solid white powder with a molecular weight of 176.17 g/mol. It is used in medicine for drug delivery given its good biocompatibility. Likewise in many coumarin derivatives, its benzene rings provide good fluorescence properties, with an absorption peak at around 320 nm and an emission peak at around 400 nm. Given its properties and its structure, it has been chosen in this work as a precursor for a coumarin-based

monomer, obtained by adding a methacrylate termination to the carbon atom in the 7th position, which can be then copolymerized with other monomers.

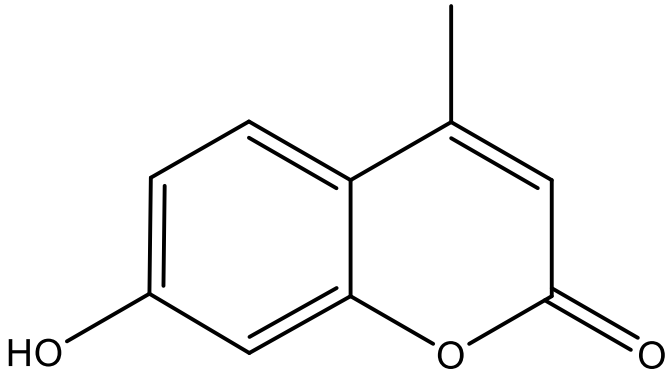

Figure 2.1 – Structure of 4-methylumbelliferone.

2-Bromoethanol

2-bromoethanol is an alcohol with a bromine atom attached, as shown in Figure 2.2, and it has a molecular mass of 124.96 g/mol. In this work, it has also been utilized as a chain extender reagent for 4-methylumbelliferone.

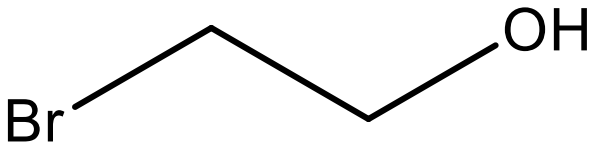

Figure 2.2 – Structure of 2-bromoethanol.

Perylene Bisimides

Perylene is a polycyclic aromatic carbon and it is the basic building block for many dyes and luminophores. In its basic structure, shown in Figure 2.3, it appears as a brown powdery solid with a molecular mass of 252.32 g/mol. It presents a strong fluorescence, with an absorption peak at 410 nm and a fluorescence peak at 435 nm.

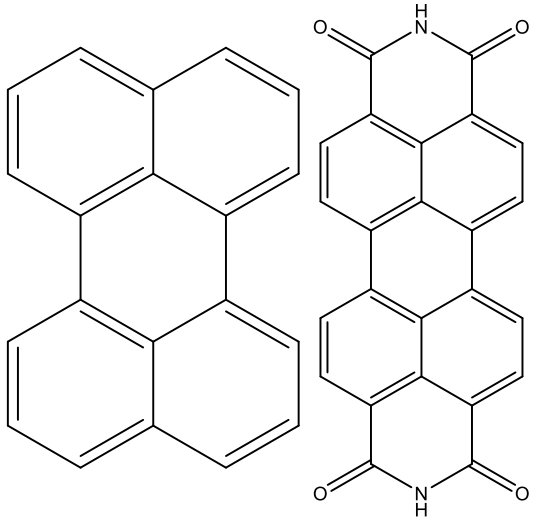

Figure 2.3 – Structure of perylene (left) and perylene bisimide (right).

Another class of dyes that have been more recently explored is perylene bisimides, also shown in Figure 2.3; compared to perylene, they display a redshifted absorption and emission peak.

Among perylene bisimides, a monofunctional hydroxyl molecule was custom synthesized by the research group of Prof. Claudia Dragonetti in the Department of Chemistry of the University of Milano. It was used in this work as a precursor for a luminescent monomer, and its structure is shown in Figure 2.4.

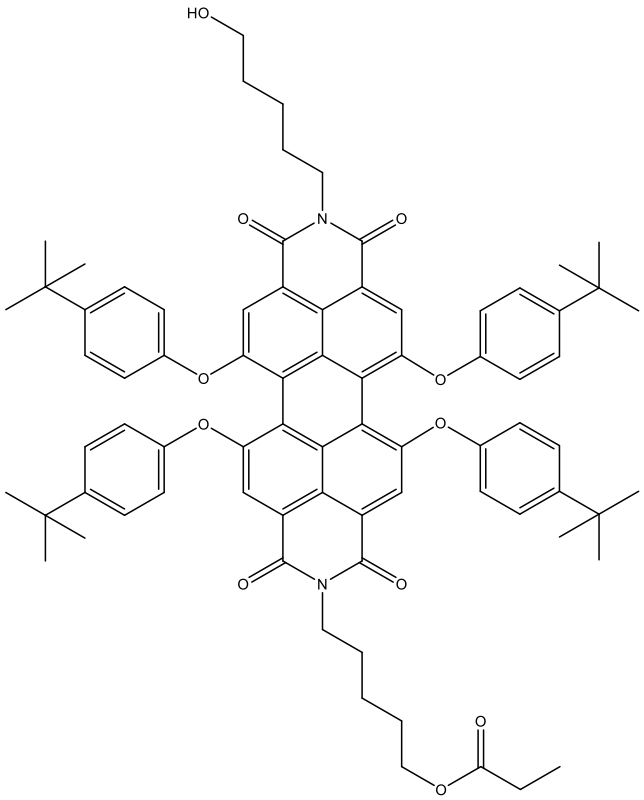

Figure 2.4 – Structure of the precursor for a perylene bisimide methacrylate monomer.

The molecule is a brown-violet solid powder with a molecular mass of 1210.59 g/mol. It has an absorption peak around 575 nm and an emission peak at 620 nm.

2-Isocyanatoethyl Methacrylate (IEM)

2-isocyanatoethyl methacrylate is an isocyanate with a methacrylate termination, as shown in Figure 2.5. It is an extremely toxic clear liquid with a molecular mass of 155.15 g/mol. In this work, IEM was utilized to confer methacrylate functionality to the 4-methylumbelliferone and the perylene bisimide derivative.

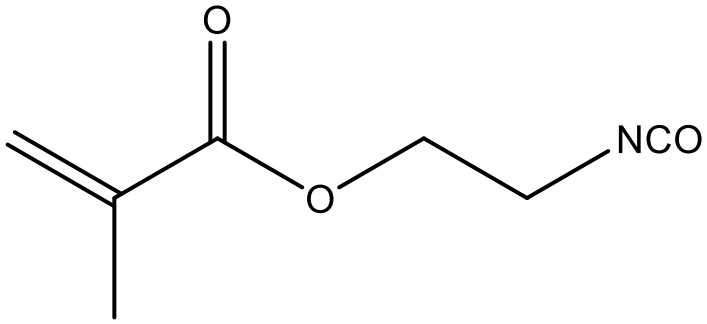

Figure 2.5 – Structure of 2-isocyanatoethyl methacrylate.

Methyl Methacrylate (MMA)

Methyl methacrylate is an organic transparent liquid with a molecular mass of 100.05 g/mol. It is the precursor for the synthesis of poly (methyl methacrylate), also known as plexiglass. In this work, it has been used as a building block for the newly synthesized copolymers. Its structure is shown in Figure 2.6.

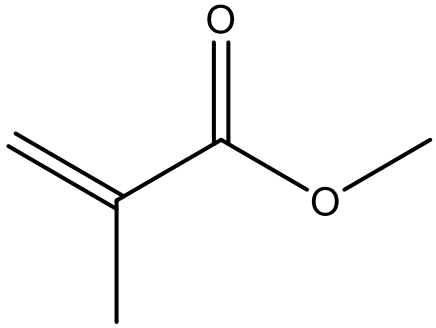

Figure 2.6 – Structure of methyl methacrylate (MMA).

Sodium Hydroxide

Sodium hydroxide, also known as caustic soda, is a white solid inorganic compound with the chemical formula NaOH and a molar mass of 39.99 g/mol, often found as solid pellets. In this work, it is used in solution with water to remove the inhibitors from monomers such as MMA, which would otherwise slow down the chemical reaction.

Sodium Sulphate

Sodium sulphate is a white solid inorganic compound, with the chemical formula Na_2SO_4 and a molar mass of 142.04 g/mol. In this work, it is used as a drying agent after the removal of inhibitors from MMA due to its strong hygroscopic properties.

2-Phenyl-2-Propyl Benzodithioate

2-phenyl-2-propyl benzodithioate, the structure of which is shown in Figure 2.7, is an organic compound used to perform RAFT polymerization. It is a bright purple coloured powder with a molar mass of 272.07 g/mol. In this work, it is used as a RAFT agent in order to promote the synthesis of a more regular block copolymer.

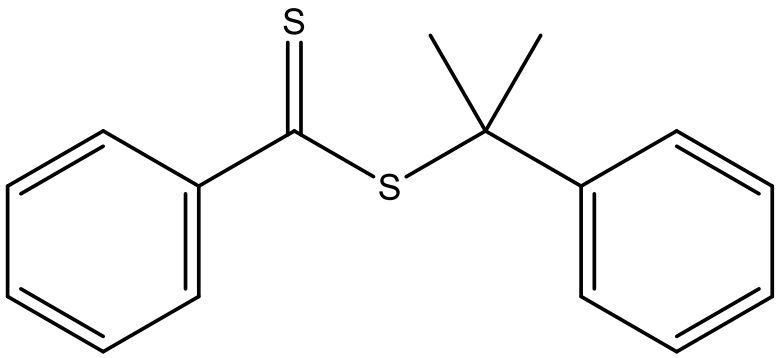

Figure 2.7 – Structure of 2-phenyl-2-propyl benzodithioate.

2.1.2 Solvents

In order to carry out chemical reactions, many solvents have been utilized. Most of them are listed below.

Acetone

Acetone is an organic compound with the chemical formula$(CH_3)_2CO$. It is the simplest ketone and it is a transparent, highly volatile and highly flammable liquid, completely miscible with water. Its molar mass is 58.08 g/mol, its density is 0.78 g/mL and its boiling point is 56 °C. It is a very common solvent, used in many fields and applications, and it is generally considered safe for humans. In this work, it has been utilized to clean LSC glass substrates and solubility tests.

Chloroform

Chloroform, also known as trichloromethane, is an organic compound with the chemical formula $CHCl_3$. It is a transparent liquid, slightly miscible with water, with a molar mass of 119.37 g/mol, a density of 1.49 g/mL and a boiling point of 61 °C. It is a very common solvent, despite its modest toxicity: other than being a powerful anaesthetic, it has been found to be an irritating and carcinogenic substance. In this

work, it has been utilized for ultrasonication, solubility tests and as a solvent for polymers. Furthermore, deuterated chloroform, with the chemical formula $CDCl_3$, has been used as a solvent for H-NMR analyses because of the absence of hydrogen atoms.

Isopropyl Alcohol

Isopropyl alcohol, also known as isopropanol, is an organic compound with the chemical formula $CH_3CHOHCH_3$. It is a transparent liquid, completely miscible with water, with a molar mass of 60.10 g/mol, a density of 0.79 g/mL and a boiling point of 83 °C. It is a fairly common chemical, mostly used as an antiseptic and disinfectant, since it evaporates very quickly and leaves no oil traces, unlike ethanol. In this work, it has been utilized to clean LSC glass substrates and solubility tests.

Tetrahydrofuran (THF)

Tetrahydrofuran is an organic compound with the chemical formula $(CH_2)_4O$. It is a heterocyclic compound, with an oxygen atom in the 1st position. It is a transparent liquid, completely miscible with water, with a molar mass of 72.11 g/mol, a density of 0.89 g/mL and a boiling point of 66 °C. It is a fairly common solvent in industry, despite being carcinogenic and irritant. In this work, it has been used as a solvent for the dissolution of monomers during various polymerization reactions, despite being sometimes substituted by dioxane or dimethylformamide due to their higher boiling point, more suitable for high-temperature reactions. THF is usually packaged with butylated hydroxytoluene (BHT) as a stabilizer to avoid the formation of shock-sensitive peroxide compounds; inhibitor-free THF has been used to perform gel permeation chromatography (GPC) analyses.

Dioxane

Dioxane is an organic compound with the chemical formula $C_4H_8O_2$. It is a heterocyclic compound, and the most common form is 1,4-dioxane, with oxygen atoms in the 1st and 4th positions. It is a transparent liquid, completely miscible with water, with a molar mass of 88.11 g/mol, a density of 1.03 g/mL and a boiling point of 101 °C. It is a common solvent, often used as a substituent for THF to its lower toxicity and higher boiling point, despite being a potential carcinogenic. In this work, it has been used as a solvent for the dissolution of monomers during various polymerization reactions.

Dimethylformamide (DMF)

Dimethylformamide is an organic compound with the chemical formula $(CH_3)_2NC(O)H$. It is a derivative of formamide, with two methyl groups bound to the nitrogen atom instead of two hydrogen atoms. It is a transparent liquid, completely miscible with water, with a molar mass of 73.10 g/mol, a density of 0.95 g/mL and a boiling point of 153 °C. It is a common solvent, despite its toxicity. In this work, it has been used as a

solvent for the dissolution of monomers and dyes during various reactions, although its high boiling point resulted in processability problems.

Toluene

Toluene is an organic compound with the chemical formula C_7H_8. It can be described as a benzene molecule with a methyl substituent in the 1st position. It is a transparent liquid, insoluble in water, with a molar mass of 92.14 g/mol, a density of 0.87 g/mL and a boiling point of 111 °C. It is a common solvent, also used as an additive in fuels, with fairly low toxicity compared to other solvents. In this work, it has been used as a solvent for the dissolution of monomers in some polymerization reactions and for solubility tests.

Dimetyhl Sulfonate (DMSO)

Dimethyl sulfonate is an organic compound with the chemical formula $(CH_3)_2SO$. Its structure is the one of acetone with a sulfur atom substituting the central carbon. It is a transparent liquid, miscible in water and a wide range of organic solvents, with a molar mass of 78.13 g/mol, a density of 1.10 g/mL and a boiling point of 189 °C. It is commonly used as a solvent due to its stability and its ability to dissolve many compounds. In this work, the deuterated form of DMSO has been used as a solvent for H-NMR analyses.

Hexane

Hexane is an organic compound with the chemical formula C_6H_{14}. It is a transparent liquid, immiscible with water, with a molar mass of 86.18 g/mol, a density of 0.66 g/mL and a boiling point of 69 °C. It is commonly used in the fuel industry and for the production of glues. In this work, it has been used to precipitate polymers after polymerization reactions, due to their insolubility in hexane, and as a purifying agent for the perylene-based monomer.

Cyclohexane

Cyclohexane is an organic cyclic compound with the chemical formula C_6H_{12}. It is a transparent liquid, immiscible with water, with a molar mass of 84.16 g/mol, a density of 0.77 g/mL and a boiling point of 81 °C. It is commonly used as a precursor to synthesize other chemicals. In this work, similarly to hexane, it has been used to precipitate polymers after polymerization reactions, due to their insolubility in cyclohexane.

Ethanol

Ethanol is an organic compound with the chemical formula C_2H_5OH. It is a transparent liquid, completely miscible with water, with a molar mass of 46.07 g/mol, a density of

0.79 g/mL and a boiling point of 78 °C. It is commonly used as a disinfectant and antiseptic, as an additive for fuels and recreationally. In this work, it has been used during chemical reactions involving isocyanates to quench their -NCO groups, in order to avoid residual toxic molecules in the polymer.

Ethyl Acetate

Ethyl acetate is an organic compound with the chemical formula $CH_3COOC_2H_5$. It is a transparent liquid, not miscible in water, with a molar mass of 88.11 g/mol, a density of 0.90 g/mL and a boiling point of 77 °C. It is commonly used as a solvent and diluent in many, including cosmetics and food. In this work, it has been used as a solvent for the recrystallization of hydrolyzed coumarin.

2.1.3 Catalysts and initiators

In order to carry out polymerizations, initiator and catalyst molecules have to be utilized to increase the rate of the reactions. They will be described below.

Potassium Carbonate

Potassium carbonate is a white inorganic salt, and its structure is shown in Figure 2.8. It is water-soluble and highly hygroscopic with a molecular mass of 138.21 g/mol. In this work, it has been utilized a catalyst in the chain extension step for 4-methylumbelliferone.

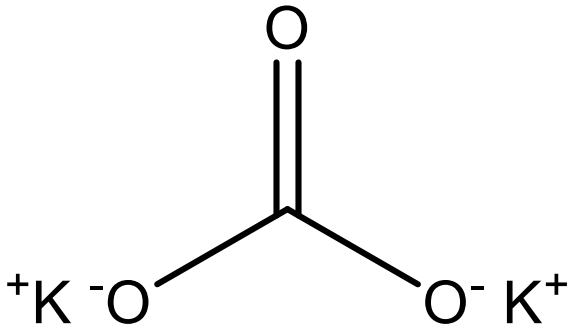

Figure 2.8 – Structure of potassium carbonate.

Azobisisobutyronitrile (AIBN)

Azobisisobutyronitrile is an organic compound, the structure of which is shown in Figure 2.9. It is a white powder with a molar mass of 164.21 g/mol, insoluble in water. It is usually dissolved in an organic solvent and then mixed with monomers. As shown in Figure 2.9, at around 70 °C the molecule breaks down and forms free radicals, which are highly reactive and can kickstart the free-radical polymerizations.

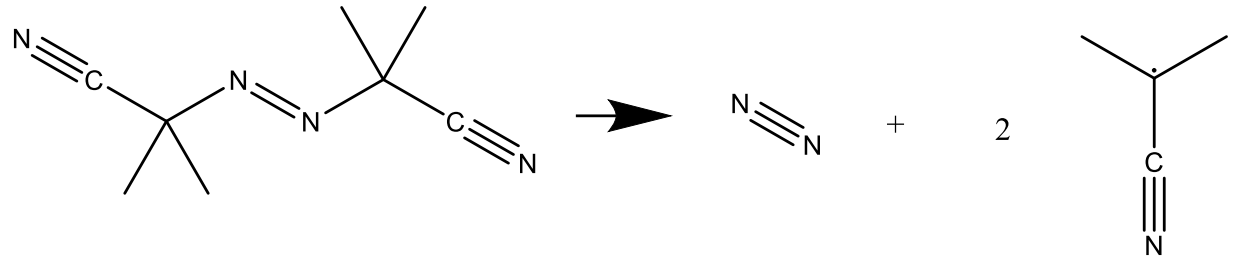

Figure 2.9 – Structure of azobisisobutyronitrile (left) and its characteristic decomposition reaction.

Dibutyltin Dilaurate (DBDTL)

Dibutyltin dilaurate is an organotin compound, the structure of which is shown in Figure 2.10. At room temperature, it is a transparent liquid with a molar mass of 631.56 g/mol. It is usually utilized as a catalyst in polyurethane production in reactions involving isocyanates. In this work, it has been utilized in the functionalization reaction of the coumarin and perylene bisimide methacrylate monomers in order to attach the isocyanate methacrylate to the bulk of the molecule.

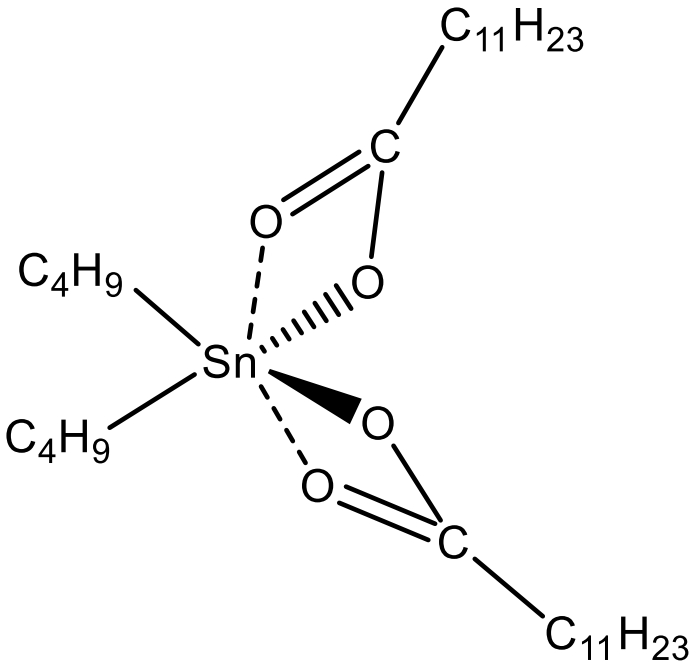

Figure 2.10 – Structure of dibutyltin dilaurate.

2.2 Syntheses

In this work, many syntheses have been carried out in order to create new molecules and polymers. The procedures are listed and described here.

2.2.1 AIBN Purification

When stored, AIBN can decompose spontaneously; consequently, decomposition products and impurities can be present in the batch. In order to remove them and obtain a purer product, recrystallization is carried out.

To do so, 3.5 g of methanol per gram of AIBN to be purified are heated up to 60 °C, and once the temperature has been reached the initiator is poured in and left in stirring to dissolve. When all the AIBN has dissolved, the solution turns completely clear and impurities become visible as white filaments. At this point, hot filtration is performed with a paper filter and a glass funnel, so that the impurities are collected in the filter while the methanol flows in a beaker. The filtrate is then cooled down overnight to promote the crystalization due to oversaturation, and the purified AIBN is collected on a paper filter via vacuum filtration.

2.2.2 MMA Purification

When packaged, inhibitor compounds such as mequinol (MeHQ) are usually added to methyl methacrylate to prevent polymerization. In order to carry out the reactions, the inhibitors need to be removed.

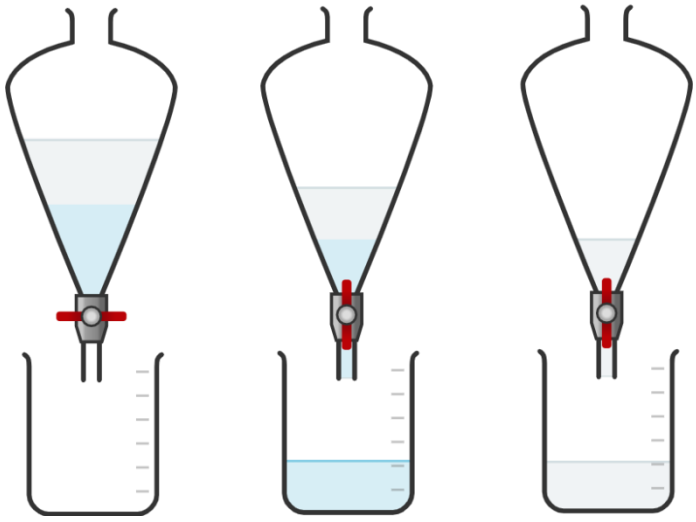

Figure 2.11 – Scheme for the purification procedure of methyl methacrylate.

To do so, a 10% weight solution of water and sodium hydroxide is produced and mixed with the same volume of MMA. As shown in Figure 2.11, the mixture is then poured into a separatory funnel: the funnel is then shaken vigorously three or four times, allowing

the two liquids to mix thoroughly, in order to let the NaOH solution dissolve the MeHQ. Since the liquids are immiscible, they quickly separate and the MMA, being less dense, forms a layer above the water. The two liquids are then poured into two different beakers using the tap in the separatory funnel, and their pH is tested with a litmus paper, in order to make sure that no NaOH remained in the methyl methacrylate. Finally, 100 mg of sodium sulfate per mL of MMA are mixed into the monomer and left in stirring for half an hour, in order to absorb any residual water.

2.2.3 Coumarin Methacrylate

In order to synthesise methacrylate copolymers with luminophores, fluorophores need to be functionalized with a methacrylate termination. The first monomer that was synthesized was coumarin methacrylate.

To start, 4 grams of 4-methylumbelliferone are dissolved in 25 mL of DMF in a round-bottom flask with a stirring rod. When the powder is completely dissolved, 4.3 g of bromoethanol and 6.3 g of potassium carbonate are added to the flask. The flask is connected to a condenser, which has a tap connected to a nitrogen-filled balloon attached to the top opening. A vacuum pump is attached to a tap positioned on one of the necks of the flask, while the other necks are closed by plugs. Three cycles of vacuum evacuation and nitrogen backfilling are then performed. The flask is then heated to 88 °C and left in a nitrogen atmosphere for 18 hours.

Afterwards, the flask is removed from the condenser, its content precipitated in cold deionized water and then vacuum filtered with a Buckner funnel. Once dried, the now-obtained compound, called 7-(2-hydroxyethoxy)-4-methylcoumarin (HEOMC) and shown in Figure 2.12, is dissolved in ethyl acetate and hot filtered to remove any impurity. After cooling, the filtrate is vacuum filtered and the recrystallized HEOMC is collected and dried overnight.

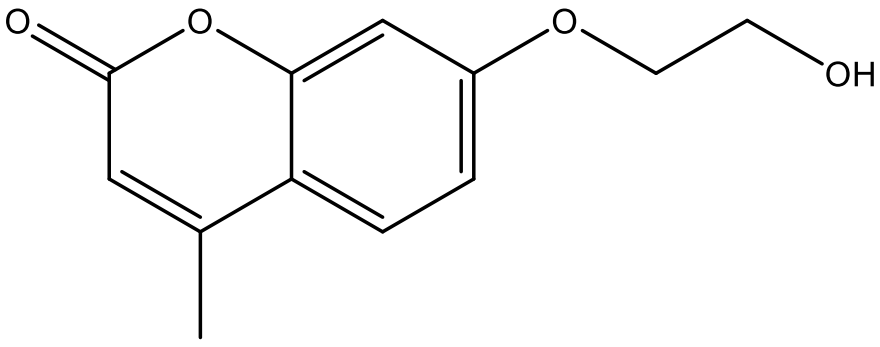

Figure 2.12 – Structure of 7-(2-hydroxyethoxy)-4-methylcoumarin.

Now, the methacrylate functionality needs to be attached to the molecule. In order to do so, 3 grams of HEOMC are dissolved in 12 mL of DMF and the flask is heated to 50 °C. Similarly to the previous step, three cycles of vacuum evacuation and nitrogen backfilling are performed to remove contaminants from the atmosphere. Afterwards,

1.92 mL of IEM (in a 1:1 molar ratio with HEOMC) and 0.048 mL of DBTDL (1% weight with respect to the reagents) are dissolved in 1 mL of DMF and syringed in the flask. The temperature is raised to 70 °C for 5 hours.

The content of the flask is then poured in cold deionized water (around 70 mL, as suggested by the rule of thumb of using a volume 5 times larger than the solution to precipitate); the content is then vacuum filtered with a Buckner funnel and dried in a vacuum oven.

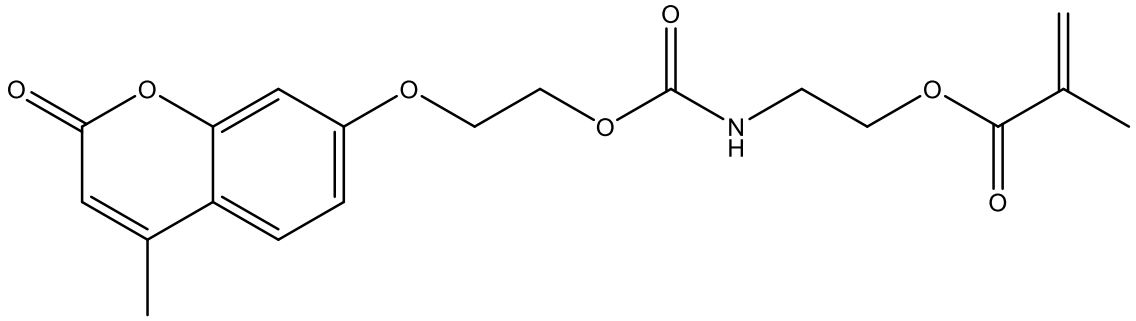

Figure 2.13 – Structure of coumarin methacrylate.

The thus-obtained compound, called coumarin methacrylate (CMA) and shown in Figure 2.13, is then utilized as a monomer for polymerization reactions.

2.2.4 Perylene Methacrylate

Similarly to coumarin, the perylene bisimide-based compound was also functionalized with IEM in order to obtain perylene methacrylate.

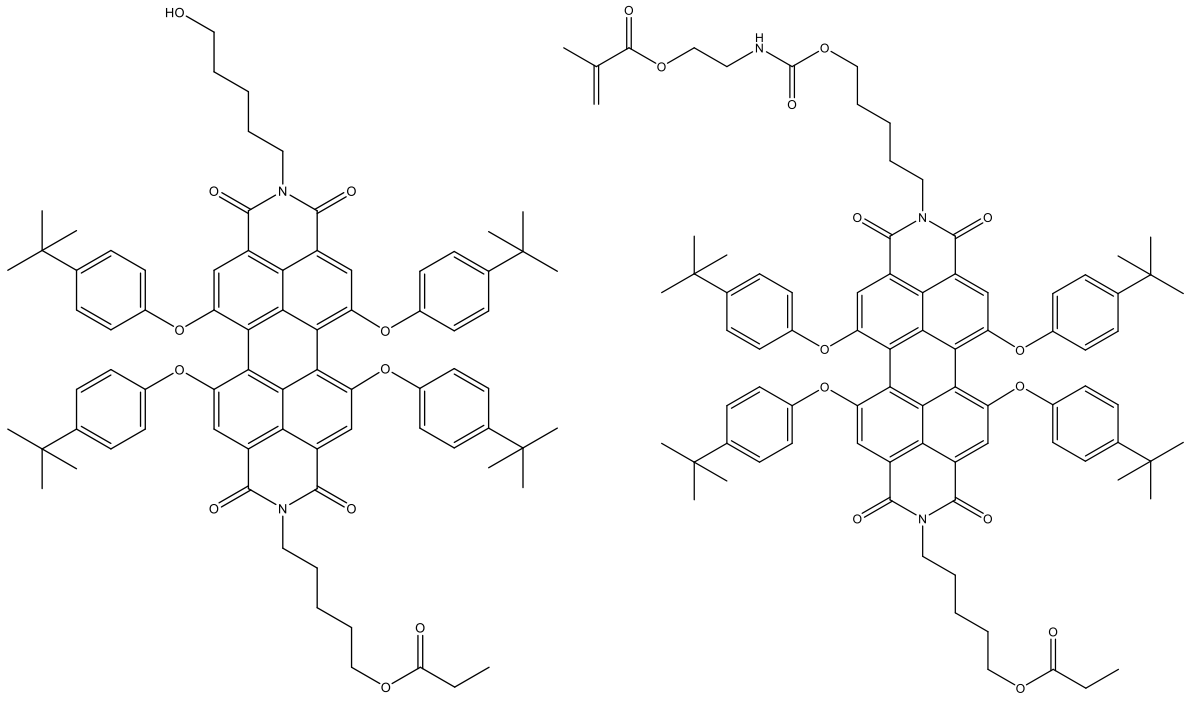

Figure 2.14 – Structure of the custom perylene bisimide (left) and its methacrylate derivate (right).

To start, 50 mg of a custom perylene molecule, shown in Figure 2.14, are dissolved in 10 mL of THF and three cycles of vacuum evacuation and nitrogen backfilling are performed. Afterwards, 1.67 µL of IEM (in a 1:1 molar ratio with PBI) and 1.06 µL of DBTDL (1% weight with respect to the reagents) are dissolved in 1 mL of THF and syringed in the flask. The temperature is then raised to 70 °C for 5 hours.

After the reaction is completed, the THF is evaporated from the flask with a rotavapor and the remaining product is dried in a vacuum oven overnight. To remove any possible unreacted IEM, the product is then washed with hexane (which is a good solvent for IEM and a bad solvent for perylene) and the dispersion is centrifugated to allow the perylene methacrylate to deposit on the bottom of the test tube.

The final product, called perylene methacrylate (PMA) and shown in Figure 2.14, is then allowed to completely dry in a vacuum oven.

2.2.5 Copolymers via Random Polymerization

Many copolymers have been synthesized with a random copolymerization reaction. The procedure is as follows: a certain total amount of monomers (e.g., methyl methacrylate, coumarin methacrylate and perylene methacrylate) is added to a round-bottom flask. The relative concentration of each monomer is varied depending on the polymer composition that is desirable to obtain.

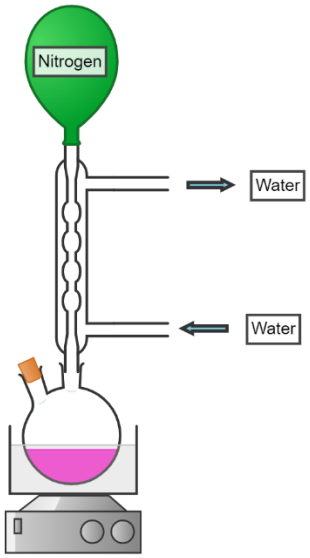

Figure 2.15 – Diagram of the setup for random free-radical polymerization reactions.

In general, MMA is mixed with both CMA in a concentration between the 0 and 15% mol/mol and PMA in concentrations in the 0 – 0.1% mol/mol range. A solvent is added into the flask, usually dioxane, THF or DMF, and monomers are left in stirring to dissolve if needed.

Afterwards, the flask is connected to a condenser and a needle attached to a nitrogen line is inserted in the round-bottom flask for around 20 minutes in order to remove

oxygen from the solution, while the flask is immersed in an ice bath to avoid excessive volatilization of the solvent. Once the needle is removed, the system is closed with nitrogen-filled balloons and the flask is heated to 83 °C. Once the temperature is reached, 0.1% molar of AIBN (with respect to the total number of moles of the monomers) is added to the flask, and the reaction is left running for 6 hours. The setup is shown in Figure 2.15. The temperature of 83 °C has been chosen because it is the temperature at which AIBN has a half-life of 1 hour. The general reaction scheme is shown in Figure 2.16.

After 6 hours, the flask is removed from the heating setup and its content is poured in cold hexane or cyclohexane. The polymer, insoluble in those solvents, precipitates and forms a solid tangle, which is then removed and left to dry in a vacuum oven overnight.

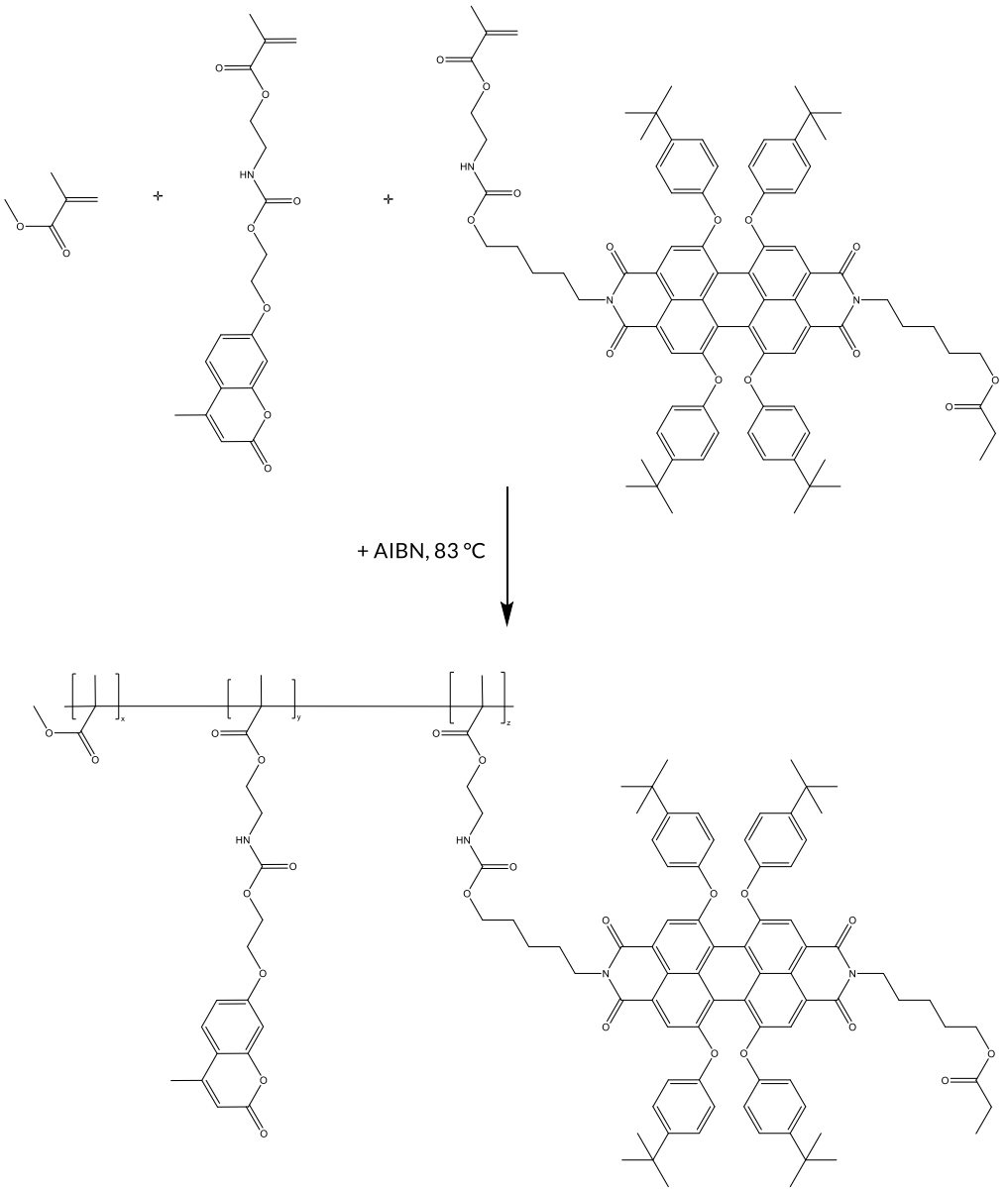

Figure 2.16 – Scheme of a random free-radical copolymerization reaction.

Listed inTable 2.1 are all the random polymers that have been synthesized in this work. The name of the polymer is given by the name of luminescent monomer present in solution followed by its molar feed concentration before polymerization. For example, CMA10 PMA0.025 MMA89.975 is the polymer resulting from the polymerization of a solution containing 89.975% molar of MMA, and 10% molar of CMA and 0.025% molar of PMA. The yield of the reaction is calculated by dividing the weight of the polymer with the weight of the monomers in the feed.

Table 2.1 – List of synthesized random fluorescent polymers.

Batch Name	**MMA**	**CMA**	**PMA**	**AIBN [mg]**	**Yield**
CMA5 MMA95	1 mL 95%$_{mol/mol}$	185 mg 5%$_{mol/mol}$	-	1.62	34%
CMA10 MMA90	1 mL 90%$_{mol/mol}$	391 mg 10%$_{mol/mol}$	-	1.71	44%
CMA15 MMA85	1 mL 85%$_{mol/mol}$	621 mg 15%$_{mol/mol}$	-	1.81	36%
PMA0.025 MMA99.975	1 mL 99.975%$_{mol/mol}$	-	3.2 mg 0.025%$_{mol/mol}$	1.54	48%
PMA0.050 MMA99.950	1 mL 99.950%$_{mol/mol}$	-	6.4 mg 0.050%$_{mol/mol}$	1.54	45%
PMA0.100 MMA99.900	0.5 mL 99.900%$_{mol/mol}$	-	6.4 mg 0.100%$_{mol/mol}$	0.77	46%
CMA10/PMA0.025 MMA89.975	1 mL 89.975%$_{mol/mol}$	391 mg 10%$_{mol/mol}$	3.2 mg 0.025%$_{mol/mol}$	1.71	51%
CMA10/PMA0.050 MMA89.950	1 mL 89.950%$_{mol/mol}$	391 mg 10%$_{mol/mol}$	6.4 mg 0.050%$_{mol/mol}$	1.71	56%
CMA10/PMA0.100 MMA89.900	1 mL 89.900%$_{mol/mol}$	391 mg 10%$_{mol/mol}$	12.8 mg 0.100%$_{mol/mol}$	1.71	53%

2.2.6 Polymers via RAFT Polymerization

RAFT polymerization reactions have been carried out in order to synthesize polymers with controllable average molecular weight, narrower molecular weight dispersion (i.e., polydispersity - PDI), and specifically designed polymer architecture. The procedure is divided into two or more steps, and it is described below.

To start, a determined amount of MMA is poured into a round-bottom flask and mixed with DMF. Afterwards, the RAFT agent (2-phenyl-2-propyl benzodithioate, abbreviated as RA) is added to the flask and stirred until complete dissolution. Nitrogen insufflation is carried out for around 30 minutes and then the flask is heated at around 70 °C. Once the temperature is reached, AIBN previously dissolved in 1 mL of DMF is syringed in the system and the reaction is left running for 5 hours. The ratios between components in the reaction can vary, but the most utilized is a 100:4.45:1 molar ratio of MMA:RA:AIBN. At the end of the process, the flask is removed from the condenser and its content is poured into a beaker containing cold hexane. The precipitated polymer is then collected and left to dry in a vacuum oven.

After this first step, a poly(methylmethacrylate) with a low polydispersity index is obtained, where the polymeric chain is terminated with the RAFT agent. The now-obtained polymer is also called macromer and can be effectively utilized as a RAFT agent in another polymerization reaction.

The second step is then to repeat the previous polymerization process, using CMA or PMA as a monomer instead of MMA, and the previously obtained macromer instead of the RAFT agent. The resulting polymer will be a block copolymer with a low polydispersity index.

A third step can be also performed with another monomer, in order to obtain a third block in the chain. This step is performed to synthesize three-block terpolymers like CMA10 PMA0.050: the MMA macromer is first polymerized with CMA in solution, then the resulting macromer is polymerized again with PMA in solution.

A picture of the reaction setup is shown in Figure 2.17.

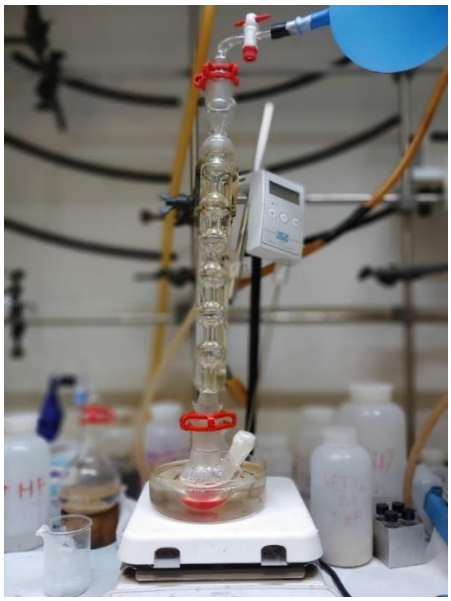

Figure 2.17 – Picture of the setup for a RAFT polymerization reaction, showing a condenser with a nitrogen balloon attached, a round-bottom flask containing the reaction solution, an oil bath and a heating plate.

Table 2.2 - List of synthesized RAFT macromers.

Batch Name	MMA	Raft Agent	AIBN
RAFT100	5 mL 100 molar ratio	569.1 mg 4.45 molar ratio	77.1 mg 1 molar ratio
RAFT205	2.5 mL 205 molar ratio	138.8 mg 4.45 molar ratio	18.8 mg 1 molar ratio
RAFT500	2.5 mL 500 molar ratio	56.9 mg 4.45 molar ratio	7.71 mg 1 molar ratio

Listed in Table 2.2 are all the RAFT macromers that have been synthesized in this work. The name of the polymer is given by the ratio of MMA to the other components of the initial solution. For example, RAFT100 is the polymer resulting from the polymerization of a solution containing MMA:RA:AIBN in a molar ratio equal to 100:4.45:1.

Listed in Table 2.3 are all the RAFT fluorescent polymers that have been synthesized in this work. The name of the polymer is given by the name of luminescent monomer present in solution followed by its molar concentration in the reaction feed. For example, CMA 10 RAFT100 is the polymer resulting from the polymerization of a solution containing 10% molar of CMA and 90% molar of the RAFT 100 MMA macromer.

Table 2.3 – List of synthesized RAFT fluorescent polymers.

Batch Name	Macromer	CMA	PMA	AIBN [mg]
CMA10 RAFT100	0.65 mg 90%$_{mol/mol}$	270.5 mg 10%$_{mol/mol}$	-	239.6
PMA0.050 RAFT100	0.65 mg 99.950%$_{mol/mol}$	-	4.4 mg 0.050%$_{mol/mol}$	239.6

2.3 Methods

In this section, methods and machinery utilized to produce and treat samples are described.

2.3.1 Centrifugation

Centrifugation is a technique used to separate components in a heterogeneous mixture. The mixture is poured into a test tube, which is placed at an angle in a centrifuge disc able to rotate onto its axis at around 3000 rpm. As a result of centrifugal force, the denser component is deposited on the bottom of the test tube, while the other components, called supernatant, float on top.

In this work, the centrifuge has been utilized after the perylene methacrylate washing with hexane: since PMA is insoluble in hexane, a heterogeneous dispersion forms and the components need to be separated. Centrifugation of the mixture, removal of the supernatant and addition of new mixture are repeated until all the PMA is deposited in the test tube.

2.3.2 Spin Coating

In order to produce thin films with uniform thickness, the spin coating technique was employed. A spin coater is a machine consisting of a rotating plate connected to a vacuum line: the substrate that needs to be coated is placed on top of the plate and locked in place with a vacuum, then a solution is pipetted on top of the substrate and the machine is turned on. The plate, together with the substrate, rotates on its axis at speeds varying from 500 to 2000 rpm for a time ranging between 30 and 300 seconds.

The solution, usually consisting of a polymer dissolved in a solvent, spreads out on the substrate due to shear forces and the solvent quickly evaporates due to the high speeds. The main parameters to control are the boiling point of the solvent, the viscosity of the solution, the rotation speed and the time of deposition; they can be linked to the film thickness with the following equation:

$$d = k\omega^{\alpha}$$

where d is the film thickness, ω is the angular speed and k and α are parameters related to the properties of the solution. The lower the boiling point of the solvent, the faster the evaporation and the harder the spreading of the coating on the substrate. Indeed, as the solvent evaporates, the viscosity of the solution increases and stronger shear forces are needed to spread the coating. The parameters need to be adjusted properly in order to avoid too thick, too thin, incomplete or irregular films: for example, a particularly viscous solution of a polymer dissolved in chloroform should be deposited at a low rotation speed, otherwise the solvent could evaporate even before coating the whole substrate.

In this work, the Laurell (WS-400BZ-6NPP/LITE) spin coater was used to coat glass slides with fluorescent polymers to test their characteristics and build LSC devices, and to coat KBr or NaCl discs for FTIR analyses.

2.4 Fabrication of LSC Devices

In this section, materials and techniques necessary to fabricate an LSC device are presented.

2.4.1 Materials

Substrate

The substrates chosen to build LSCs are soda-lime glass slabs with dimensions of 4.4x4.4x0.6 cm^3. Soda-lime glass is one of the most common and inexpensive materials among glasses, although it has a quite large absorption coefficient between 400 and 1100 nm compared to other materials, and has an average transmission coefficient of 90%.

Polymers

The polymers deposited on the substrates to produce LSCs are the fluorescent polymers synthesized with the polymerization techniques described above. All the polymers that have been produced and used to fabricate an LSC are listed in Table 2.1.

2.4.2 Film Deposition

Polymers, once completely dried, are solubilized in chloroform in order to be spin-coated on the glass substrates. 3% or 10% weight solutions of polymer in chloroform are prepared; sometimes stirring and heating is required to achieve complete dissolution of the polymer.

After the solution is ready, 1 mL is pipetted onto the glass substrate and spin-coated for one minute at 600 rpm, which seems to be the optimal velocity to obtain a uniform coating with these polymers.

2.4.3 Coupling with PV Cells

In order to convert light into electricity, LSCs have to be matched with photovoltaic cells. The cells that were used in this work are IXYS KXOB25-12X1L monocrystalline silicon solar cells with dimensions 2.2x0.6 cm, shown in Figure 2.18. They have high efficiency, around 24.5%, and a good external quantum efficiency between 300 and 1100 nm.

To test its power conversion efficiency, two opposite edges of the LSC are coupled with solar cells, each of which is composed of two modules soldered together in series mode. Moreover, the two cells are connected in series and to a multimeter to perform PV tests.

Figure 2.18 – Picture of IXYS KXOB22-12X1L *monocrystalline silicon solar cells.*

In order to match the solar cells to the glass and avoid unwanted optical effects that could distort the truthfulness of the results, strips of ethyl vinyl acetate (EVA) glue with a refractive index value similar to that of soda-lime glass (1.52) is utilized and placed in between the LSC and the PV cell.

2.5 Characterization Techniques

In this section are described the most important characterization techniques used to characterize monomers, polymers and LSCs.

2.5.1 UV-Vis Spectroscopy

UV-Vis spectroscopy is a technique used to measure the light absorption of a certain material. Unlike IR light, which induces vibrational transitions in molecules, UV (190-400 nm) and visible (400-700 nm) light promote electronic transitions; thus, molecules absorb specific wavelengths in different ways depending on the structure of the electronic states. A UV-Vis spectrometer uses a light source to shine a light beam on a sample, and a detector on the other side to measure the percentage of transmitted and absorbed light.

In particular, UV light is produced by a deuterium lamp, while to produce visible light a tungsten/halogen light is used: in this way, light from 200 to 900 nm can be easily produced. Light passes through a filter and a monochromator in order to be able to shine light on the sample with a precision of up to 1 nm. The light beam also passes through a beam splitter, so that one of the beams will hit the sample while the other one will hit a reference sample. The schematic structure of a spectrometer is shown in Figure 2.19.

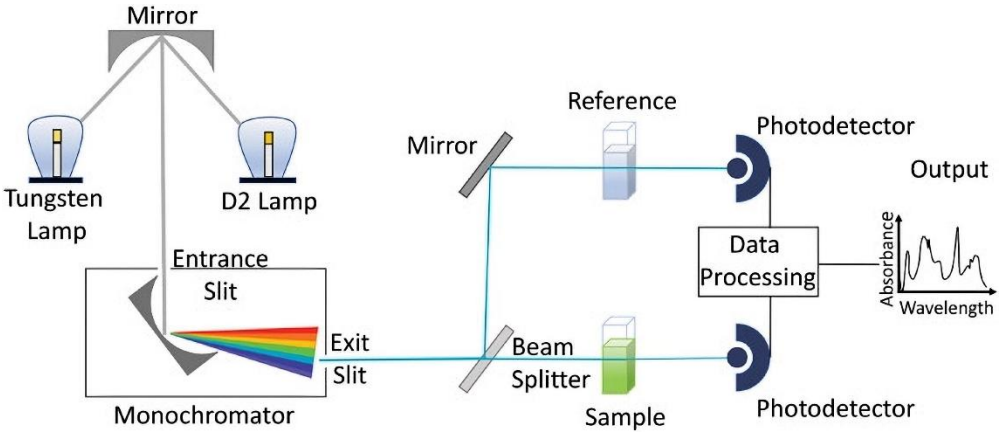

Figure 2.19 – Schematic structure of a UV-Vis spectrometer.

The intensity of light passing through the sample I (for example, a glass slide coated with a fluorescent polymer) is compared with the intensity through the reference sample I_0 (for example, a glass slide identical to the other one but not coated with a polymer) to calculate the light absorbance A. Since the intensity of light decreases exponentially when it passes through an absorbing medium, the absorbance can be calculated as:

$$A = \log_{10} \frac{I_0}{I} = \log_{10} \frac{1}{T}$$

The absorbance can also be calculated with the Lamber-Beer law as:

$$A = \varepsilon c l$$

where c is the concentration of the absorbing medium (mol/L), l is the length of the optical path (cm) and ε is the extinction coefficient (cm^{-1} mol^{-1} L), an intrinsic property of the absorbing species. This law is useful to calculate calibration curves by measuring the absorbance of samples at different known concentrations of absorbing species; this way, a linear correlation is established and by measuring the absorbance of a sample it is possible to interpolate its concentration.

In this work, an Evolution 600 UV-vis spectrometer has been used to measure the absorption spectrum of fluorescent polymers. The scans were performed in room temperature air, after the acquisition of a baseline, with a bandwidth of 2 nm, a scan speed of 120 nm/min, a data interval of 1 nm, lamp change at 350 nm and spectral range from 280 to 800 nm. The samples were prepared by spin-coating a square lab quartz slide for 60 seconds at 600 rpm with 330 µL of a 3% weight fluorescent polymer solution.

2.5.2 Fluorescence Spectroscopy

When a molecule absorbs a photon, an electron is excited from the ground state to a higher energy level; this state is intrinsically unstable, and the electron will rapidly lose its excess energy and decade to the ground state via various processes, shown by the Perrin-Jablonski diagram in Figure 2.20.

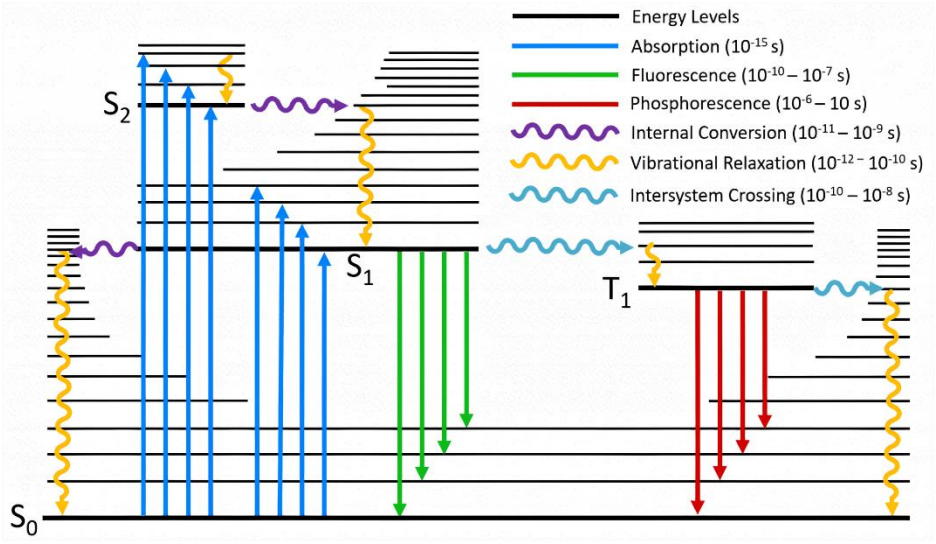

Figure 2.20 – Perrin-Jablonski diagram.

In particular, an electron can be excited from the ground state S_0 to a singlet excited state (S_1, S_2...). From there, the electron will likely lose energy due to vibrational relaxation, decade to the ground state (fluorescence), undergo internal conversion or

exploit spin-orbital coupling to make a non-radiative transition to a triplet excited state (T_1, T_2...), from where the electron can undergo a radiative transition to the ground state (phosphorescence).

To calculate the efficiency of the fluorescence process, a parameter called quantum yield of fluorescence Φ is introduced, defined as the number of photons that are emitted by fluorescence over the total number of absorbed photons. The intensity of fluorescence I_F, measured by instruments such as fluorescence spectrometers, can then be calculated as:

$$I_F = kI_0\Phi(1 - 10^{-\varepsilon cl})$$

where k is a constant of the instrument, I_0 is the intensity of the incident light, ε the extinction coefficient, c the concentration of the luminescent species and l the length of the optical path.

For the molecules treated in this work, the most important process is fluorescence, since luminophores are characterized by a high quantum yield of fluorescence, and phosphorescence is a much weaker, less probable process.

As shown in Figure 2.21, a spectrofluorometer is an instrument consisting of a xenon lamp in series with a monochromator, in order to precisely select an excitation wavelength, a sample compartment, another monochromator to precisely select the emission wavelength and finally a detector.

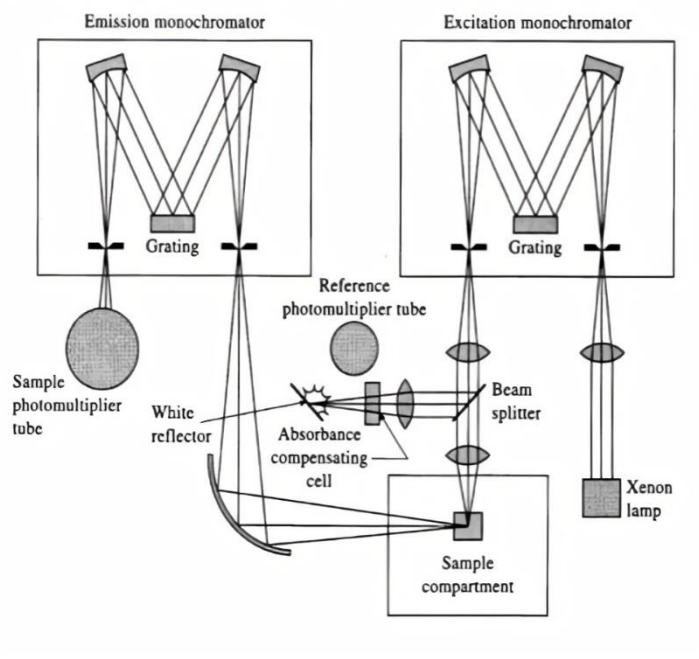

Figure 2.21 – Schematic structure of a spectrofluorometer.

With such an instrument, it is possible to perform emission and excitation measurements: the former consists in exciting a sample with a constant wavelength and measuring the emission intensity for a sweep of wavelengths, while the latter

consists in exciting a sample with a sweep of wavelengths while measuring the fluorescence intensity at a fixed wavelength.

In this work, emission spectra of the fluorescent polymers (spin-coated on lab quartz slides) were measured using a Jasco FP-6600 Spectrofluorometer with low sensitivity, a response of 2 seconds, data pitch of 1 nm, an excitation band width of 3 nm, an emission band width of 6 nm and a scanning speed of 200 nm/min. The emission spectra were recorded with spectral range from 360 to 750 nm when exciting at 350 nm and from 460 to 750 nm when exciting at 450 nm.

2.5.3 Nuclear Magnetic Resonance Spectroscopy (NMR)

Nuclear magnetic resonance spectroscopy is a characterization technique that relies on the interaction between a magnetic field and an atomic nucleus. When simultaneously subjected to a strong constant magnetic field (usually around 20 T) and to a weak oscillating field (usually oscillating at 60 -1000 MHz), the nucleus can emit an electromagnetic signal. This phenomenon occurs at the resonance frequency of the sample, which is also directly proportional to the strength of the applied constant magnetic field. The most common spectroscopy techniques investigate the NMR properties of ^{1}H and ^{13}C; due to their nuclear spin, the NMR effect only occurs with nuclei that consist of an odd number of particles between protons and neutrons.

NMR spectroscopy measures the chemical shift induced by the chemical environment of a certain molecule. More in detail, each electron can generate a magnetic field that effectively screens the nucleus from the external static field: if the investigated nucleus is surrounded by atoms with low electronegativity, electrons will be surrounding the nucleus, the shielding effect will be stronger and the resonance effect will occur at lower frequencies; conversely, an electronegative atom will draw electrons from the nuclei, which will be less shielded and they will resonate at higher frequencies.

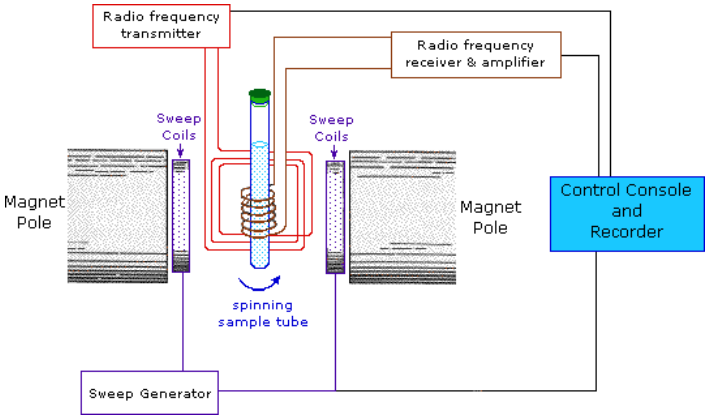

Figure 2.22 – Schematic of an NMR spectrometer.

Moreover, if ^1H atoms are close together, their spin states interact and the J-coupling phenomenon occurs. Effectively, the signal relative to the neighbouring ^1H atoms will be split in $n + 1$ peaks, where n is the number of ^1H atoms.

NMR spectroscopy is thus very useful to determine the chemical structure of a molecule, since every ^1H nucleus provides a different signal depending on its chemical environment. A schematic of an NMR spectrometer is shown in Figure 2.22.

In this work, H-NMR spectroscopy has been used to determine whether the structure of the synthesized molecules was as expected: for example, it was used to investigate the degree of incorporation of luminophore monomers into the polymeric chain in order to compare the initial concentration of monomers to the final one after the reaction. Around 10 mg of analyte were dissolved in 0.8 mL of deuterated $CHCl_3$ or deuterated DMSO and pipetted into an NMR tube. The spectrometer is a Bruker Avance 400 and works at a frequency of 400 MHz.

2.5.4 Fourier Transform Infrared Spectroscopy (FTIR)

Fourier Transform Infrared Spectroscopy is a technique used to analyze molecules and compounds and obtain their infrared spectrum.

As with visible light, when molecules are hit by IR photons they absorb part of their energy and convert it into vibrational energy: more precisely, a molecule absorbs IR radiation when the frequency of the photon resonates with one of the vibrational modes of the molecule and a simultaneous change in molecular dipole moment occurs.

The most typical vibrational modes are stretching and bending: the former is an oscillatory change of bond length between two atoms, while the latter is an oscillatory modification of bond angle. Bending can be further divided into scissoring, rocking, wagging and twisting.

Like in the case of NMR spectroscopy, different atoms and functional groups in the molecule result in different IR peaks and spectra; this phenomenon can be exploited to identify a molecule from its IR spectrum, which almost becomes a fingerprint of that specific molecule. More specifically, some functional groups like -NH, -C=C or -C=O produce very recognizable IR peaks, since they usually vibrate at a different frequency compared to the rest of the molecule.

To acquire an FTIR spectrum, a spectrometer is used: the instrument consists of an IR light source coupled with an interferometer to modulate the wavelength, a sample compartment and a detector. The IR light passes through the sample and the absorbed/transmitted radiation is recorded from the detector; the data is then sent to a computer that performs Fourier transform calculations. The schematic diagram of an FTIR spectrometer is reported in Figure 2.23.

The data is usually plotted as intensity (on the y-axis) over wavenumber (on the x-axis). The wavenumber is related to the wavelength of the radiation through a simple formula:

$$\nu[cm^{-1}] = \frac{10^4}{\lambda[nm]}$$

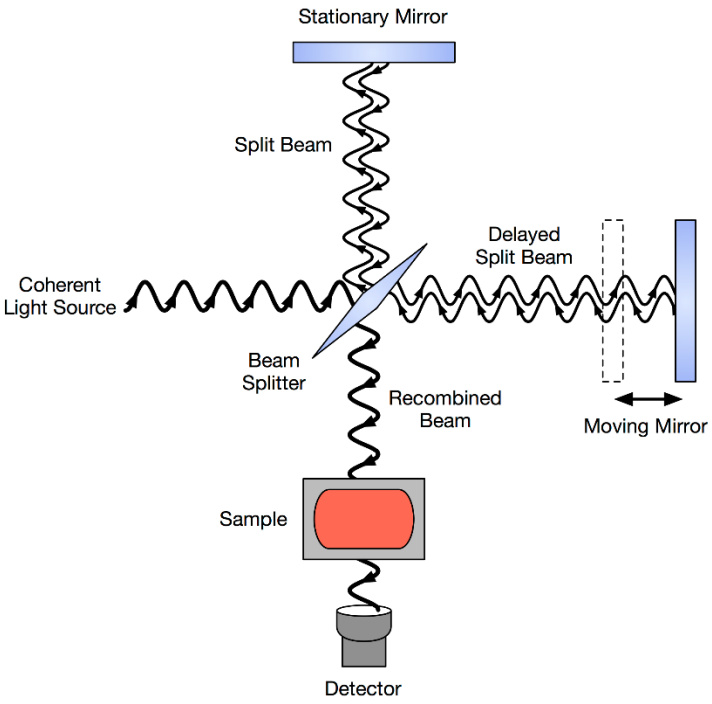

Figure 2.23 – Schematic diagram of an FTIR spectrometer.

In this work, FTIR spectroscopy has been used to perform spectral measurements on the synthesized monomers and polymers, in order to analyze their structure and verify the presence of key functional groups. The measurements were carried out by spin coating polymers on KBr or NaCl disks or by pressing monomers into a powder to create a KBr tablet. The spectrometer used was a Jasco FT/IR-615, in air at room temperature, with a resolution of 4 cm^{-1}, a number of scans of 32 and wavenumber spectral range from 4000 cm^{-1} to 400 cm^{-1}.

2.5.5 Differential Scanning Calorimetry (DSC)

Differential scanning calorimetry is a thermal characterization method that investigates the phase transitions in materials as a function of time and temperature. In particular, it measures the difference in heat flow or power needed to raise the temperature of a sample and a reference: two metal crucibles, one empty and one containing the sample to investigate, are heated and the heat flow is measured. When the sample undergoes a phase transformation, the variation in power needed to maintain a temperature constant is recorded

The resulting plot presents the time and temperature progress on the x-axis and the power needed to heat the sample on the y-axis. As phase transitions occur, power can increase or decrease depending on the type of transition: negative peaks correspond to

an endothermic transition, while positive peaks correspond to an exothermic one. Furthermore, the integral of the area of a peak gives the value of the enthalpy variation corresponding to a certain phase transition.

In this work, DSC analyses were performed on polymers in order to verify their phase transitions and find out their glass transition temperature. The analyses were carried out with a DSC/823e-Mettler Toledo calorimeter calibrated with n-hexane and indium.

The polymers were tested with a scan speed of 20 °C/min, in three thermal runs going from 25 to 200 °C, from 200 to 25 °C and finally from 25 to 200 °C.

2.5.6 Gel Permeation Chromatography (GPC)

Gel permeation chromatography is a technique used to determine the molecular weights and the polydispersity index of macromolecules such as polymers.

GPC allows to physically fractionate components of a polymeric solution based on their molecular weight: as shown in Figure 2.24, a solvent flows into the instrument, usually THF or dichlorobenzene, and collects the injected sample before reaching the chromatographic columns. The columns are packed with porous beads, which slow down the elution of polymers depending on their polymeric weight: more precisely, smaller molecules are more easily trapped by the pores of the beads, and their elution time is greatly increased, while polymers with a larger molecular weight flow much easier and reach the detector in a slower time.

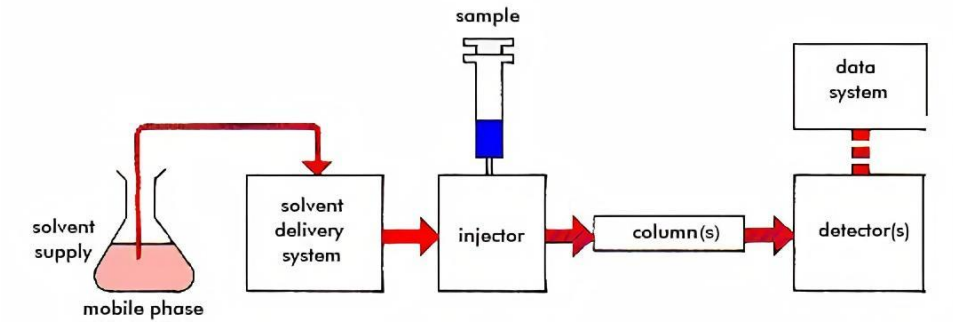

Figure 2.24 – Schematic diagram of GPC instrumentation.

When choosing the solvent to flow into the system, it's important to consider that the polymer must be soluble in it in order to inject it into the columns. Furthermore, it's important to have a general idea of the molecular weight of the polymer beforehand, since there exist different columns that can fractionate polymers with different ranges of polymeric weights.

In this work, GPC has been used to determine the polymeric weight of the synthesized fluorescent polymers. The instrument utilized is a Waters 486, together with a Waters 515 HPLC pump and a Waters 2410 refractive index detector, set with a range of 1250 mV and a rate of 12,5 mV/s.

2.5.7 Time-Resolved Fluorescence Spectroscopy

Time-resolved fluorescence spectroscopy is a technique employed to investigate the fluorescence characteristics of compounds with particular attention to the time needed for certain processes to occur.

More precisely, the fluorescence of a sample, after being excited by irradiating light, is recorded and monitored in time. The characteristics time of fluorescence phenomena is around tens of nanoseconds; in order to record it, a technique called time-correlated single-photon counting (TCSPC) is employed.

In this work, time-resolved fluorescence spectroscopy has been employed to evaluate the time of fluorescence in fluorescent polymers. More specifically, it has been used to evaluate the efficiency of FRET phenomena in terpolymers by recording the fluorescence lifetime of the donor species.

Fluorescence time-resolved TCSPC measurements have been performed with a NanoLog composed of an iH320 spectrograph equipped with a PPD-850 single-photon detector module and a DeltaTime series DD-405L DeltaDiode Laser and analysed with the instrument software DAS6.

2.5.8 Photovoltaic Tests

In order to evaluate the optical and photovoltaic characteristics of LSCs, a solar simulator, a spectroradiometer and a digital multimeter were employed.

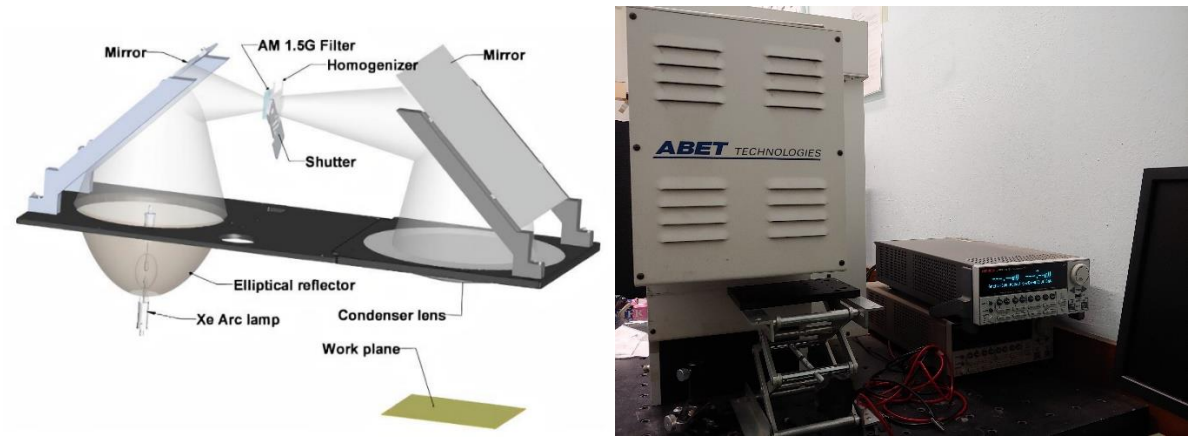

Figure 2.25 – Schematic diagram of a solar simulator (left), picture of the solar simulator and the multimeter (right).

An ABET Technologies Sun 2000 solar simulator with an AM 1.5 filter and an irradiance of 1000 W/m corresponding to 1 SUN was utilized to reproduce the solar spectrum. As shown in Figure 2.25, the instrument consists of a xenon short-arc lamp which radiation is focused onto an integrated lens that helps produce a uniform divergent beam. The light then passes through a spectrum shaping element like an AM filter and finally is

deflected on the work plane by a mirror. As explained in page 3, the air mass standard is useful to assure constant measurement conditions across the globe.

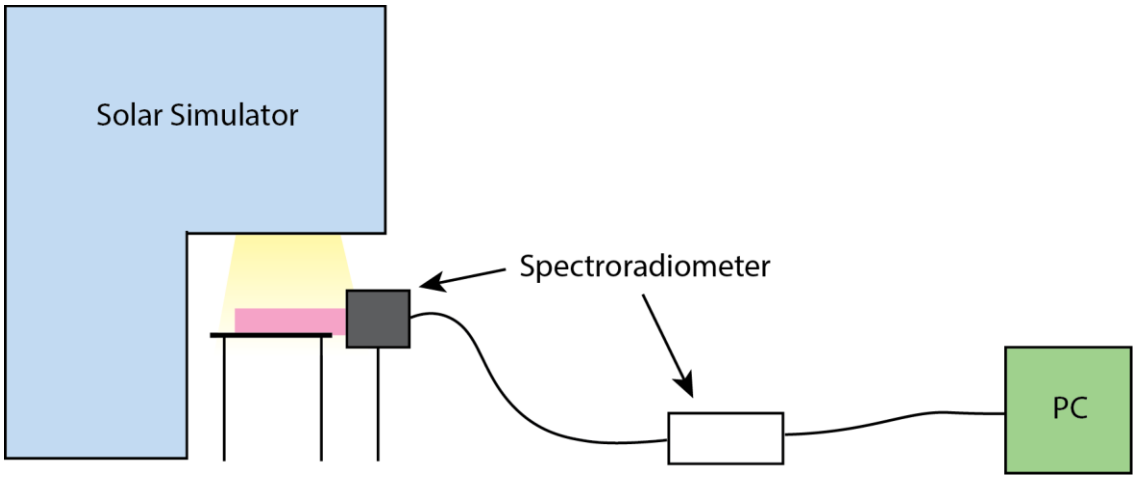

Figure 2.26 – Diagram showing the setup for edge-emission irradiance measurements.

As shown in Figure 2.26, in order to measure the optical characteristics of LSCs, the devices were put on a workbench so to illuminate their top face with the solar simulator. As shown in Figure 2.27, an International Light Technologies ILT950 spectroradiometer with a cosine corrector was mounted on one of the sides of the LSC and the emission spectra were recorded with the software Spectrilight. With this data, the external η_{EXT} and internal η_{INT} photon efficiencies could be calculated.

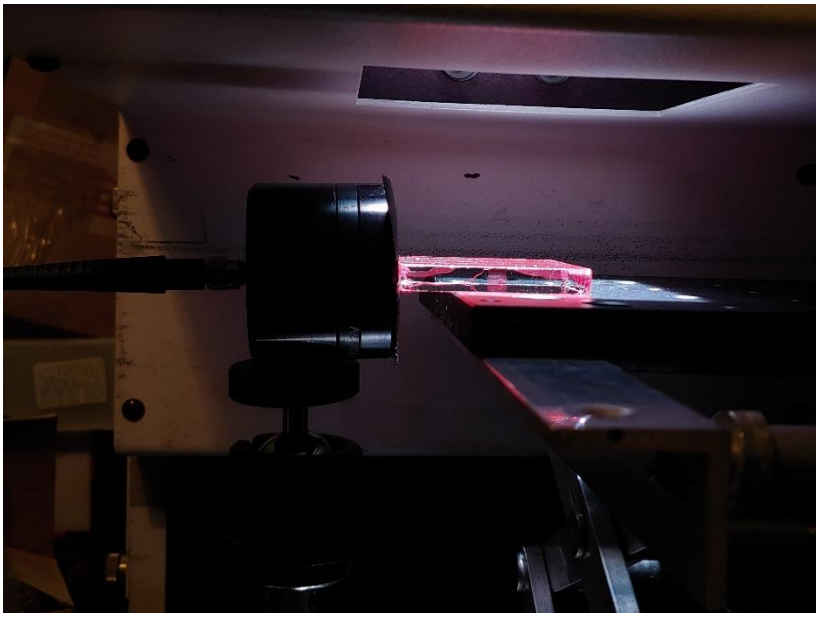

Figure 2.27 – Setup of the ILT950 spectroradiometer for edge-emission irradiance measurements.

After connecting the LSC and the PV cells to the multimeter, as described in paragraph 2.4.3, photovoltaic efficiencies of the LSCs could be calculated. The multimeter runs a sweep of voltages in order to record the response of the solar cell in terms of electrical current. The resulting plot is the I-V characteristic of the device; by knowing the area

of the LSC and the efficiency of the PV cells it's possible to calculate the efficiency of the LSC and the geometric gain.

The multimeter parameters used to perform PV efficiency tests are as follows: voltage range from -0.5 to 3.0 V, data pitch of 0.05 V, 71 points and light intensity of 100 mW/cm^2.

Chapter 3
Results and Discussion

This chapter will be divided into three parts.

The first part will be focused on the characterization of the synthesized luminescent monomers.

The second part will be focused on the characterization of the luminescent polymers synthesized by random polymerization.

The third and final part will be focused on the characterization and properties of the LSC devices.

3.1 Luminescent Monomers

After synthesizing luminescent monomers, some characterization tests were performed in order to ensure that the reaction was successful.

3.1.1 Coumarin Methacrylate

As described in paragraph 2.2.3, coumarin methacrylate (CMA) was synthesized starting from methylumbelliferone. Described below are the characterization tests that were performed on the molecule.

Differential Scanning Calorimetry

DSC analysis was performed on the molecule. As shown in Figure 3.1, no heat flow peak was observed while heating the crucible, which means that no phase transitions and no degradation occur in the sample between 25 and 250 °C, as expected from a methacrylate monomer. Also, since a glass phase transition is not present on the curve, we can infer that the monomer did not self-polymerize during the reaction or storage.

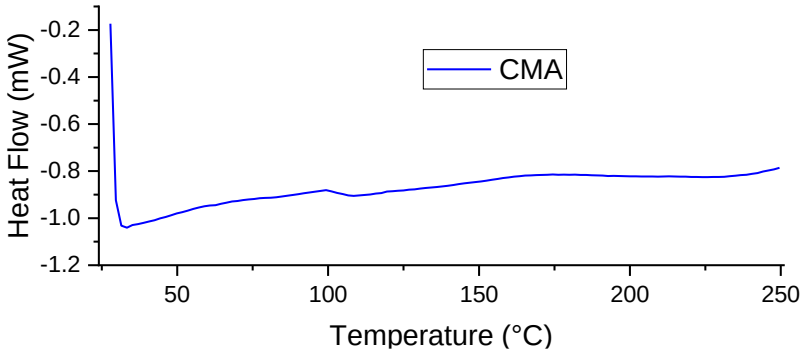

Figure 3.1 – DSC analysis of CMA.

Fourier Transform Infrared Spectroscopy

Both 7-(2-hydroxyethoxy)-4-methylcoumarin (HEOMC) and coumarin methacrylate were characterized through FTIR spectroscopy, as shown in Figure 3.2.

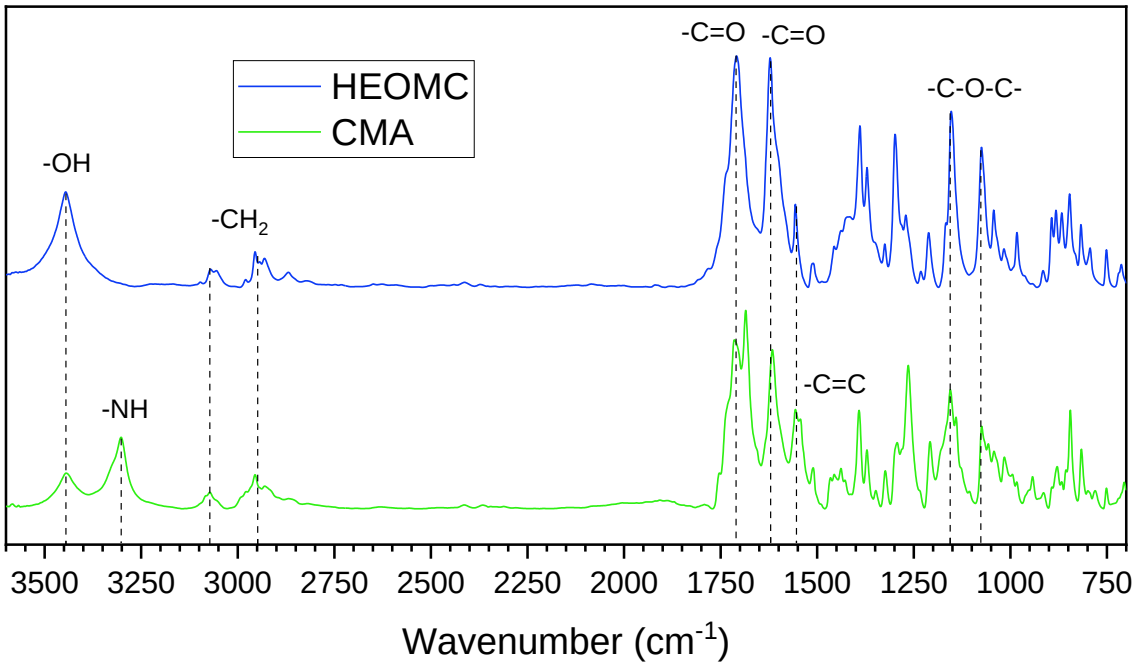

Figure 3.2 – FTIR spectroscopy analysis of CMA and HEOMC.

Starting from the left of the spectrum, we can observe sharp peaks at 3450 and 3300 cm^{-1}: the former can be attributed to the -OH termination of HEOMC, while the latter can be assigned to the -NH group formed on the CMA chain. As we can observe, the peak at 3300 cm^{-1} is only present in the CMA thus proving the successfulness of the reaction and the formation of the urethane bond. Furthermore, the peak at 3450 cm^{-1} should completely disappear in the CMA, since the -OH termination of the HEOMC reacts with the isocyanate ethyl methacrylate to form the urethane bond; its residual presence may indicate an incomplete conversion or the presence of humidity in the sample.

Going forward to the right, the group of peaks between 3050 and 2900 cm^{-1} can be attributed to aliphatic in-chain $-CH_2$ groups. One thing to note is the absence of any peak around 2270 cm^{-1}: this peak is typical of the cyanate -N=C=O group and its presence would signify that the isocyanate ethyl methacrylate (IEM) is still present in the sample. This is yet another confirmation that the reaction was successful.

The CMA peaks at 1740 and 1610 cm^{-1} are typical of the stretching of the -C=O group: while the former is present in both spectra and can be attributed to the carbonyl group on the coumarin backbone, the latter is present only in the CMA spectrum and is typical of the stretching movement of the -C=O group on the secondary amide given by the urethane bond.

Moving further, a peak at 1550 cm^{-1} denoting the stretching of the C=C bonds on the coumarin rings and peaks at 1150 and 1080 cm^{-1} that can be attributed to the stretching of -C-O-C- bonds in the coumarin are found.

Nuclear Magnetic Resonance Spectroscopy

Nuclear magnetic resonance spectroscopy analyses were performed on CMA samples in order to characterize the chemical structure of the molecule.

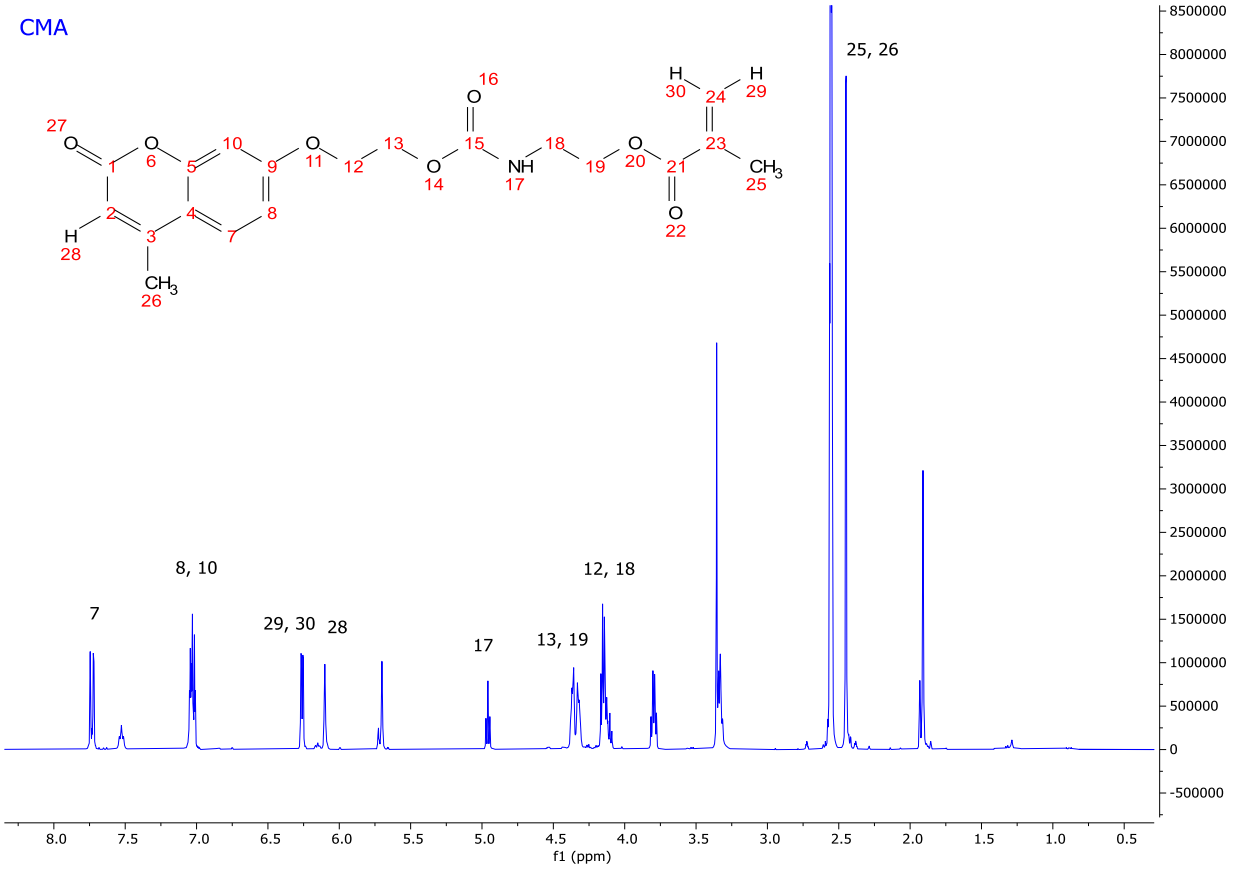

Figure 3.3 – NMR analysis of coumarin methacrylate.

The NMR spectrum of CMA is reported in Figure 3.3. The signals of the coumarin bulk, except for the methyl bound with the carbon atom number 3, are mainly found between 6.0 and 8.0 ppm. Starting from higher chemical shifts, we can find the benzylic H7 (dd, 1H) at 7.73 ppm, two other benzenic hydrogen atoms H8 and H10 (m, 2H) at 7.03 ppm, two CH_2 hydrogens H29 and H30 (d, 2H) at 6.27 ppm, the H17 hydrogen bound to the nitrogen atom of the urethane bond (t, 1H) at 4.94 ppm, two in-chain CH_2 hydrogens H13 and H19 (m, 4H) at 4.35 ppm, H12 and H18 (m, 4H) at 4.14 ppm and finally the peaks corresponding to the two methyl groups H25 and H26 (d, 6H) at 2.45 ppm.

The NMR spectra of HEOMC and IEM are also reported in Figure 3.4 and Figure 3.5.

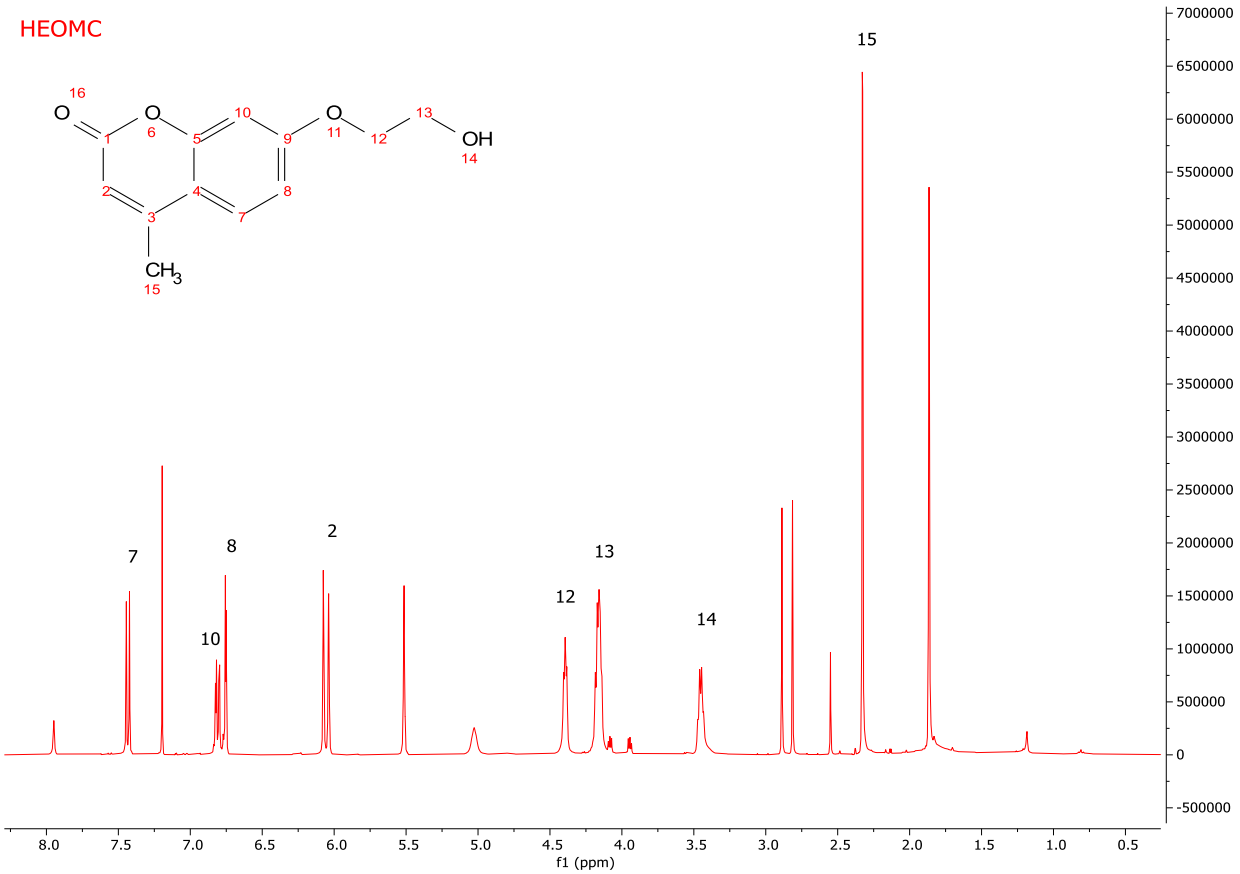

Figure 3.4 – NMR analyses of HEOMC.

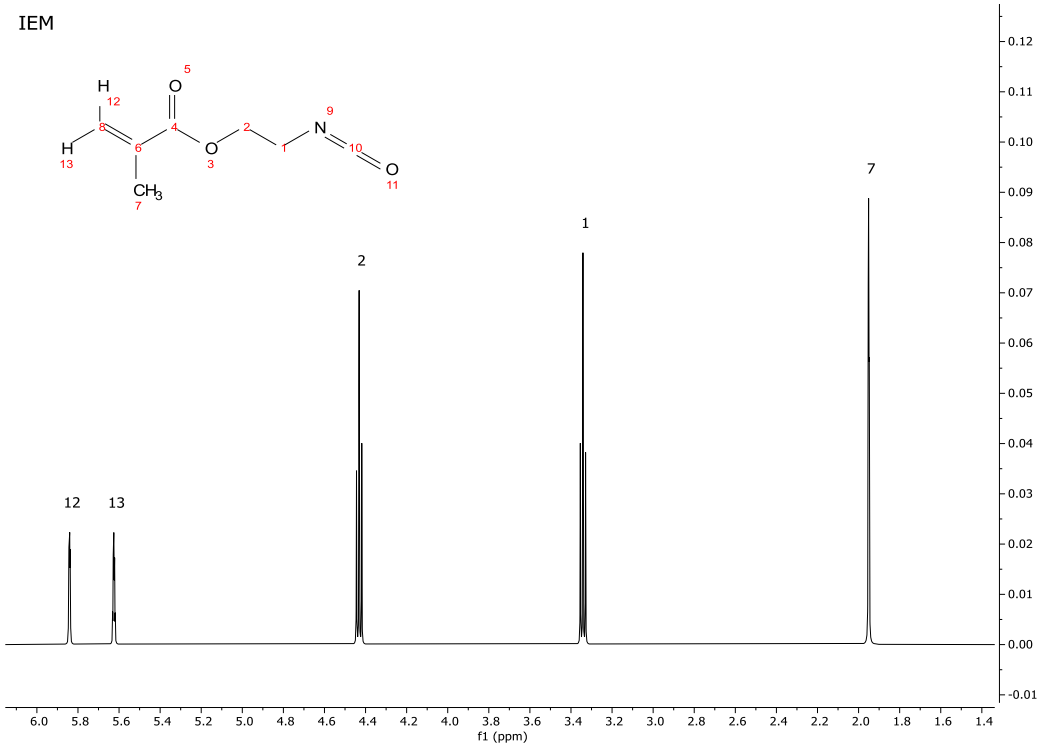

Figure 3.5 – NMR analyses of IEM.

Furthermore, a comparison between the NMR spectra of isocyanate ethyl methacrylate (IEM), HEOMC and CMA is reported in Figure 3.6.

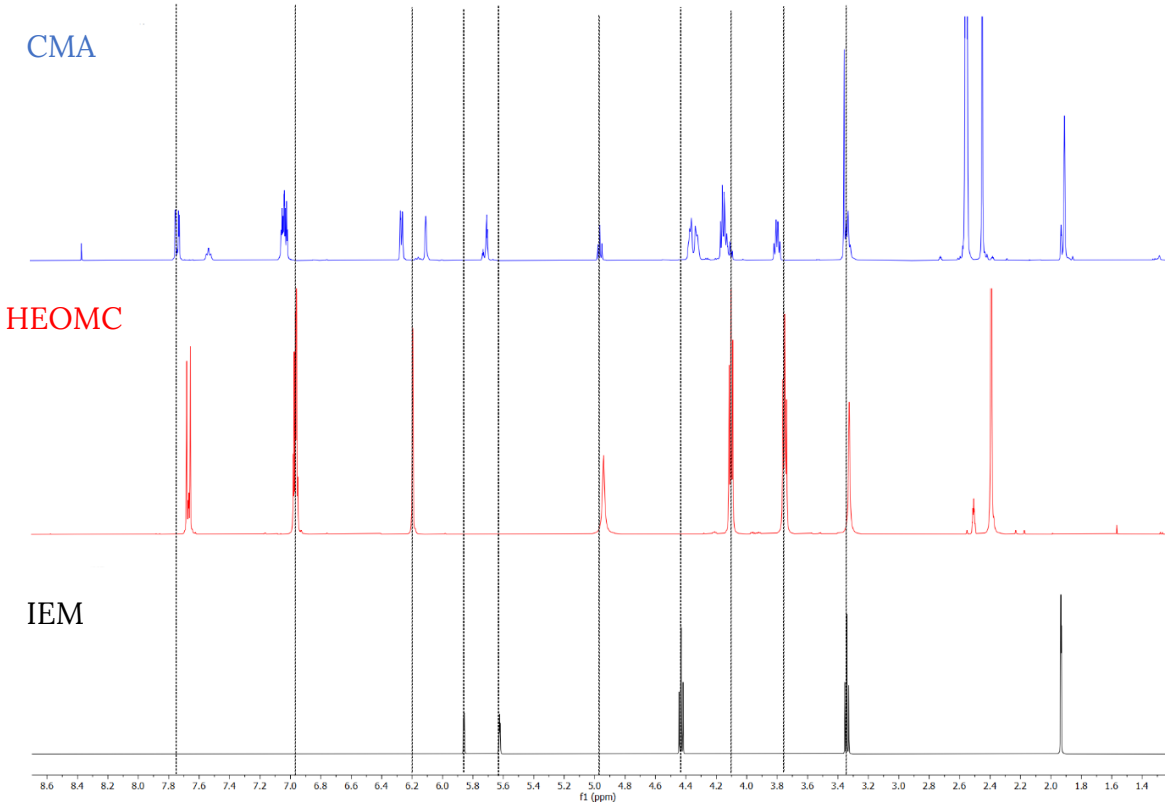

Figure 3.6 – Comparison between the NMR spectra of IEM (bottom, black), HEOMC (middle, red) and CMA (top, blue).

All the reported peaks of the reagents seem to have shifted in the spectra of the final product; this is a probable indication that the reaction was successful.

UV-Vis Absorbance

In order to assess the absorption spectrum of the dye, measurements with a UV-Vis spectrometer have been performed. Reported in Figure 3.13is the normalized absorption spectra of both HEOMC and its methacrylate counterpart (CMA).

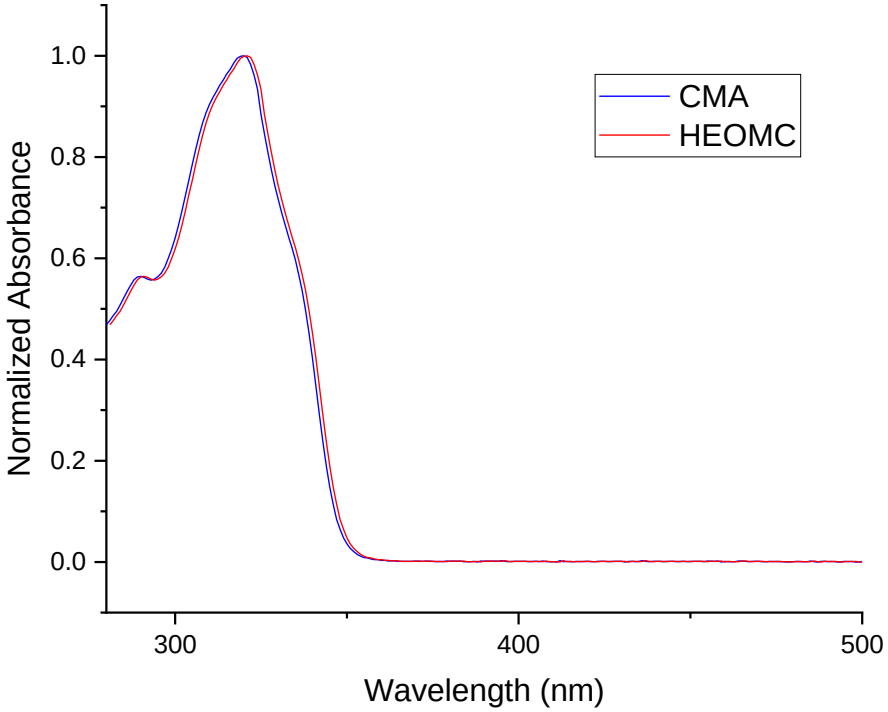

Figure 3.7 - Normalized absorption spectra of CMA and HEOMC.

The two spectra are completely superimposable, proof that the functionalization reaction did not affect the optical characteristics of the dye. The molecules present an absorption maximum at $\lambda = 320\,nm$, a secondary peak at $\lambda = 290\,nm$ and a tertiary shoulder around 340 nm.

Fluorescence Spectroscopy

Fluorescence spectroscopy measurements were carried out on CMA in order to assess its emission characteristics. Reported in Figure 3.8 are the fluorescence spectra of HEOMC and its methacrylate counterpart when excited at a wavelength $\lambda = 330\,nm$.

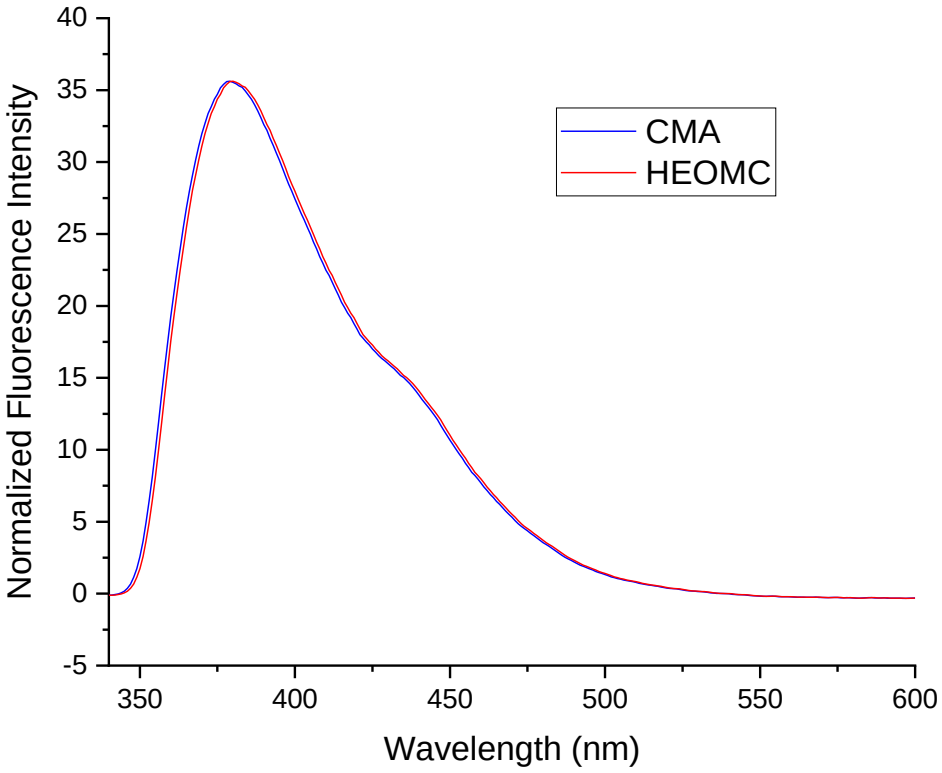

Figure 3.8 – Normalized fluorescence spectra of HEOMC and CMA.

Similarly to the absorption spectra, these spectra are also completely superimposable, thus further corroborating that the methacrylate functionality does not affect the optical properties of the dye.

3.1.2 Perylene Methacrylate

As described in paragraph 2.2.4, a custom perylene bisimide molecule was functionalized in order to obtain perylene methacrylate. Described below are the characterization tests that were performed on the molecule.

Differential Scanning Calorimetry

DSC analysis was performed on the molecule. As shown in Figure 3.9, no heat flow peak was observed while heating the crucible, which means that no phase transitions and no degradation occur in the sample in the 25 - 200 °C temperature range. Also, since no glass phase transition is present on the profile, we can infer that the monomer did not self-polymerize during the reaction or storage.

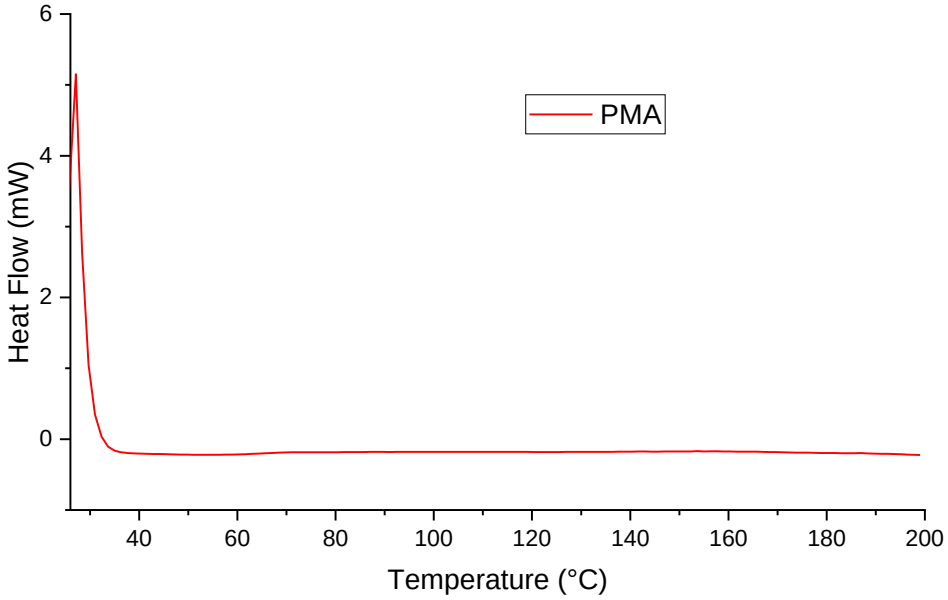

Figure 3.9 – DSC analysis of PMA.

Fourier Transform Infrared Spectroscopy

Both the custom PDI molecule and PMA were characterized through Fourier transform infrared spectroscopy in order to interpret their chemical structure, as shown in Figure 3.10.

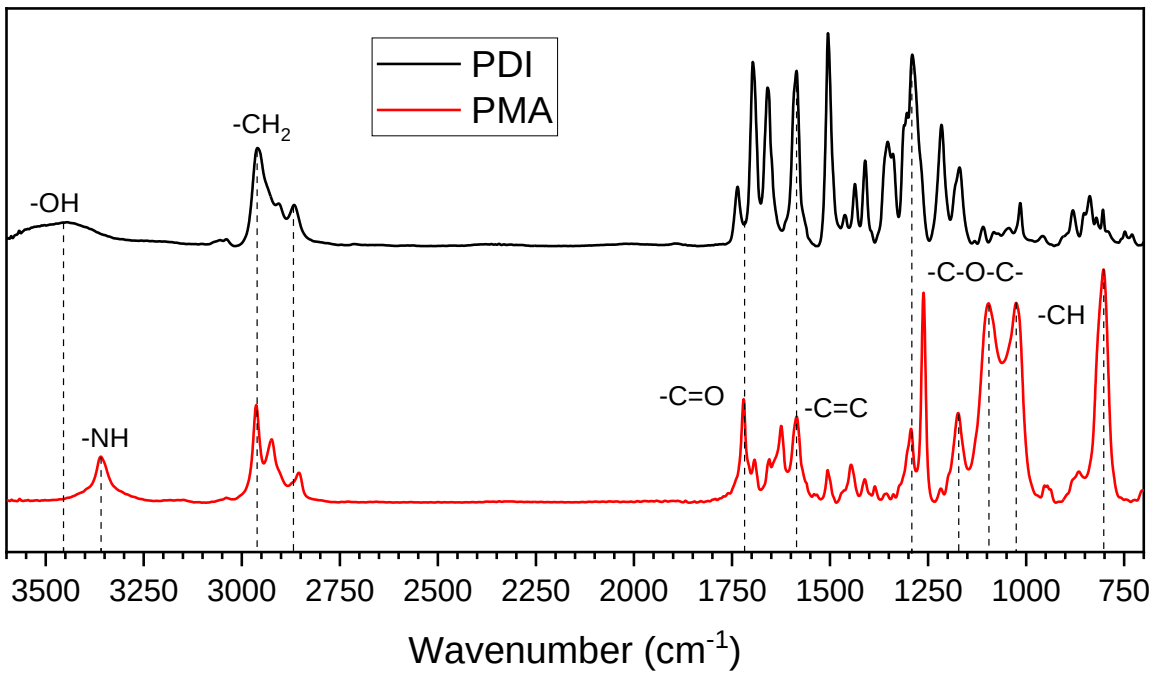

Figure 3.10 - FTIR spectroscopy analysis of PMA and the custom PDI.

Starting from the left of the spectrum, we can observe a broad peak at 3450 and a sharp peak at 3350 cm^{-1}: the former can be attributed to the -OH termination of the PDI, while

the latter can be assigned to the -NH group formed on the PMA chain. Moreover, the peak centred at 3350 cm^{-1} is only present in the PMA thus demonstrating the successfulness of the end-capping reaction with the formation of the urethane bond.

Going forward to the right, the group of peaks between 2950 and 2850 cm^{-1} can be attributed to aliphatic in-chain -CH_2 groups. Like in the case of PMA, the absence of any peak around 2270 cm^{-1} is to be noted: this peak is typical of the cyanate -N=C=O group and its presence would signify that the isocyanate ethyl methacrylate (IEM) is still present in the sample. This is yet another evidence that the reaction was successful.

The PMA peak at 1720 cm^{-1} is typical of the stretching movement of the -C=O group on the secondary amide given by the urethane bond.

Moving further, we find a peak at 1600 cm^{-1} denoting the stretching of the C=C bonds and peaks between 1300 and 1000 cm^{-1} that can be attributed to the stretching of -C-O-C- bonds in the PMA molecule.

Finally, the peak at 750 cm^{-1} in PMA can be attributed to the bending of-CH bonds.

Nuclear Magnetic Resonance Spectroscopy

Nuclear magnetic resonance spectroscopy analyses were performed on PMA samples in order to characterize the chemical structure of the molecule.

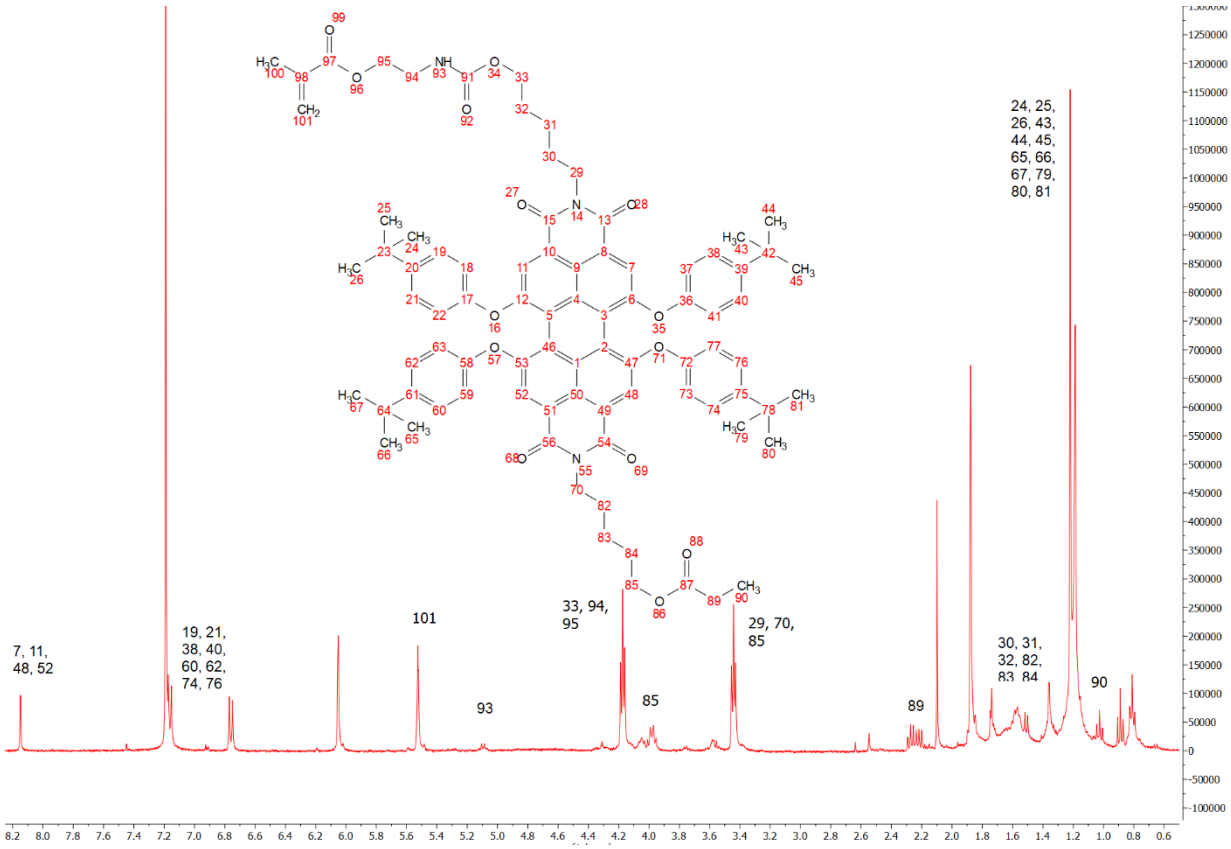

Figure 3.11 – NMR analysis of perylene methacrylate.

The NMR spectrum of PMA is reported in Figure 3.11. Starting from higher chemical shifts, we can find the benzylic hydrogens H7, H11, H48 and H52 belonging to the perylene bulk (s, 4H) at 8.15 ppm, the other benzylic hydrogens H19, H21, H38, H40, H60, H62, H74 and H76 belonging to the external benzene rings (m, 16H) at 7.16 and 6.76 ppm, two CH_2 hydrogens H101 (t, 2H) at 5.53 ppm, the H93 hydrogen bound to the nitrogen atom of the urethane bond (t, 1H) at 5.11 ppm, three in-chain CH_2 groups H33, H94 and H95 (m, 6H) at 4.17 ppm, three others in-chain CH_2 groups H29, H70 and H85 (m, 6H) at 3.44 ppm, the in-chain CH_2 H89 (m, 1H) at 2.26 ppm, the in-chain CH_2 H30, H31, H32, H82, H83 and H84 (m, 12H) at 1.88 ppm, the peaks relative to the external methyl groups H24. H25, H26, H43, H44, H45, H65, H66, H67, H79, H80, H81 (d, 36H) at 1.20 ppm and finally the peak corresponding to the chain-terminating methyl group H90 (5, 3H) at 1.05 ppm.

Furthermore, a comparison between the NMR spectra of IEM, the custom PDI and PMA is reported in Figure 3.12.

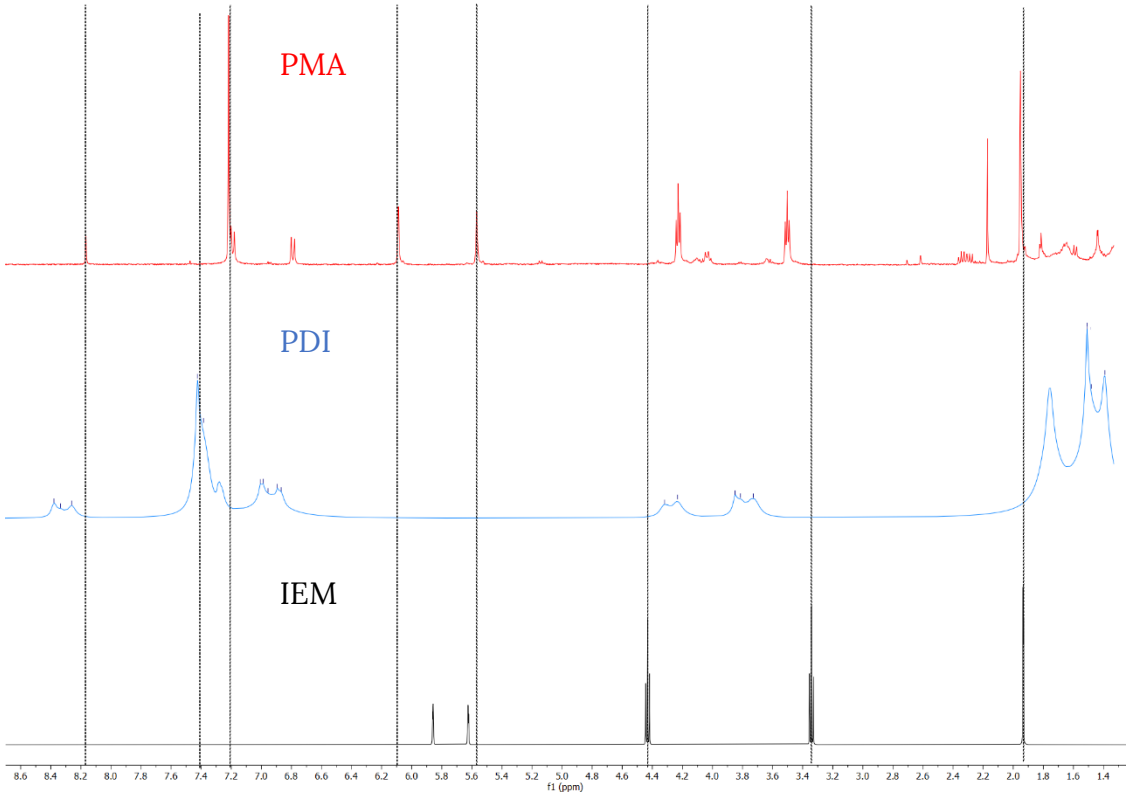

Figure 3.12 – Comparison between the NMR spectra of IEM (bottom, black), PDI (middle, blue) and PMA (top, red).

All the reported peaks of the reagents seem to have shifted in the spectra of the final product; this is a probable indication that the reaction was successful.

UV-Vis Absorbance

In order to assess the absorption spectrum of the dye, measurements with a UV-Vis spectrometer have been performed. Reported in Figure 3.13 is the normalized

absorption spectra of both the custom PDI molecule and its methacrylate counterpart (PMA).

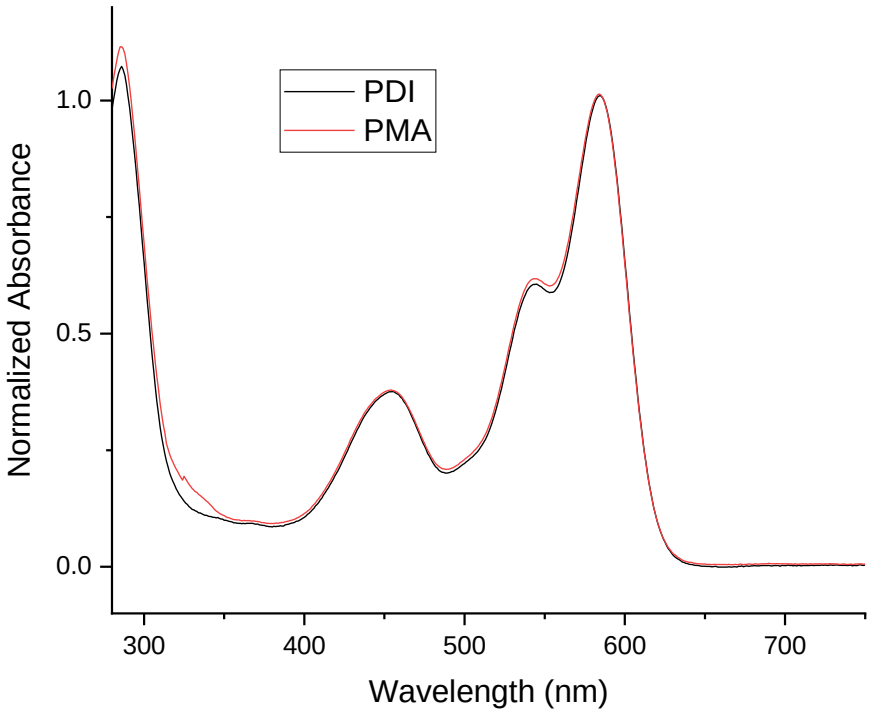

Figure 3.13 – Normalized absorption spectra of the custom PDI and PMA.

As in the case of CMA and MU, the two spectra are completely superimposable, proof that the functionalization reaction didn't affect the optical characteristics of the dye. The molecules present an absorption maximum at $\lambda = 580\ nm$, a secondary peak at $\lambda = 540\ nm$ and a third one at $\lambda = 450\ nm$. As further explained later, this third peak will be chosen as the excitation peak for fluorescence spectroscopy measurements.

Fluorescence Spectroscopy

Fluorescence spectroscopy measurements were carried out on PMA in order to assess its emission characteristics. Reported in Figure 3.14 are the fluorescence spectra of the custom PDI molecule and its methacrylate counterpart when excited at a wavelength $\lambda = 450\ nm$.

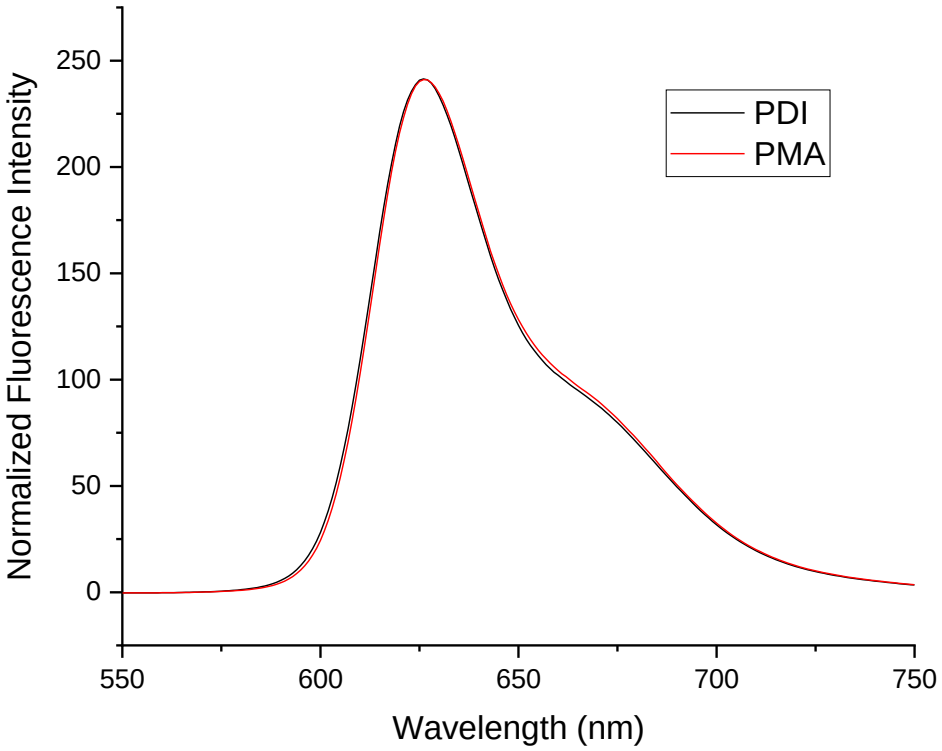

Figure 3.14 – Normalized fluorescence spectra of the custom PDI and PMA.

Similarly to the absorption spectra, these spectra are also completely superimposable: this is a further confirmation of the fact that the methacrylate functionality doesn't affect the optical properties of the dye.

The molecules present a fluorescence peak at $\lambda = 625\ nm$, with a secondary shoulder at around $\lambda = 670\ nm$.

3.2 Luminescent Copolymers via Random Polymerization

After the synthesis of luminescent polymers, characterization tests were performed on the sample to determine their properties.

3.2.1 Coumarin Methacrylate/Methyl Methacrylate Copolymers

Copolymers with 5%, 10% and 15% molar of CMA (while the rest is MMA) were synthesized. In the following graphs, they are referred to as CMA5/MMA95, CMA10/MMA90 and CMA15/MMA85, respectively.

Gel Permeation Chromatography

GPC analyses were performed on the samples to determine their molecular weight. The resulting elution curves are reported in Figure 3.15.

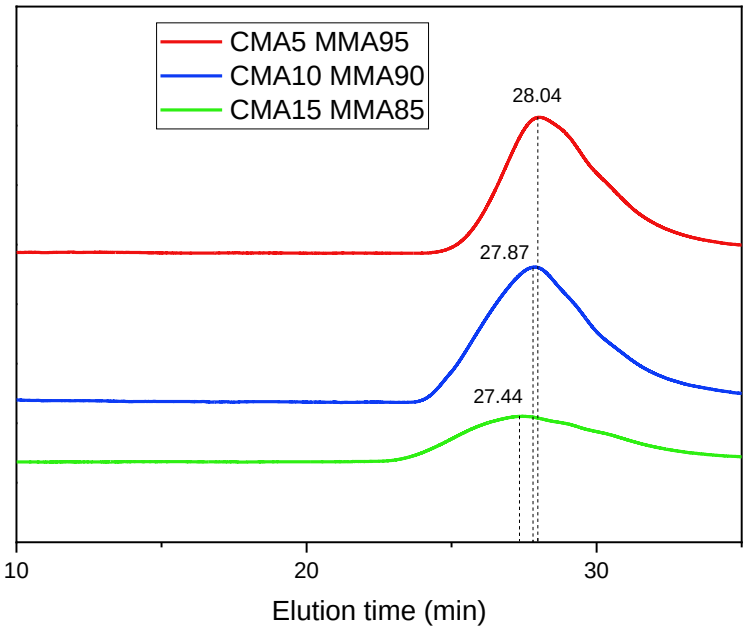

Figure 3.15 – GPC analyses of CMA-MMA random copolymers.

Reported in Table 3.1 are the main results of GPC analyses on CMA random polymers, showing the number averaged molecular weight, the weight averaged molecular weight and the polydispersity index.

Table 3.1 – Results of GPC analyses on CMA-MMA random copolymers.

Batch Name	Mn	Mw	PDI
CMA5/MMA95	39914	75039	1.88
CMA10/MMA90	43116	94156	2.18
CMA15/MMA85	48508	115289	2.38

From these results, it can be inferred that the final molecular weight of the polymers increased with the amount of coumarin in the reaction solution, probably because CMA has a higher molecular weight with respect to MMA; however, the polydispersity index also slightly increases, making the polymer less regular.

Differential Scanning Calorimetry

DSC analyses were performed on the polymers in order to measure their glass transition temperature. The results are shown in Figure 3.16.

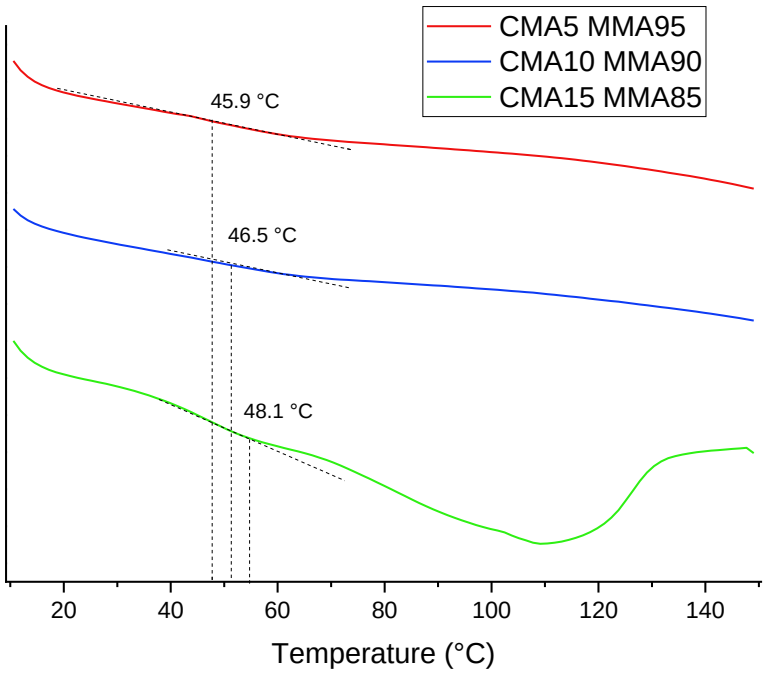

Figure 3.16 – DSC analyses of CMA-MMA random copolymers.

From the curves, it can be inferred that the polymerization was successful since there is only one transition peak. Furthermore, it seems that the concentration of CMA in the reaction solution does not have a significant impact on the Tg of the final polymer, which is around 47 °C for all the samples, although the Tg seems to increase slightly with the amount of CMA. The peak visible around 110 °C in the CMA15/MMA85 curve could be attributed to the evaporation of residual dioxane.

Fourier Transform Infrared Spectroscopy

In order to characterize their chemical structure, FTIR spectroscopy measurements were carried out on random CMA-MMA copolymers. Reported in Figure 3.17 are the overlapping FTIR spectra of the three polymers.

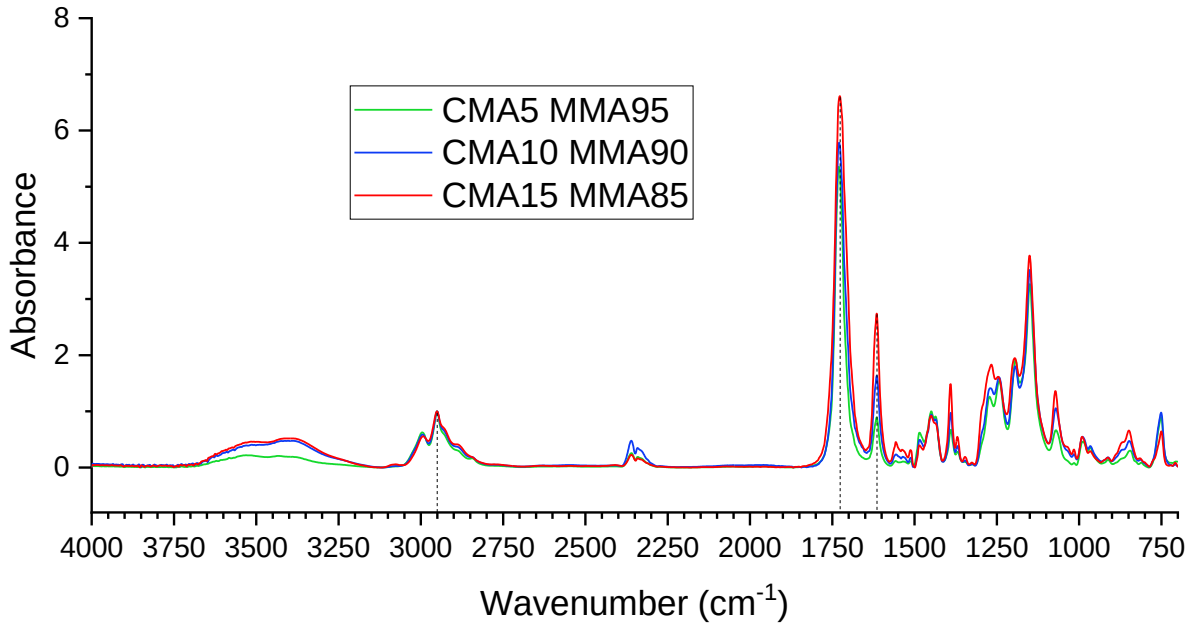

Figure 3.17 – Overlap of FTIR spectra of CMA-MMA random copolymers.

From the graph, peaks between 1150 and 1300 cm^{-1} are visible: these peaks are associated with C-O-C and C-C-O stretching and are characteristic of methyl methacrylate and poly methyl methacrylate. This is a first proof of the presence of MMA in the sample.

The peak at 2350 cm^{-1} is instead to be attributed to O=C=O stretching of carbon dioxide in the air and its intensity is independent of the concentration of the sample.

As better highlighted in Figure 3.18, the main peaks associated with coumarin increase proportionally with the amount of monomer in the sample.

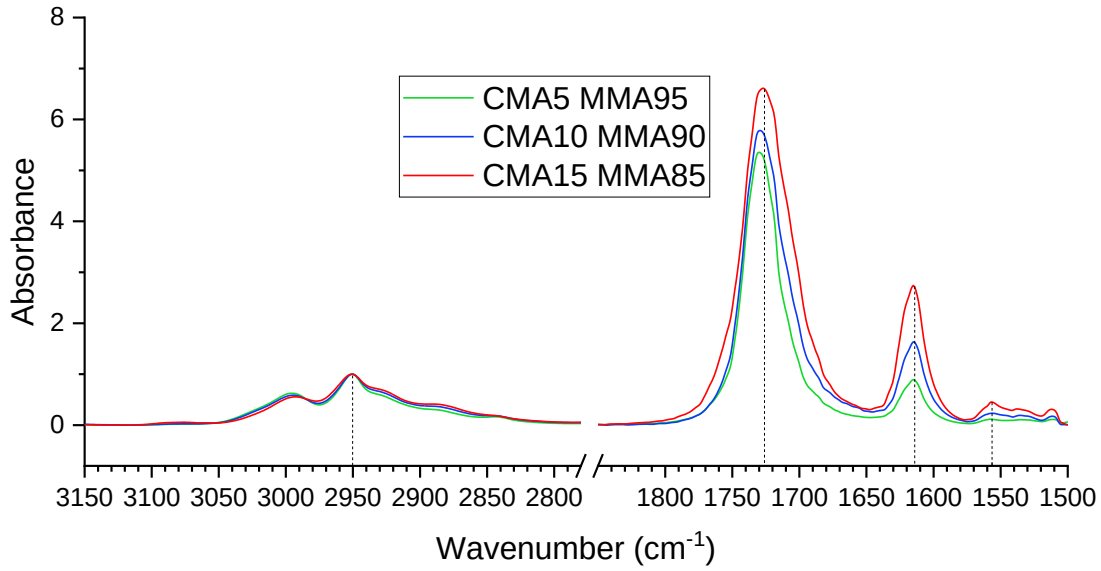

Figure 3.18 – Highlight of characteristics peaks in FTIR analyses of CMA-MMA random copolymers.

In particular, peaks ascribed to the stretching of C=O groups at 1720 and 1610 cm^{-1} seem to increase with an increased concentration of CMA in the polymer. On the contrary, peaks between 2900 and 3050 cm^{-1}, associated with aliphatic CH_2 groups, seem to neither decrease nor increase while varying the concentrations of monomers. Around 1550 cm^{-1}, the peak associated with the stretching of C=C peaks seems to increase as the concentration of CMA in the polymer increases.

Nuclear Magnetic Resonance Spectroscopy

NMR analyses were performed on polymer samples in order to assess their chemical structure; the results are reported in Figure 3.19.

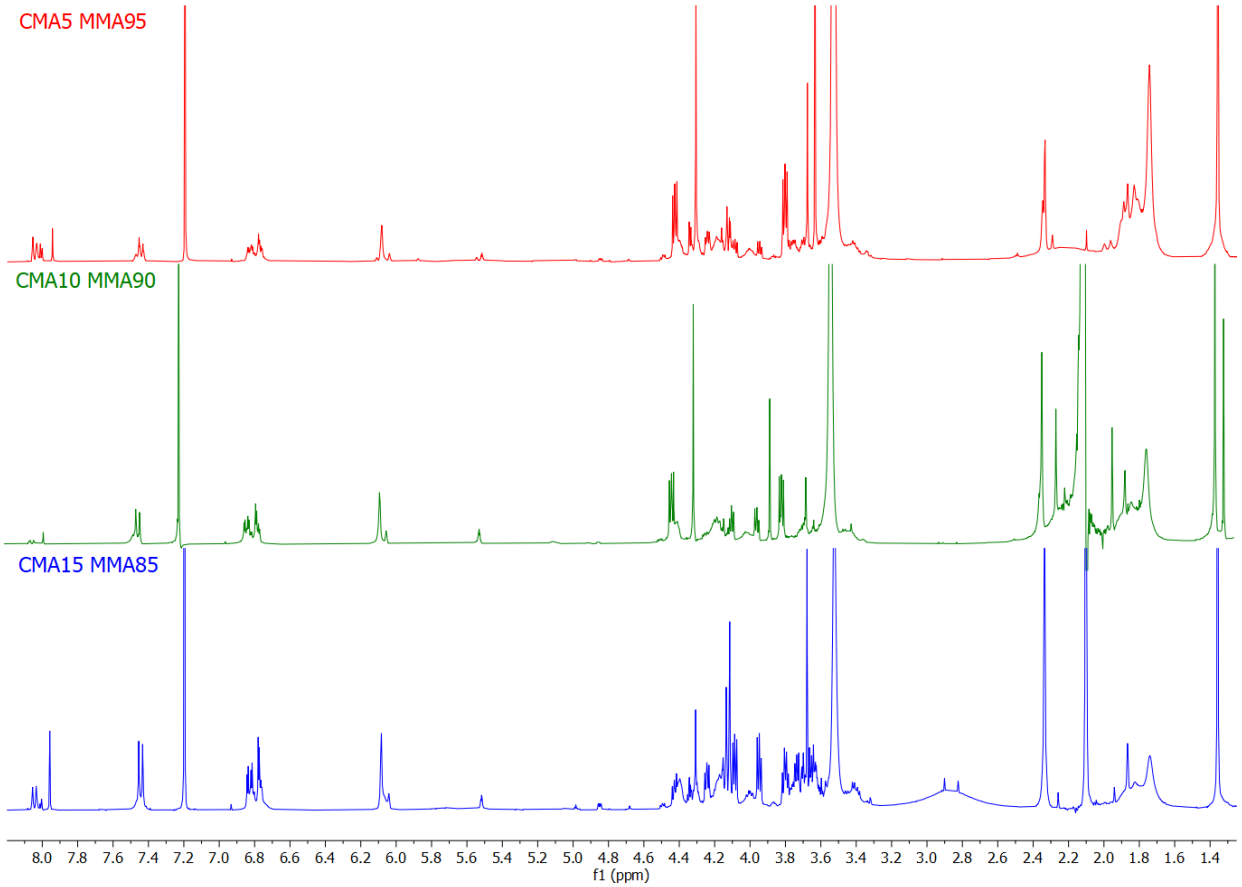

Figure 3.19 – NMR spectra of CMA-MMA random copolymers.

In the graph, characteristic peaks of both monomers are present and visible. In order to verify the successfulness of the polymerization, some calculations were performed on the NMR spectra.

First, a test to make sure that the reaction was successful was carried out: as shown in Figure 3.20, the signal between 2.0 and 1.62 ppm, corresponding to CH_2 groups in the polymeric chain, and the peaks between 1.07 and 0.62 ppm, corresponding to CH_3 groups in the chain, were integrated to obtain their area. By imagining an ideal polymethacrylate polymeric chain constituted by 100 repeating units, we can establish that the number of hydrogen atoms relative to CH_2 and CH_3 groups in the polymeric chain is always the same regardless of the composition of the polymer; that is, the concentration of monomers does not affect the number of hydrogen atoms in the backbone of the polymer since the methacrylate termination is common to all the monomers considered in this work. More specifically, every polymeric chain composed of 100 repeating units carries 200 hydrogen atoms from CH_2 groups and 300 hydrogen atoms from CH_3 groups. After the integration of the peaks, the so-obtained values of the area were normalized by dividing them respectively by 200 and 300 and compared between each other: if the polymerization is successful, the two resulting values, relative to the normalized integrals associated respectively to the CH_2 and CH_3 signals,

should be the same, otherwise it could mean that some unreacted monomers are still present in the polymeric sample.

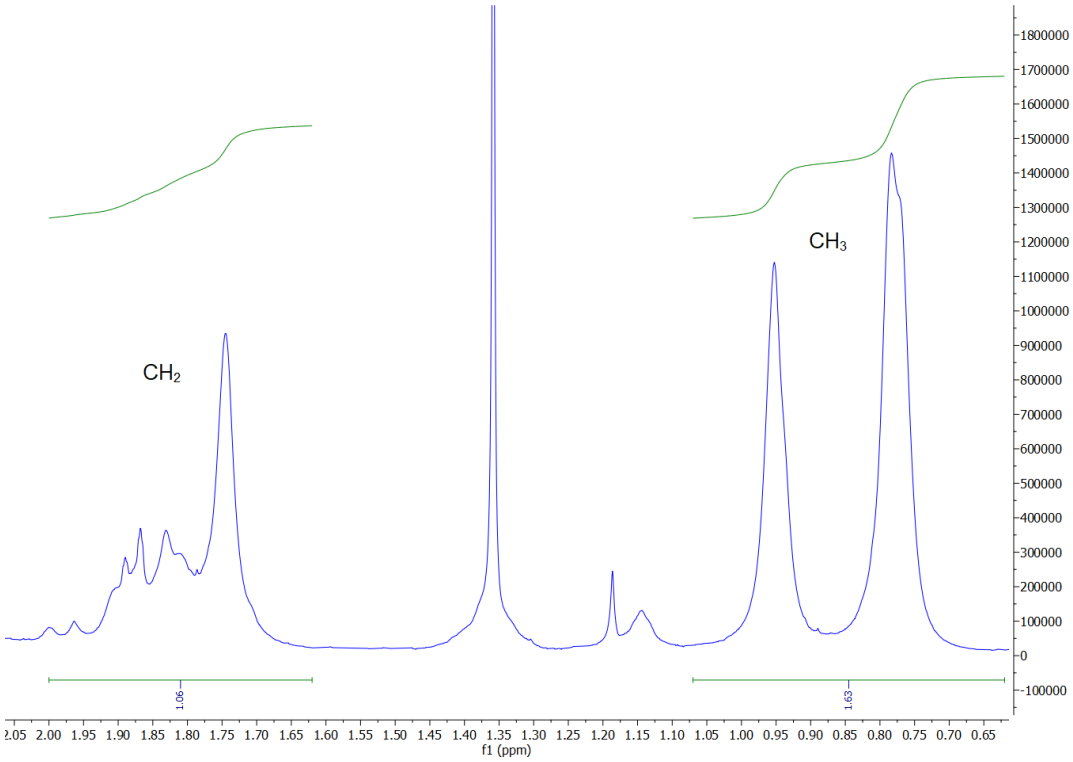

Figure 3.20 – NMR integration of in-chain CH_2 and CH_3 groups in CMA-MMA random copolymers.

Results of these calculations are reported in Table 3.2.

Table 3.2 – Results of NMR calculations on the number of in-chain H atoms in CMA-MMA random copolymers.

Batch Name	**Normalized CH_2**	**Normalized CH_3**
CMA5 MMA95	1	1.024
CMA10 MMA90	1	0.958
CMA15 MMA85	1	1.043

From these results, it seems like the polymerization was successful and all of the monomeric units were converted into a polymer.

A second test was performed to assess the concentration of the different monomeric units in the polymer samples. As shown in Figure 3.21, the signal centered around 6.1 ppm, corresponding to the hydrogen on the left ring of the coumarin bulk (H28 in Figure 3.3) in the CMA molecule, was chosen to infer the quantity of coumarin methacrylate in the copolymer, while the signal centered around 3.5 ppm, corresponding to the ester methyl on MMA, was chosen to assess the quantity of methyl methacrylate in the copolymer.

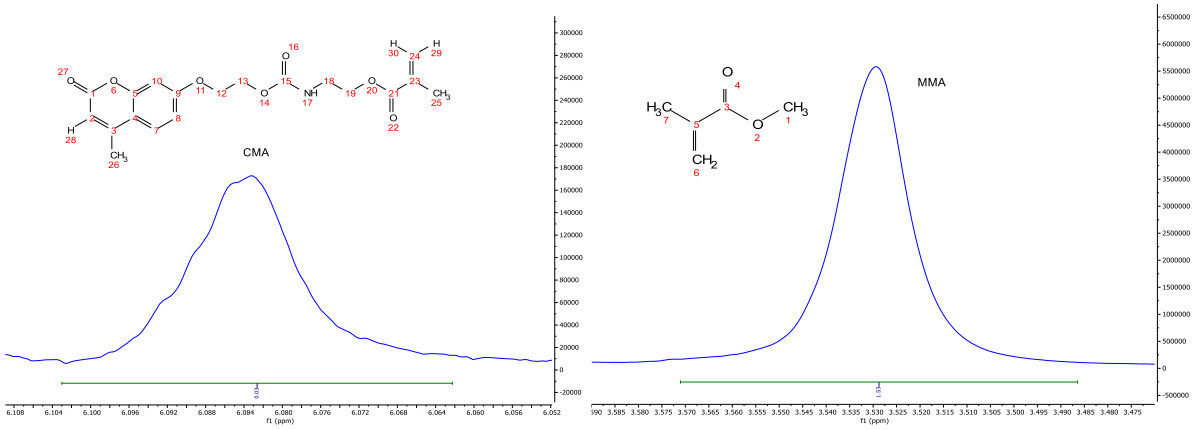

Figure 3.21 – NMR peaks corresponding to CMA and MMA in CMA-MMA random copolymers.

Similarly to the previous procedure, the peaks were integrated to obtain the value of their underlying area; these values were then compared with the theoretical values obtained by multiplying the area of the in-chain CH_2 previously calculated with the number of hydrogens relative to the monomers' peak and their initial concentration.

The formula used to calculate the theoretical areas is as follows:

$$A_{MONOMER_{TH}} = A_{CH_2} \cdot number\ of\ hydrogens\ relative\ to\ the\ signal \cdot feed\ \%_{mol}$$

For example, the theoretical areas for the polymer CMA5 MMA95 were obtained with this formula:

$$A_{CMA_{TH}} = A_{CH_2} \cdot 1 \cdot 5 \qquad A_{MMA_{TH}} = A_{CH_2} \cdot 3 \cdot 95$$

The theoretical (relative to the feed) and real area values are then compared to check the grade of luminophore incorporation. By normalizing the real area values obtained from the NMR graphs it was possible to obtain the real composition of the polymers, reported in Table 3.3, using the formula reported below:

$$CMA\%_{mol/mol} = \frac{\frac{A_{CMA_{REAL}}}{n^{\circ}\ of\ H\ relative\ to\ the\ signal}}{\frac{A_{CMA_{REAL}}}{n^{\circ}\ of\ H\ relative\ to\ the\ signal} + \frac{A_{MMA_{REAL}}}{n^{\circ}\ of\ H\ relative\ to\ the\ signal}}$$

Table 3.3 – Real composition of CMA-MMA random copolymers.

Batch Name	**Feed CMA%$_{mol/mol}$**	**Normalized CMA%$_{mol/mol}$**	**Feed MMA%$_{mol/mol}$**	**Normalized MMA%$_{mol/mol}$**
CMA5 MMA95	5%	5.96%	95%	94.04%
CMA10 MMA90	10%	13.03%	90%	86.97%
CMA15 MMA85	15%	22.12%	85%	77.88%

From these results, it can be inferred that the polymerization is less controllable as the concentration of coumarin is increased in the initial reaction solution. In fact, while the final and initial concentrations are almost the same in CMA5 MMA95, the real coumarin methacrylate concentration in CMA15 MMA85 is much higher than the ideal one. This

could be due to the fact that a higher initial concentration of CMA prevents the total conversion of MMA during the polymerization reaction; furthermore the reactivity ratio of CMA could be higher than that of MMA, resulting in easier incorporation in the chain.

UV-Vis Absorbance

As will be better described later on, UV-Vis absorbance measurements were performed on copolymers spin-coated on soda glass slabs. The coatings were made by depositing a 3% weight solution of polymer in chloroform with the same operating conditions, so that the coatings had the same thickness. The results from the UV-Vis measurements are reported in Figure 3.22.

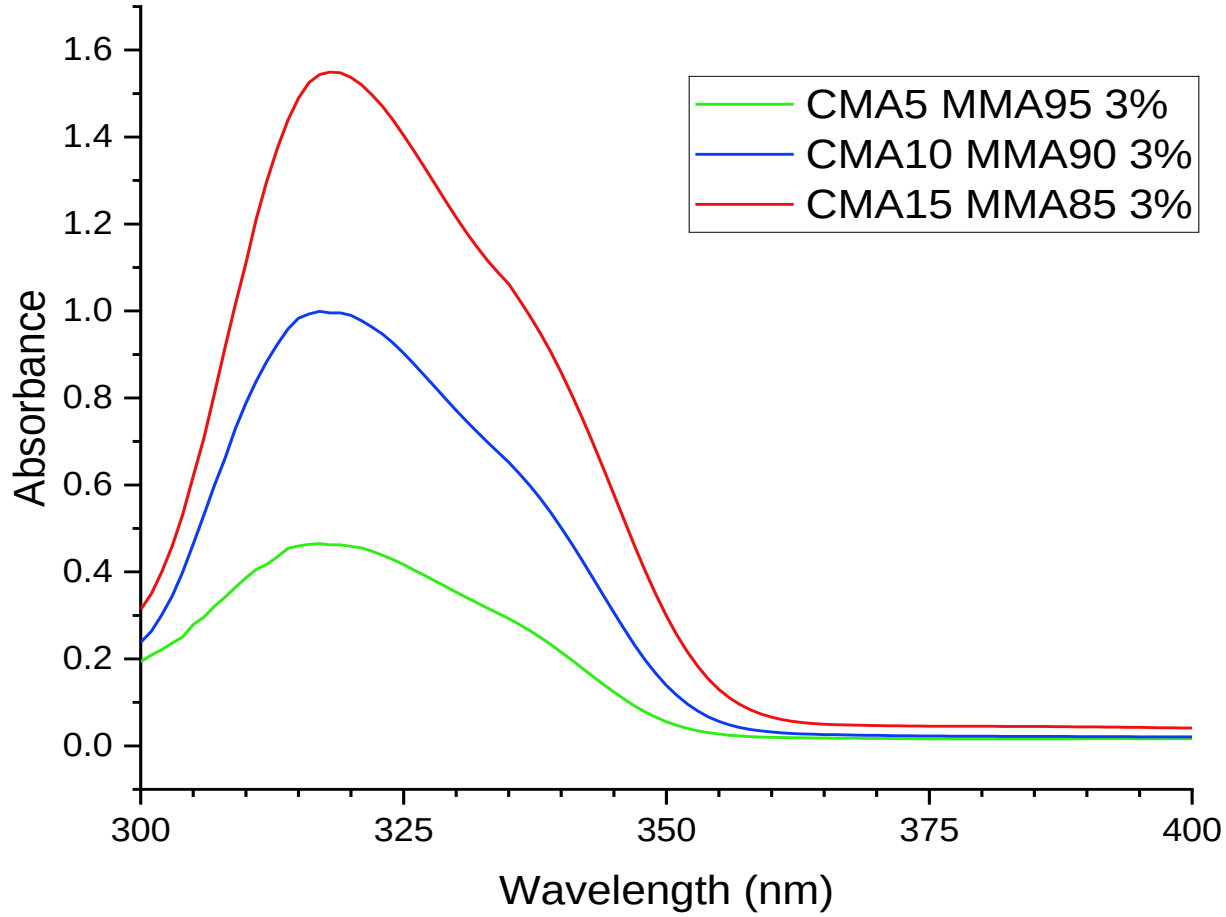

Figure 3.22 – UV-Vis absorbance measurements on CMA-MMA random copolymers.

From the graph, the linear increase in absorbance of the samples with the concentration of the methacrylate dye in the polymer indicates the excellent incorporation of CMA monomer into polymer chains during the polymerization reaction.

Fluorescence Spectroscopy

After absorbance measurements, fluorescence spectroscopy measurements were performed on the same glass slabs excited at $\lambda = 350\,nm$. The results are shown in Figure 3.23.

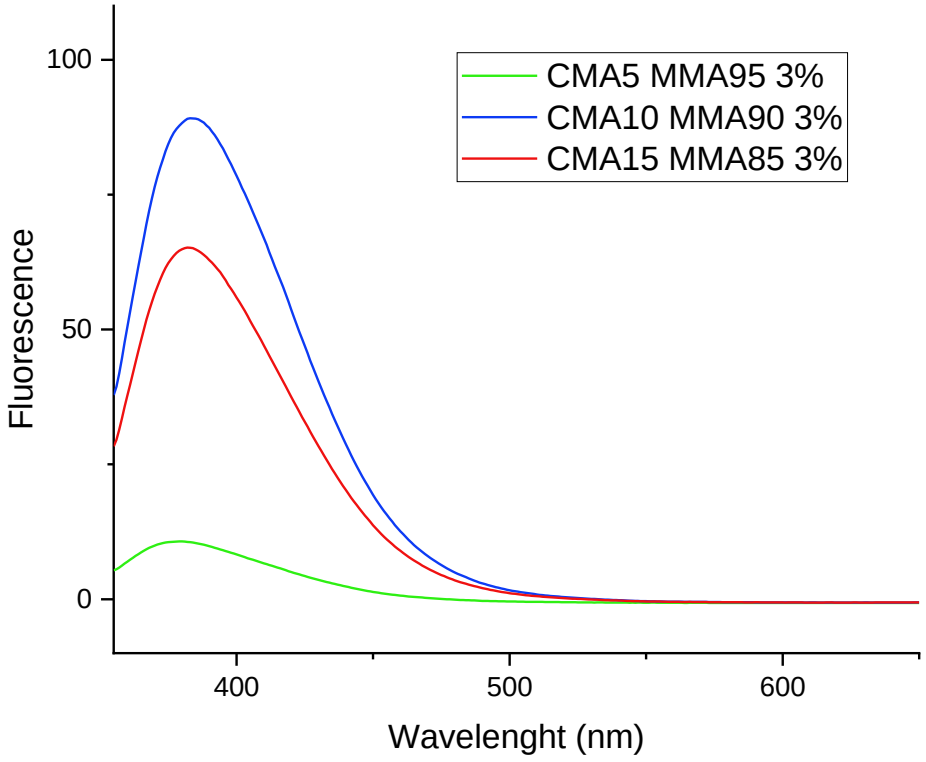

Figure 3.23 – Fluorescence spectroscopy measurements on CMA-MMA random copolymers.

As it can be noticed, the fluorescence increases with the concentration of coumarin in the polymer.

3.2.2 Perylene Methacrylate/Methyl Methacrylate Copolymers

Polymer samples with 0.025%, 0.050% and 0.100% molar of PMA (while the rest is MMA) were synthesized. In the following graphs, they are called PMA0.025 MMA99.975, PMA0.050 MMA99.950 and PMA0.100 MMA99.900, respectively.

Gel Permeation Chromatography

GPC analyses were performed on the samples to determine their molecular weight. The resulting elution curves are reported in Figure 3.24.

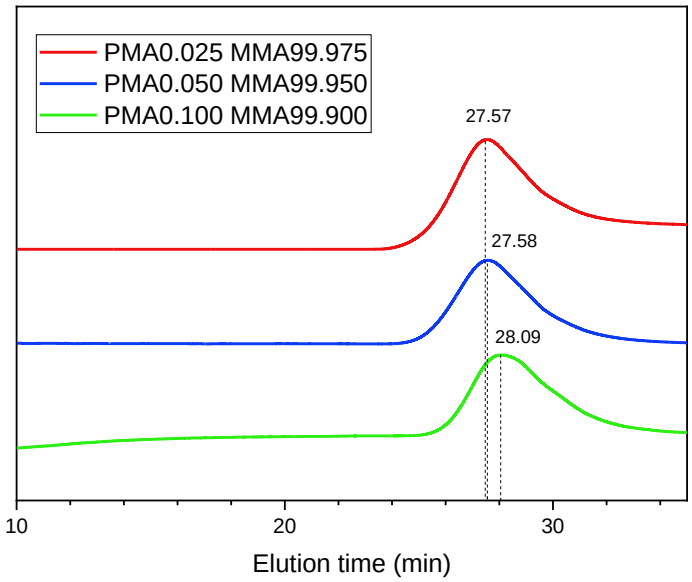

Figure 3.24 – GPC analyses of PMA-MMA random copolymers.

Reported in Table 3.4 are the main results after the integration of the GPC curves, showing the number averaged molecular weight, the weight averaged molecular weight and the polydispersity index.

Table 3.4 – Results of GPC analyses on PMA-MMA random copolymers.

Batch Name	**Mn**	**Mw**	**PDI**
PMA0.025 MMA99.975	69164	99899	1.44
PMA0.050 MMA99.950	64700	96062	1.48
PMA0.100 MMA99.900	43534	71462	1.64

These findings demonstrate that while increasing the concentration of PMA in the reaction solution, the molecular weight of the final polymer slightly decreases. One possible explanation is that since PMA is such a large molecule, its steric hindrance is too high and it results in harder incorporation of the luminescent monomer.

Differential Scanning Calorimetry

Differential scanning calorimetry measurements were performed on PMA-MMA random copolymers. The results are shown in Figure 3.25.

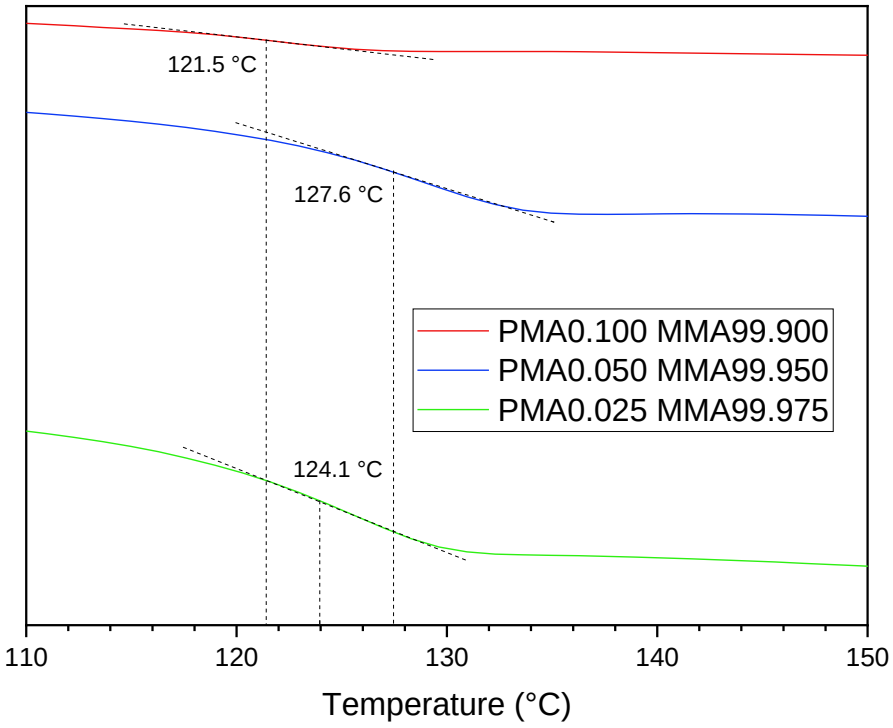

Figure 3.25 – DSC analyses on PMA-MMA random copolymers.

From the DSC scans, it can be proved that the polymerization was successful since only one transition peak is present. Furthermore, it seems that the initial concentration of PMA does not have a significant impact on the Tg of the final polymer, which is around 121 - 127 °C for all the samples. The Tg seems to follow a decreasing trend while the concentration of the PMA increases, as will be later confirmed by NMR calculations.

Fourier Transform Infrared Spectroscopy

Fourier transform IR spectroscopy measurements were performed on PMA-MMA random copolymers, as shown in Figure 3.26.

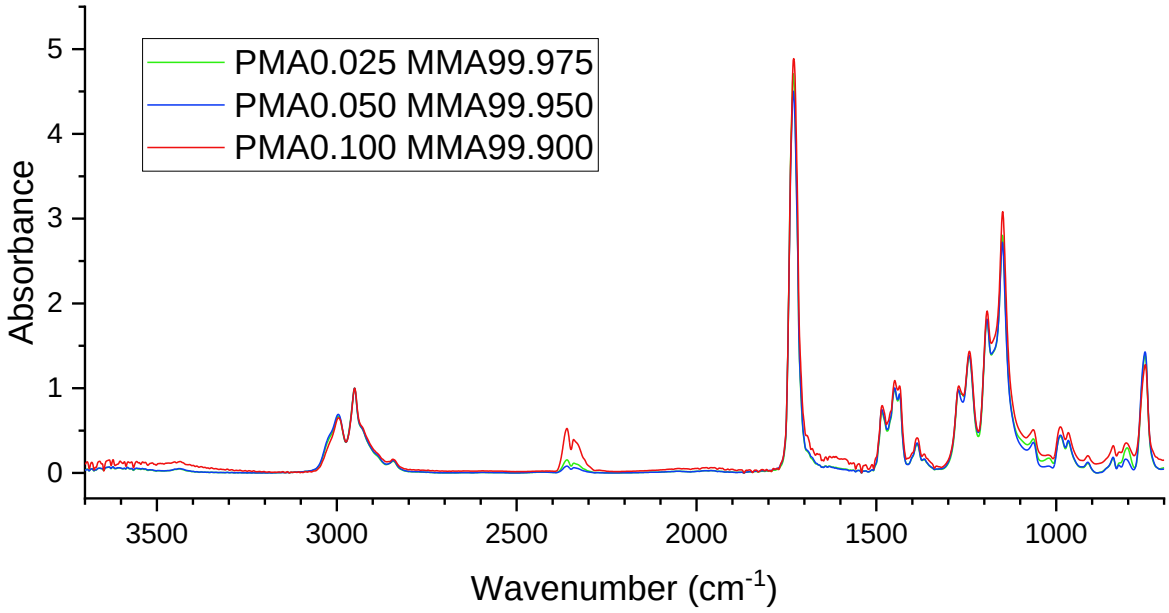

Figure 3.26 – FTIR spectroscopy results on PMA-MMA random copolymers.

As better highlighted in Figure 3.27, the characteristic peaks associated with aliphatic CH_2 bonds between 2850 and 3050 cm^{-1} are almost constant while increasing the concentration of perylene in the polymer.

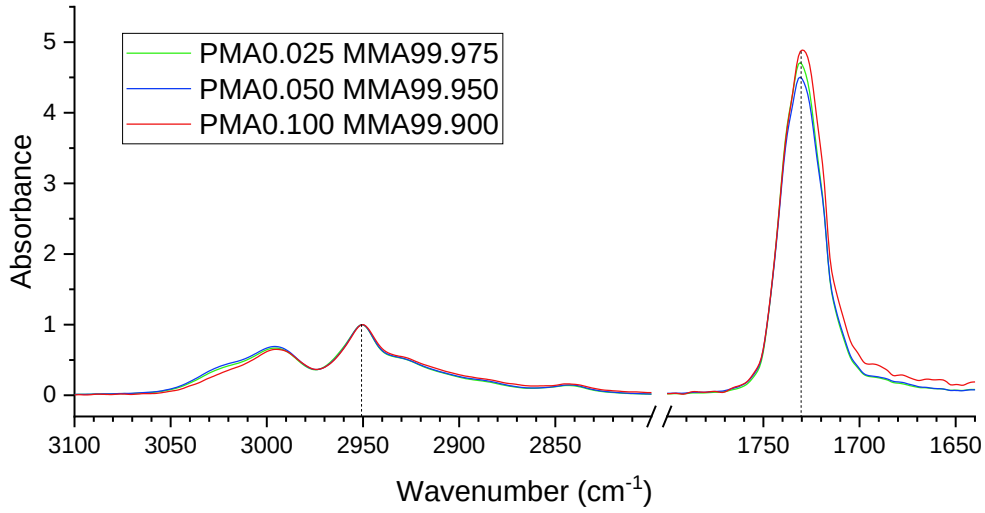

Figure 3.27 – Highlight of characteristic peaks in FTIR analyses of PMA-MMA random copolymers.

On the other hand, the intensity of the peak at 1730 cm^{-1}, associated with the stretching movement of the C=O bond of the secondary amide, seems to be correlated with the quantity of PMA in the sample. The trend, however, is not clear: this is probably due to the fact that the concentration of PMA in the polymer is very low, and such a small change is hardly distinguishable via FTIR spectroscopy.

Nuclear Magnetic Resonance Spectroscopy

NMR analyses were performed on polymer samples in order to assess their chemical structure; the results are reported in Figure 3.28.

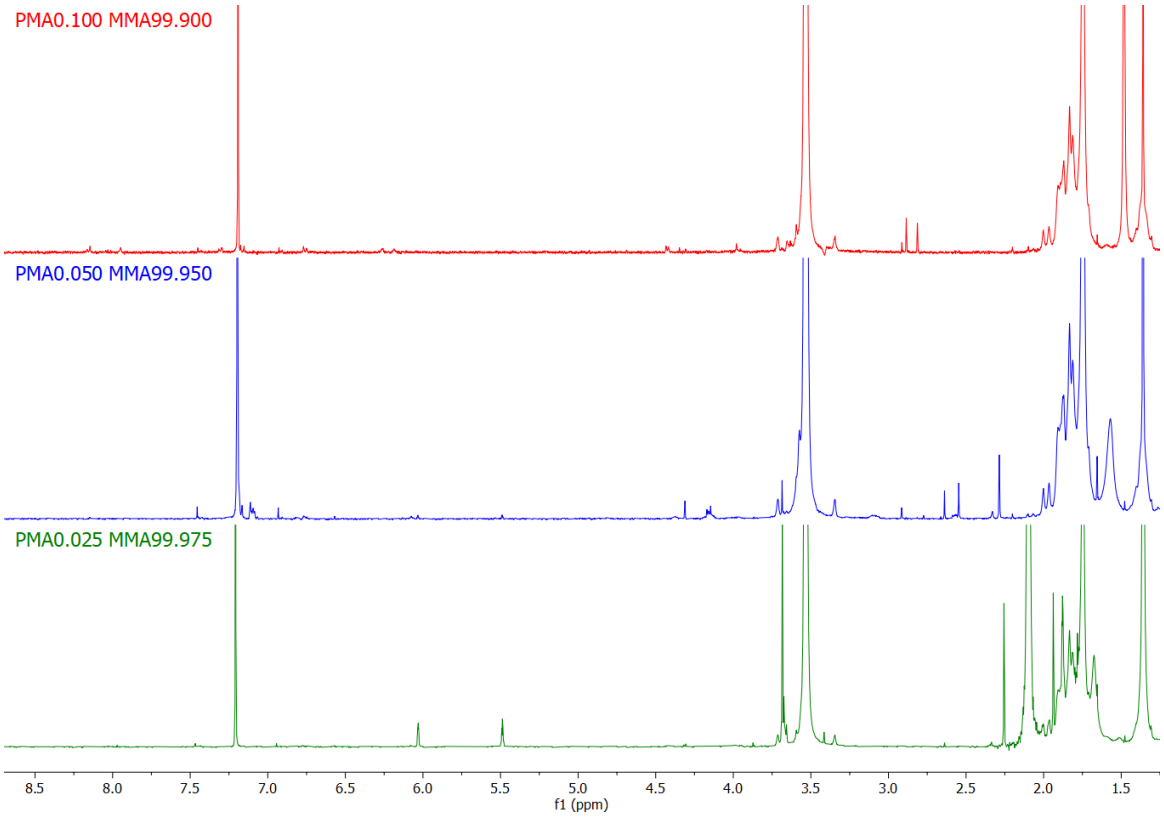

Figure 3.28 – NMR spectra of PMA-MMA random copolymers.

In the graph, characteristic peaks of both monomers are present. In order to verify the successfulness of the polymerization, some calculations were performed on the NMR spectra.

Similarly to the case of CMA-MMA random copolymers, a comparison between the normalized area value of CH_2 and CH_3 groups was made to verify the successfulness of the polymerization reaction. The results of these calculations are reported in Table 3.5.

Table 3.5 - Results of NMR calculations on the number of in-chain H atoms in PMA-MMA random copolymers

Batch Name	**Normalized CH_2**	**Normalized CH_3**
PMA0.025 MMA99.975	1	0.847
PMA0.050 MMA99.950	1	1.070
PMA0.100 MMA99.900	1	1.120

From these results, it seems like the polymerization was successful and the vast majority of monomeric units were converted into a polymer.

Again, a second test was performed to assess the concentration of the different monomeric units in the polymer samples. The peak around 8.15 ppm, corresponding to the 4 external hydrogen atoms in the perylene bulk rings in the PMA molecule, was chosen to infer the quantity of perylene methacrylate in the copolymer. Like before, the peak around 3.5 ppm was chosen to check the quantity of MMA.

Similarly to the previous procedure, the peaks were integrated to obtain the value of their underlying area; these values are then compared with the theoretical values obtained by multiplying the area of the in-chain CH_2 previously calculated with the number of hydrogens relative to the peak and the initial concentration of the monomers. For example, the theoretical areas for the polymer PMA0.025 MMA99.975 were obtained with this formula:

$$A_{PMA} = A_{CH_2} \cdot 4 \cdot 0.025 \qquad A_{MMA} = A_{CH_2} \cdot 3 \cdot 99.975$$

The theoretical (relative to the feed) and real area values are then compared to check the grade of luminophore incorporation. By normalizing the real area values obtained from the NMR graphs it was possible to obtain the real composition of the polymers, reported in Table 3.6, using the formula reported below:

$$PMA\%_{mol/mol} = \frac{\frac{A_{PMA_{REAL}}}{n^{\circ}\ of\ H\ relative\ to\ the\ signal}}{\frac{A_{PMA_{REAL}}}{n^{\circ}\ of\ H\ relative\ to\ the\ signal} + \frac{A_{MMA_{REAL}}}{n^{\circ}\ of\ H\ relative\ to\ the\ signal}}$$

Table 3.6 – Real composition of PMA-MMA random copolymers.

Batch Name	**Feed PMA%$_{mol/mol}$**	**Normalized PMA%$_{mol/mol}$**	**Feed MMA%$_{mol/mol}$**	**Normalized MMA%$_{mol/mol}$**
PMA0.025 MMA99.975	0.025%	0.021%	99.975%	99.979%
PMA0.050 MMA99.950	0.050%	0.015%	99.950%	99.985%
PMA0.100 MMA99.900	0.100%	0.077%	99.900%	99.923%

NMR calculations results show that the amount of PMA in the feed does not correspond perfectly with the final amount of perylene methacrylate present in the copolymer. In particular, PMA0.050 MMA99.950 seems to have a lower concentration of incorporated perylene than PMA0.025 MMA99.975. While this does not seem to be confirmed by absorption and fluorescence spectroscopy measurements, it may be an indication of the fact that being PMA such a big molecule, the results of random polymerization could be unpredictable and not as expected.

Another thing to note is that since the concentration of PMA in the polymers is very low, the NMR signal associated with the perylene hydrogens is also very small compared to the MMA signal. Thus, the calculations could be subject to a higher degree of error than in the case of CMA-MMA random copolymers.

UV-Vis Absorbance

As will be better described later on, UV-Vis absorbance measurements were performed on copolymers spin-coated on soda glass slabs. The slabs were prepared by depositing a 3% weight solution of polymer in chloroform. The results from the UV-Vis measurements are reported in Figure 3.29.

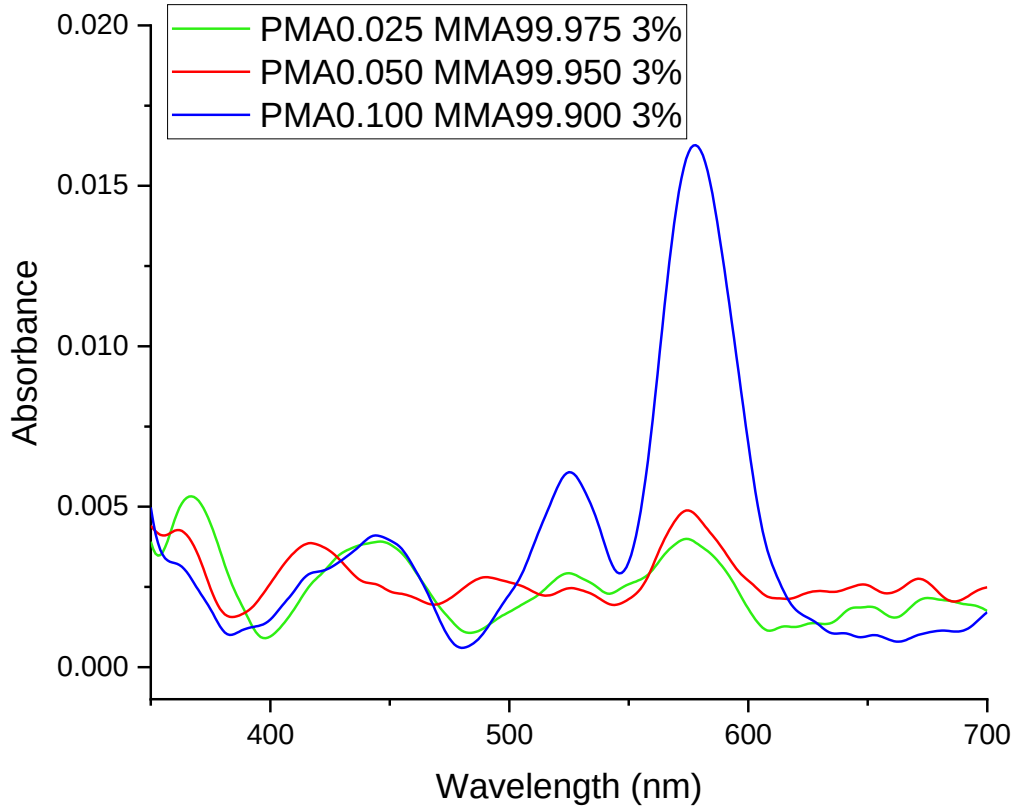

Figure 3.29 – UV-Vis absorbance measurements on PMA-MMA random copolymers.

As noticeable from the graph, a higher concentration of perylene in the polymer corresponds to a higher final absorbance, although no trend is observed. In particular, PMA0.025 MMA99.975 and PMA0.050 MMA99.950 seem to have similar values of absorbance.

In general, the absorbance of the samples is very low and the signal is noisy; this is probably due to the very low concentration of dye present on the glass slab. Measurements at higher polymer concentrations were not performed due to a lack of material.

Fluorescence Spectroscopy

After absorbance measurements, fluorescence spectroscopy measurements were performed on the same glass slabs excited at $\lambda = 350\,nm$ and $\lambda = 450\,nm$. The results are shown in Figure 3.30.

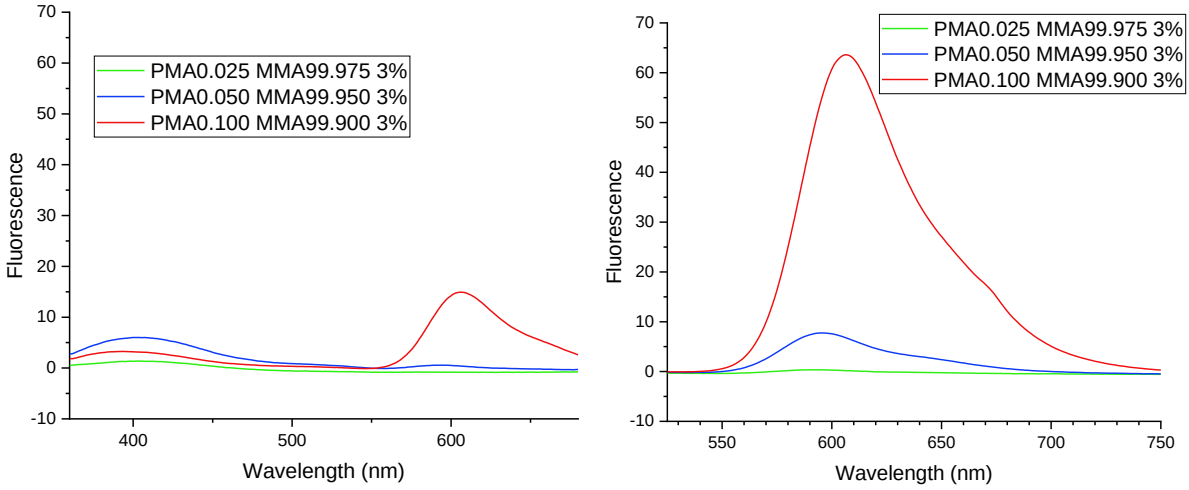

Figure 3.30 – Fluorescence spectroscopy measurements on PMA-MMA random copolymers excited at 350 nm (left) and 450 nm (right).

The polymers were excited at both wavelengths to check whether or not perylene showed a fluorescence emission when excited at the maximum absorption wavelength of coumarin. As it can be seen, the fluorescence of the samples is much higher when excited at 450 nm, since perylene absorbs much more at that wavelength. Furthermore, it can be seen from the graph on the right how the fluorescence emission increases with the amount of PMA present in the polymer.

3.2.3 Terpolymers

Polymer samples with 10% molar of CMA and 0.025%, 0.050% and 0.100% molar of PMA (while the rest is MMA) were synthesized. In the following graphs, they are called respectively CMA10 PMA0.025 MMA89.975, CMA10 PMA0.050 MMA89.950 and CMA10 PMA0.100 MMA89.900. The 10% molar concentration for CMA was chosen because, as seen in Figure 3.23, it seems like the best compromise between low absorbance and fluorescence (displayed by CMA5 MMA95) and quenching or reabsorption losses phenomena (displayed by CMA15 MMA85).

Gel Permeation Chromatography

GPC analyses were performed on the samples to determine their molecular weight. The resulting elution curves are reported in Figure 3.31.

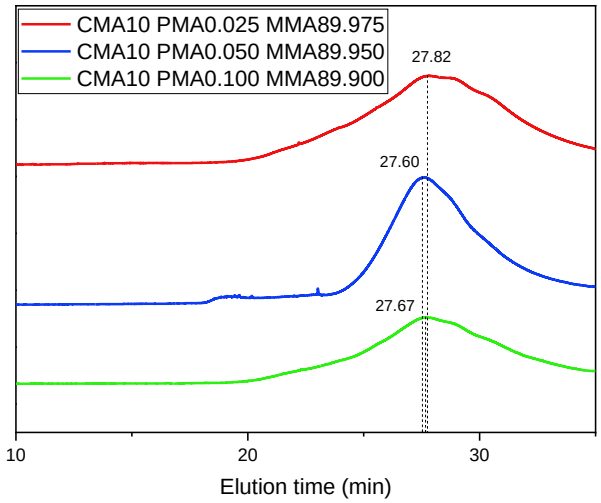

Figure 3.31 – GPC analyses of CMA-PMA-MMA terpolymers.

Reported in are the main results after the integration of the GPC curves, showing the number averaged molecular weight, the weight averaged molecular weight and the polydispersity index.

Table 3.7 – Results of GPC analyses on CMA-PMA-MMA random terpolymers

Batch Name	**Mn**	**Mw**	**PDI**
CMA10 PMA0.025 MMA89.975	35526	176224	4.96
CMA10 PMA0.050 MMA89.950	50858	178279	3.51
CMA10 PMA0.100 MMA89.900	48528	94592	1.95

It is clear from these results that no clear trend can be established since the molecular weight of the samples and their composition do not seem to be strictly correlated. Instead, it is possible that the molecular weight and the polydispersity index are more influenced by the conditions in which the reaction occurs, since both methacrylate dyes are bulky and can interfere with the progress of the radical polymerization.

The PDI of the polymers is also quite broad: this is undesirable since it could affect the processability of the polymer.

Differential Scanning Calorimetry

Differential scanning calorimetry measurements were performed on terpolymer samples. The results are shown in Figure 3.32.

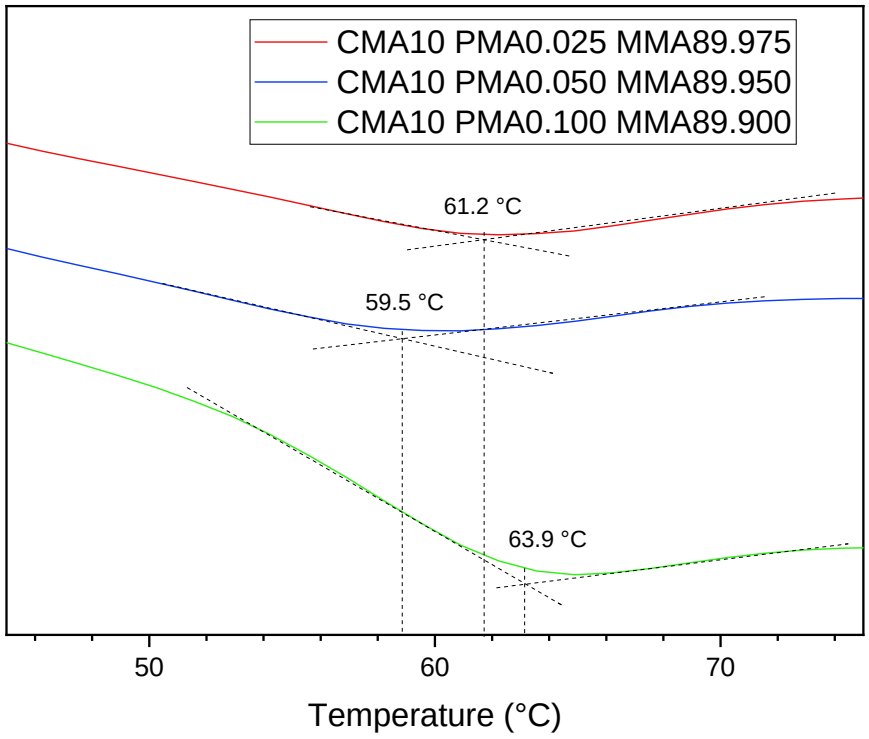

Figure 3.32 – DSC curves of CMA-PMA-MMA random terpolymers.

From the curves, it can be noticed that only one transition signal centered is present: this is an indicator that the polymerization was successful. Still, no influence of the composition of the terpolymer on the glass transition temperature was established. This could be ascribed to the low PMA content. The Tg is around 61 °C for all three samples.

Fourier Transform Infrared Spectroscopy

FTIR spectroscopy measurements were performed on random CMA-PMA-MMA terpolymers; the results are shown in Figure 3.33.

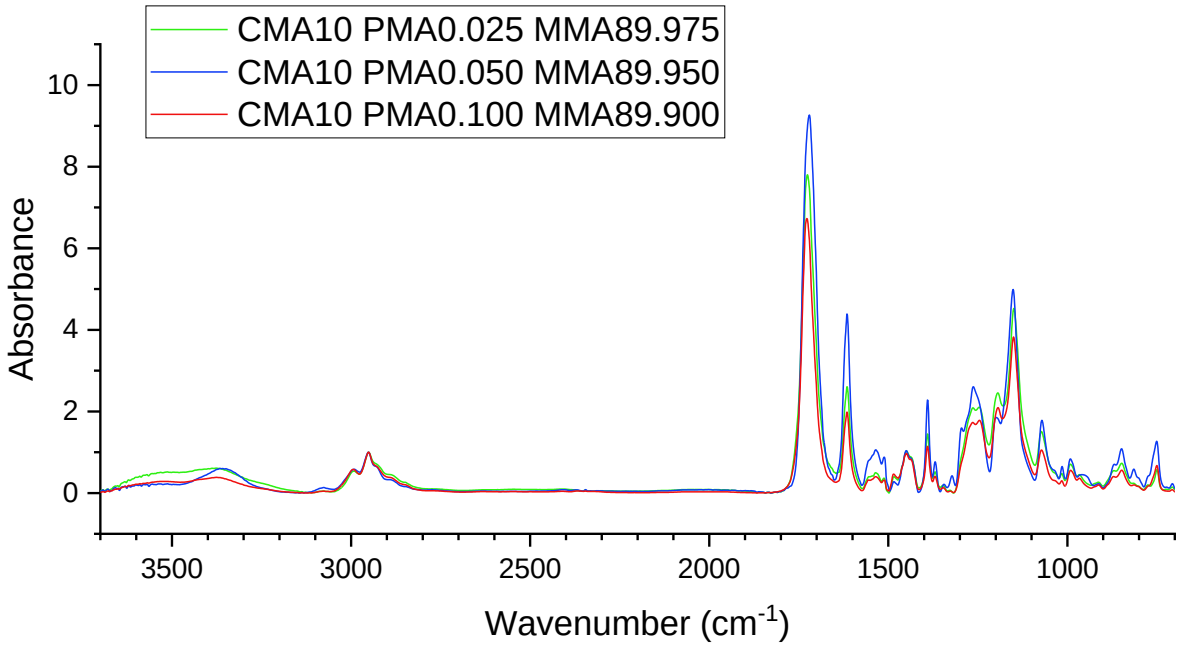

Figure 3.33 – Results of FTIR spectroscopy analyses on CMA-PMA-MMA random terpolymers.

As better highlighted in Figure 3.34, no clear trend can be established between the composition and the intensity of the FTIR peaks.

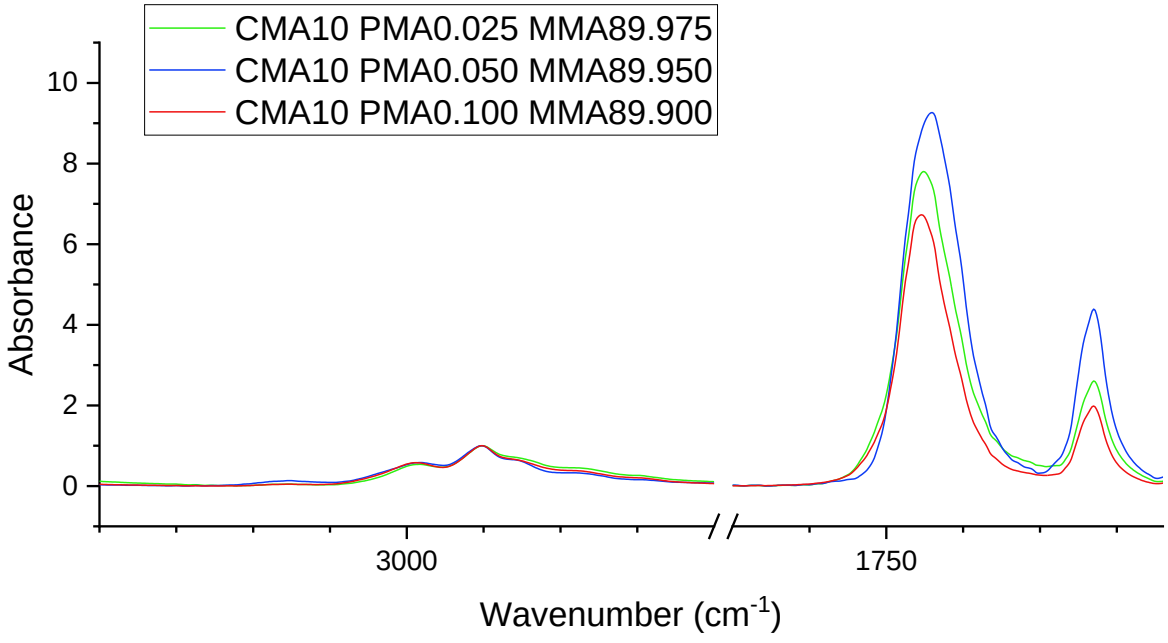

Figure 3.34 – Highlight of characteristic peaks in FTIR analyses of CMA-PMA-MMA random terpolymers.

Finally, owing to the very low amount of PMA incorporated into the terpolymer with respect to CMA, in FTIR spectra the peaks related to PMA were found to be not clearly distinguishable. Hence, more sensitive characterization techniques, such as NMR

spectroscopic analysis was also performed with the aim of assessing the real terpolymer composition.

Nuclear Magnetic Resonance Spectroscopy

NMR analyses were performed on the terpolymers, as shown in Figure 3.35.

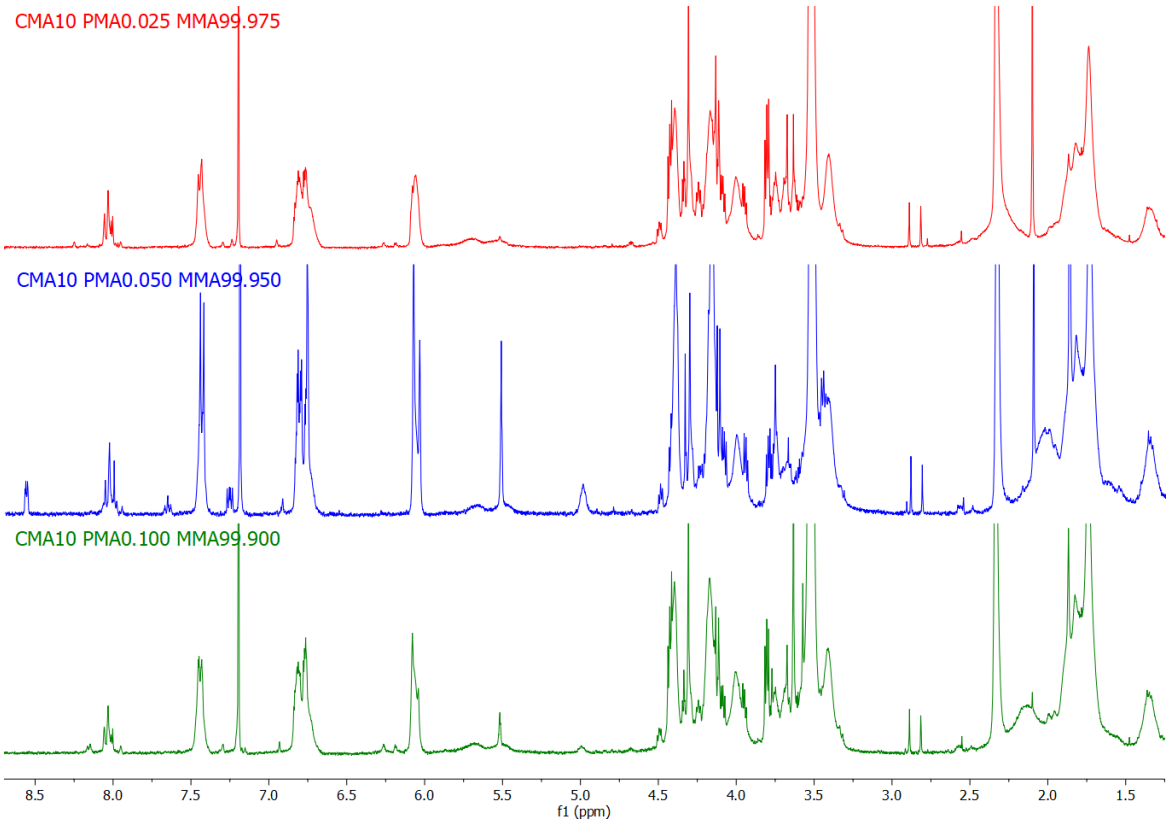

Figure 3.35 – Results of NMR analyses on CMA-PMA-MMA terpolymers.

In the graph, characteristic peaks of all three monomers are present and visible. Like before, some calculations were performed on the NMR spectra in order to verify the successfulness of the polymerization.

Table 3.8 - Results of NMR calculations on the number of in-chain H atoms in CMA-PMA-MMA random terpolymers

Batch Name	**Normalized CH_2**	**Normalized CH_3**
CMA10 PMA0.025 MMA89.975	1	1.111
CMA10 PMA0.050 MMA89.950	1	1.051
CMA10 PMA0.100 MMA89.900	1	0.866

A comparison between the normalized area value of CH_2 and CH_3 groups was made to verify the successfulness of the polymerization reaction. The results of these calculations are reported in Table 3.8.

These findings showed that the polymerization was mostly successful and the vast majority of monomeric units were converted into a polymer.

Again, a second test was performed to assess the concentration of the different monomeric units in the polymer samples. Some characteristic peaks were considered for each monomer: the singlet around 8.15 ppm for PMA, the one around 6.1 ppm for CMA and the peak around 3.5 ppm for MMA.

Similarly to the previous procedure, the peaks were integrated to obtain the value of their underlying area; these values are then compared with the theoretical values obtained by multiplying the area of the in-chain CH_2 previously calculated with the number of hydrogens relative to the peak and the initial concentration of each monomer.

The theoretical (relative to the feed) and real area values are then compared to check the grade of luminophore incorporation. By normalizing the real area values obtained from the NMR graphs it was possible to obtain the real composition of the polymers, reported in Table 3.9, using the formula reported below:

$$CMA\% = \frac{\frac{A_{CMA_{REAL}}}{n\ of\ H\ relative\ to\ signal}}{\frac{A_{CMA_{REAL}}}{n\ of\ H\ relative\ to\ signal} + \frac{A_{PMA_{REAL}}}{n\ of\ H\ relative\ to\ signal} + \frac{A_{MMA_{REAL}}}{n\ of\ H\ relative\ to\ signal}}$$

Table 3.9 – Real composition of CMA-PMA-MMA random terpolymers.

Batch Name	**Normalized vs feed CMA%$_{mol/mol}$**	**Normalized vs feed PMA%$_{mol/mol}$**	**Normalized vs feed MMA%$_{mol/mol}$**
CMA10 PMA0.025 MMA89.975	18.124% 10%	0.035% 0.025%	81.841% 89.975%
CMA10 PMA0.050 MMA89.950	18.035% 10%	0.039% 0.050%	81.926% 89.950%
CMA10 PMA0.100 MMA89.900	15.764% 10%	0.120% 0.100%	84.116% 89.900%

The results of the calculations seem to confirm the data obtained from the NMR calculations on random copolymers. More specifically, the amount of incorporated CMA seems to be higher than the theoretical value, while the amount of PMA is variable

and no clear trend can be established, although the real amount of perylene seems to somewhat follow the theoretical one.

UV-Vis Absorbance

The absorption spectra of random CMA-PMA-CMA terpolymers was measured with a UV-Vis spectrometer. 3% and 10% weight solutions of terpolymers in chloroform were spin-coated on soda glass slabs, and the resulting spectra are shown in Figure 3.36

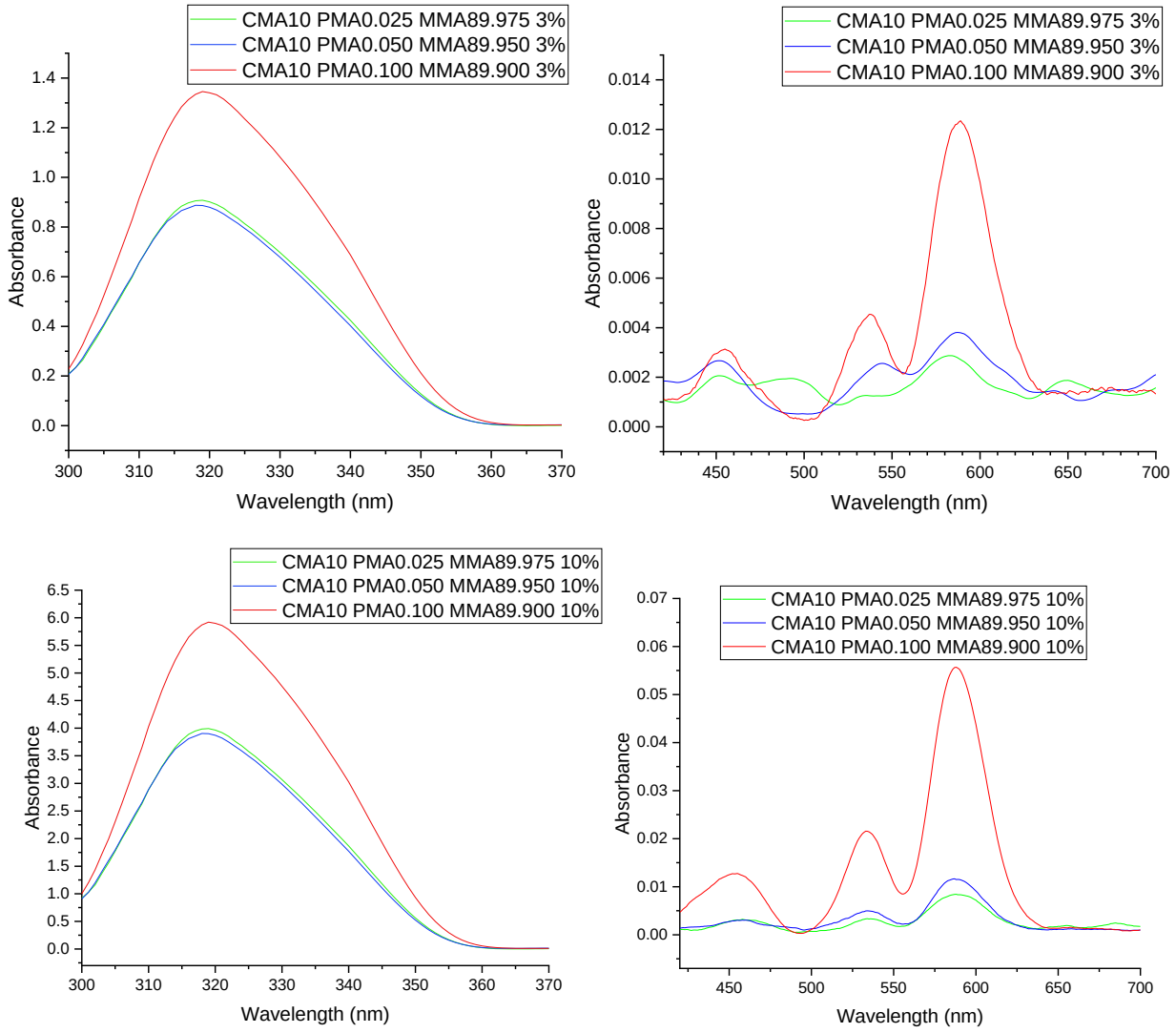

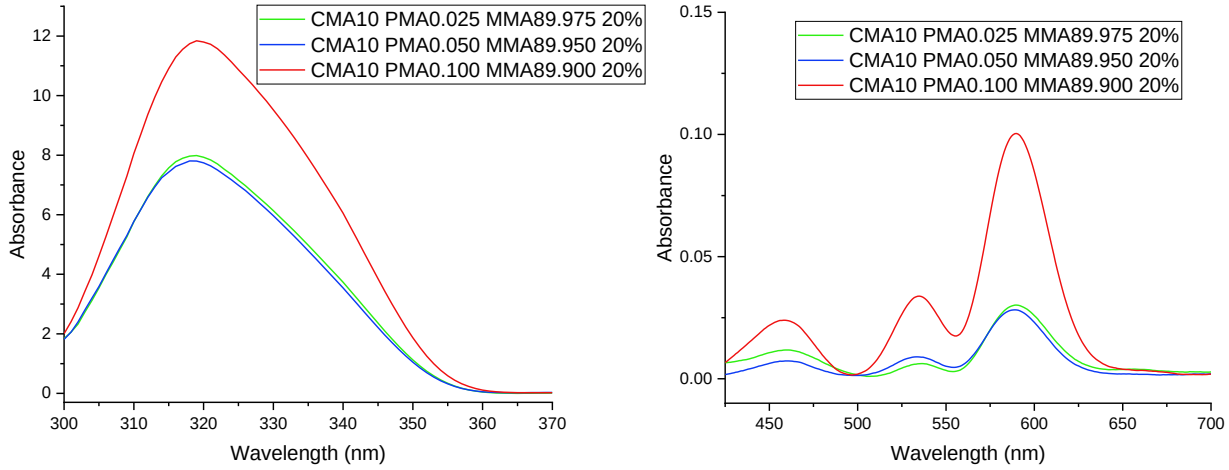

Figure 3.36 – UV-Vis absorption spectra of random CMA-PMA-MMA terpolymers in 3% (above) and 10% concentration (center) and 20% weight (below).

As it can be noticed from the figure above, the absorption spectrum relative to coumarin methacrylate resulted to be much higher compared to the absorption of perylene, given the much higher concentration in the polymer. Furthermore, it is clear that the absorbance relative to the CMA content should be similar between all the terpolymers since the content of coumarin is constant; the reason the absorbance of CMA10 PMA0.100 MMA89.900 is higher compared to the other samples is that the polymer solution in chloroform is much more viscous due to its molecular weight characteristics and a film with higher thickness results from the spin-coating process.

Fluorescence Spectroscopy and FRET Assessment

The fluorescence spectra of CMA-PMA-MMA random terpolymers were also measured with a fluorescence spectrometer, as shown in Figure 3.37.

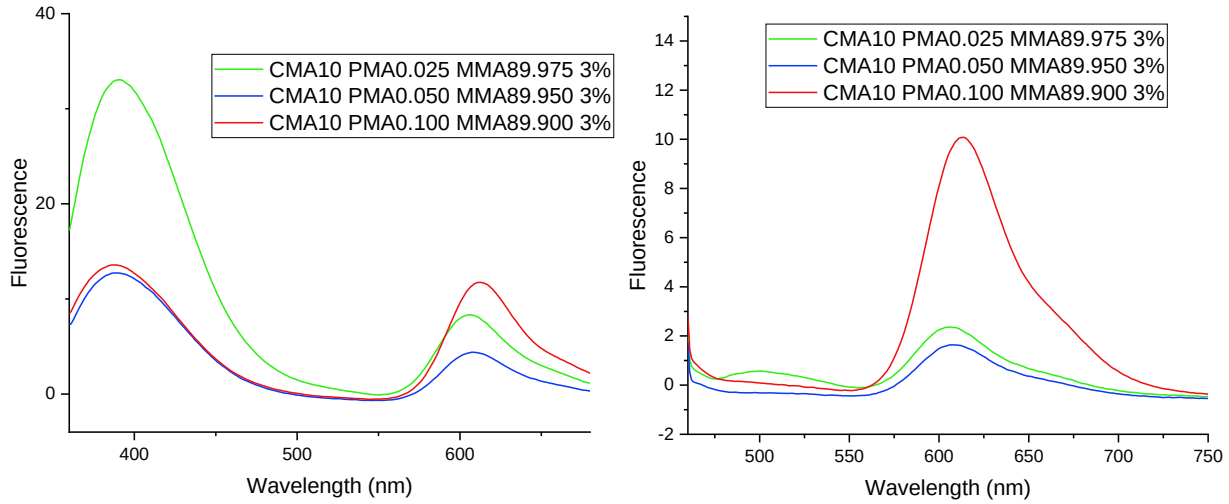

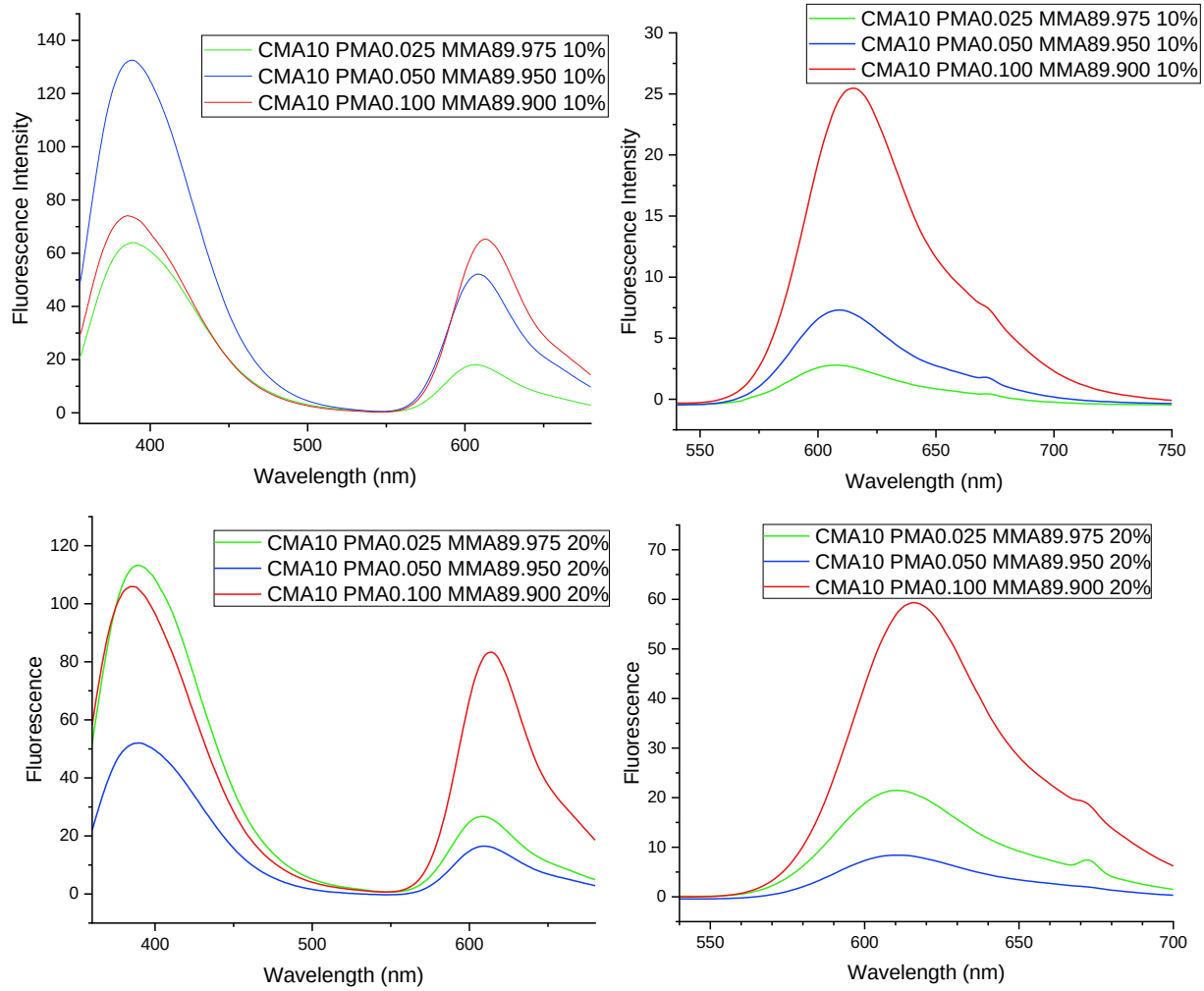

Figure 3.37 – Fluorescence spectra of CMA-PMA-MMA random terpolymers excited at $\lambda = 350\ nm$ (left column) and $\lambda = 450\ nm$ (right column).

As it is clear from the graph, the terpolymers show good fluorescence characteristics around 600 nm even when excited at $\lambda = 350\ nm$. As underlined in previous chapters, the fluorescence peak at 600 nm is typical of perylene, which in turn does not show good absorption properties in the region around $\lambda = 350\ nm$. Another thing to note is how the fluorescence peak relative to perylene seems to increase in intensity compared to the peak relative to coumarin while increasing the concentration of perylene in the polymer, especially when compared with the fluorescence intensities of the PMA-MMA random copolymer at the same PMA concentrations (shown in Figure 3.30). This is a first experimental proof of energy transfer between the fluorescent dyes incorporated in the polymers.

As described in paragraph 1.3.3, FRET is a phenomenon that consists in the transfer of energy between two fluorophores: a donor molecule absorbs photons and, instead of releasing energy it transfers it to an acceptor molecule that in turn emits photons at a higher wavelength. One fundamental requirement is that the emission spectrum of the

donor molecule should overlap with the absorption spectrum of the acceptor. The overlap of the spectra is shown in Figure 3.38.

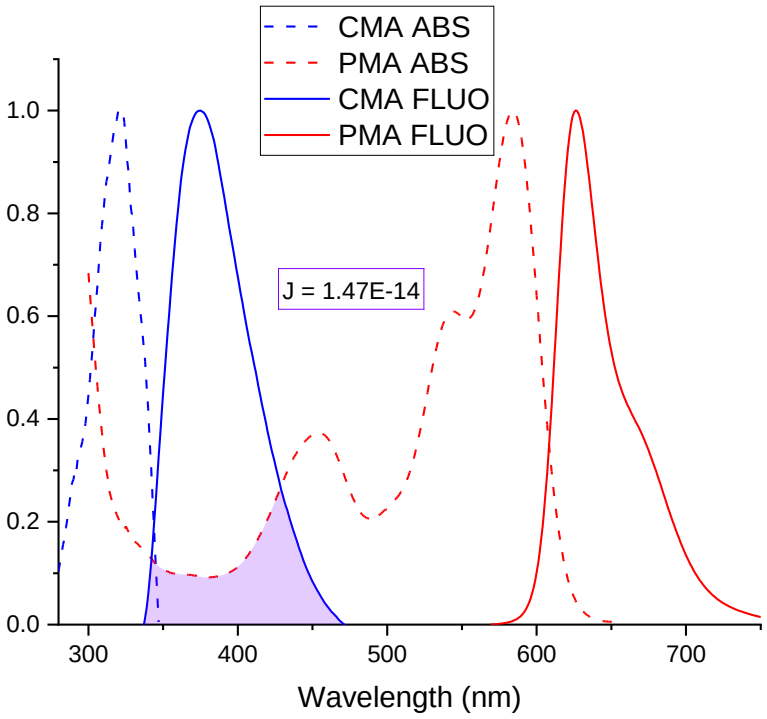

Figure 3.38 – Overlap of absorption and emission spectra of coumarin and perylene methacrylate with the value of the overlap integral J.

Using the formula introduced in paragraph 1.3.3, the value J of the overlap integral was calculated. By considering the extinction coefficient of the custom perylene bisimide and the fluorescence spectrum of the CMA10 MMA90 copolymer, a total value of 1.4712E-14 $cm^3\ M^{-1}$ resulted from the calculations, which is in line with the values found in the literature [4], [28].

To check whether energy transfer occurs in the polymer, the excitation spectra of both CMA10 PMA0.100 MMA89.900 and PMA0.100 MMA89.900 were measured by detecting fluorescence at $\lambda = 610\ nm$, corresponding to the maximum fluorescence value of perylene. In Figure 3.39, it is clearly visible that the terpolymer displays fluorescence at $\lambda = 610\ nm$ also when excited between 280 and 350 nm, corresponding to the absorption peak of coumarin. This is the first qualitative evidence of energy transfer between the two luminophores.

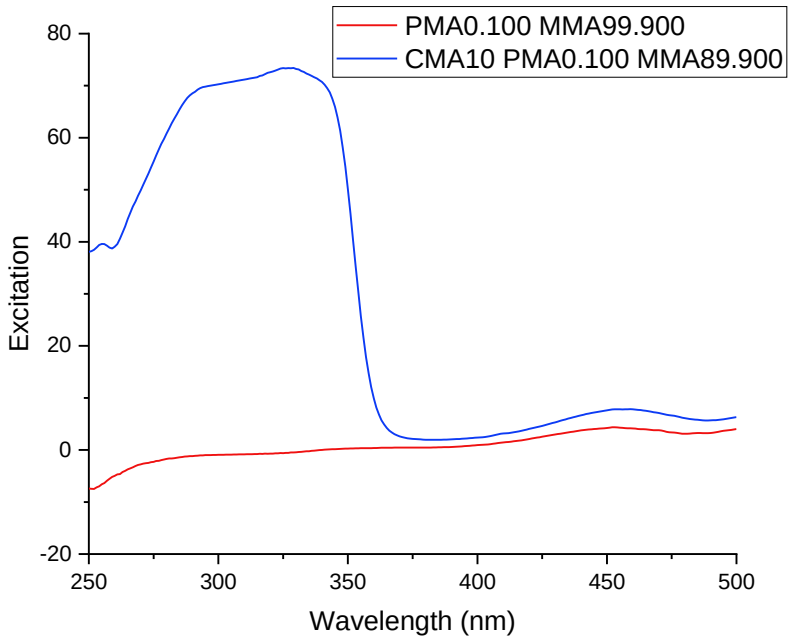

Figure 3.39 – Excitation spectra of a terpolymer and a PMA-MMA copolymer as evidence of energy transfer.

In order to quantitatively evaluate the energy transfer between the two fluorescent dyes, two techniques, previously described in paragraph 1.3.3, have been employed.

The first method is based on time-resolved fluorescence spectroscopy measurements. By measuring the fluorescence time of the polymers, it's possible to note how the τ_D (fluorescence time of the donor) decreases in the terpolymers while increasing the concentration of PMA. This effect is due to the fact that the donor is transferring energy to the acceptor instead of emitting photons itself. The efficiency of FRET is calculated with the formula reported below:

$$E = 1 - \frac{\tau_{DA}}{\tau_D}$$

where τ_{DA} is the fluorescence time of the donor molecule (CMA in this work) in a terpolymer with both luminophores and τ_D the fluorescence time of the donor molecule in a copolymer without the acceptor (PMA in this work).

The results of FRET efficiencies calculated with this method are reported inTable 3.10.

Table 3.10 – FRET efficiencies calculated with time-resolved fluorescence method.

Batch Name	**τ_{DA} (ns)**	**τ_D (ns)**	**E_{FRET}**
CMA10 MMA90	-	1.71	-
CMA10 PMA0.025 MMA89.975 10%	1.60	1.71	6.5%
CMA10 PMA0.050 MMA89.950 10%	1.59	1.71	7.0%
CMA10 PMA0.100 MMA89.900 10%	1.26	1.71	26%

The time-resolved fluorescence profiles of the terpolymers while varying the concentration of PMA is reported in Figure 3.40.

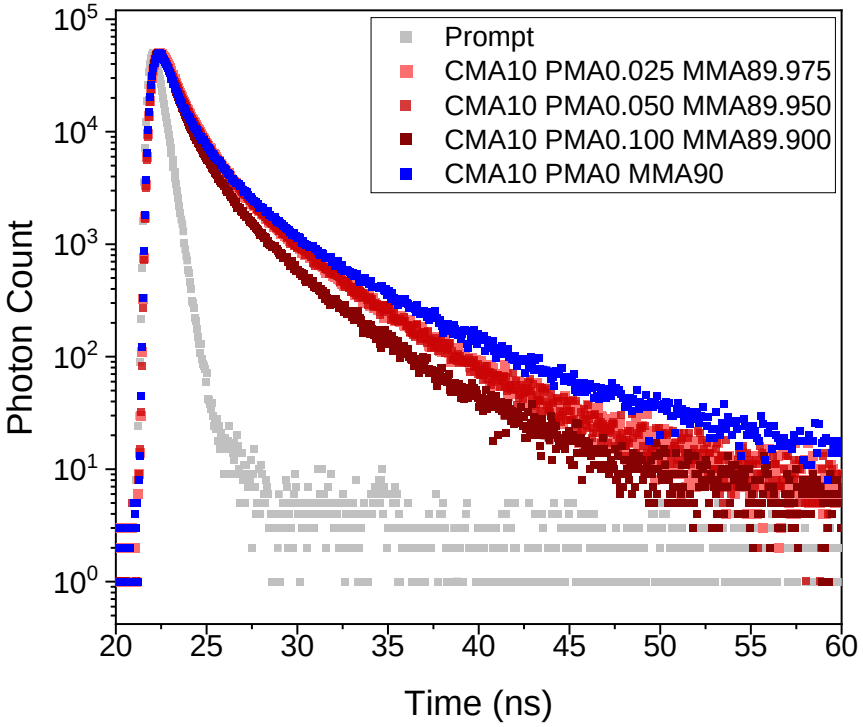

Figure 3.40 – Time-resolved fluorescence profiles of the terpolymers.

A second technique exploited to calculate the efficiency of the FRET process is based on the following formula:

$$E = 1 - \frac{F_{DA}}{F_D}$$

where F_{DA} is the maximum fluorescence emission of a terpolymer with both luminophores incorporated and F_D is the maximum fluorescence emission of a copolymer containing the donor molecule only.

By adjusting the spin-coating parameters, glass slabs of terpolymers with the same optical density were fabricated. That is, the concentration of the polymer-chloroform solutions is varied in order to control their viscosity and obtain samples with the same absorbance value in the 300-350 nm range, corresponding to the coumarin.

After that, the fluorescence of these samples was measured and compared to the fluorescence of a sample of CMA10 MMA90 with the same optical density, as shown in Figure 3.41.

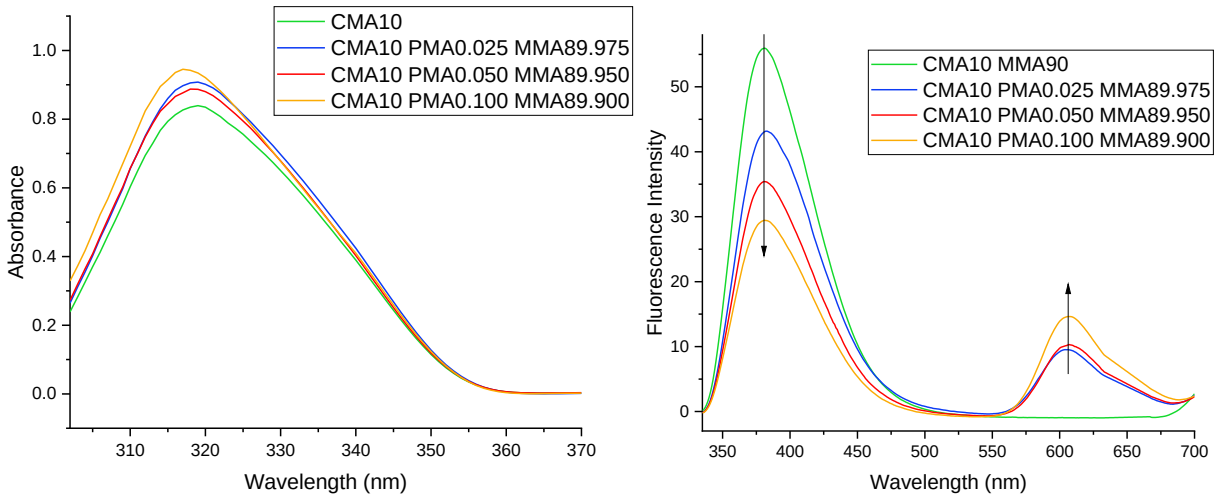

Figure 3.41 – Absorbance and fluorescence spectra of CMA10 MMA90 and terpolymers with the same optical density.

Two pieces of evidence can be noted from the graph: first of all, the fluorescence intensity of perylene increases, as expected, with the concentration of perylene. The second effect is that the fluorescence of coumarin actually decreases while increasing the concentration of PMA in the polymer, even though the absorbance is the same: this is yet another experimental confirmation of the energy transfer process.

Using the formula cited above, the efficiency of FRET was calculated for every terpolymer. The results are reported in Table 3.11.

Table 3.11 – FRET efficiencies calculated with donor fluorescence method.

Batch Name	**F_{DA}**	**F_D**	**E_{FRET}**
CMA10 PMA0.025 MMA89.975	43.169	55.969	22.87%
CMA10 PMA0.050 MMA89.950	35.398	55.969	36.75%
CMA10 PMA0.100 MMA89.900	29.443	55.969	47.39%

The value of FRET efficiency obtained with the latter methods are higher with respect to that achieved by means of time-resolved fluorescence measurements. Still, the latter are more reliable as less subjected to experimental error.

3.3 LSC Devices

In order to determine the photonic and photovoltaic efficiency of LSCs prepared with a thin film of random luminescent polymer, several tests, previously described in paragraph 2.5.8, were performed on the devices. A photograph of three LSC devices under a UV light is shown in Figure 3.42.

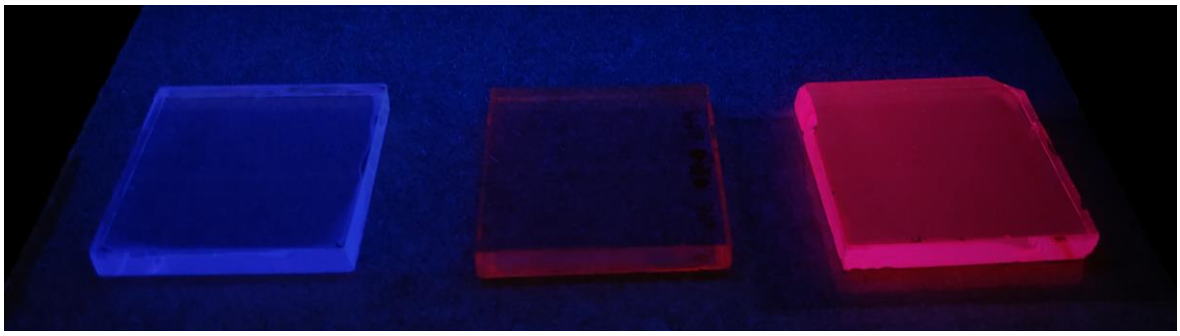

Figure 3.42 – Photograph of CMA10 MMA90 (left), PMA0.100 MMA99.900 (center) and CMA10 PMA0.100 MMA89.900 (right) under a UV light.

Edge Emission Irradiance

First, the LSCs were characterized using the ILT950 spectroradiometer. The devices are placed under the solar simulator and their edge emission is recorded. This data, together with the absorption spectra of the devices, was used to calculate the absorption efficiency and the internal and external photon efficiency, introduced in paragraph 1.3.2, with the following formulas:

$$\eta_{INT} = \frac{no.\,of\ edge - emitted\ photons}{no.\,of\ total\ absorbed\ photons} \qquad \eta_{EXT} = \frac{no.\,of\ edge - emitted\ photons}{no.\,of\ total\ incident\ photons}$$

$$\eta_{ABS} = \frac{fraction\ of\ light\ absorbed\ by\ the\ LSC}{spectral\ irradiance\ input}$$

The results of the calculations are reported in Table 3.12.

Table 3.12 – Calculations results of internal and external photon efficiencies.

Batch Name	$\eta_{INT\,SINGLE\,EDGE}$	$\eta_{EXT\,SINGLE\,EDGE}$	$\eta_{INT\,FOUR\,EDGES}$	$\eta_{EXT\,FOUR\,EDGE}$	η_{ABS}
CMA5	3.00%	0.05%	12.00%	0.19%	1.87%
CMA10	2.63%	0.06%	10.54%	0.26%	2.79%
CMA15	1.30%	0.06%	5.19%	0.24%	5.34%
PMA0.050	8.19%	0.08%	32.78%	0.32%	1.09%
PMA0.100	4.04%	0.14%	16.15%	0.55%	3.88%
CMA10 PMA0.025	3.83%	0.05%	15.33%	0.20%	1.51%

MMA89.975 3%					
CMA10 PMA0.050 MMA89.950 3%	12.10%	0.06%	48.40%	0.22%	0.54%
CMA10 PMA0.100 MMA89.900 3%	3.06%	0.12%	12.25%	0.47%	4.34%
CMA10 PMA0.025 MMA89.975 10%	8.96%	0.10%	35.83%	0.38%	1.22%
CMA10 PMA0.050 MMA89.950 10%	8.20%	0.10%	32.82%	0.40%	1.36%
CMA10 PMA0.100 MMA89.900 10%	10.56%	0.23%	42.24%	0.92%	2.33%
CMA10 PMA0.025 MMA89.975 20%	14.86%	0.31%	59.42	1.23%	2.35%
CMA10 PMA0.050 MMA89.950 20%	7.00%	0.16%	27.99%	0.66%	2.62%
CMA10 PMA0.100 MMA89.900 20%	13.71%	0.57%	54.84%	2.28%	4.44%

Some general trends can be extrapolated from these results:

- The absorbance efficiency η_{ABS} generally increases while increasing the concentration of luminophore in the polymer. This is an expected result since a greater amount of fluorophore is able to absorb a higher quantity of photons.

- The external efficiency η_{EXT} generally increases while increasing the concentration of luminophore in the polymer. This is also an expected behaviour since a higher amount of fluorophore can also emit a larger quantity of photons. Also, this demonstrates that no fluorescence emission quenching occurs, thus demonstrating the great potential brought by the insertion of fluorescent species in the polymeric chain
- The internal efficiency η_{INT} generally decreases while increasing the concentration of luminophore in the polymer. This is probably due to the fact that by increasing the concentration of dyes the absorption efficiency of the device increases more than the emission efficiency does. Thus, the devices absorb a larger quantity of photons but they are not able to scale their emission proportionally.

The four-edges external photon efficiency of the LSCs are plotted in Figure 3.43.

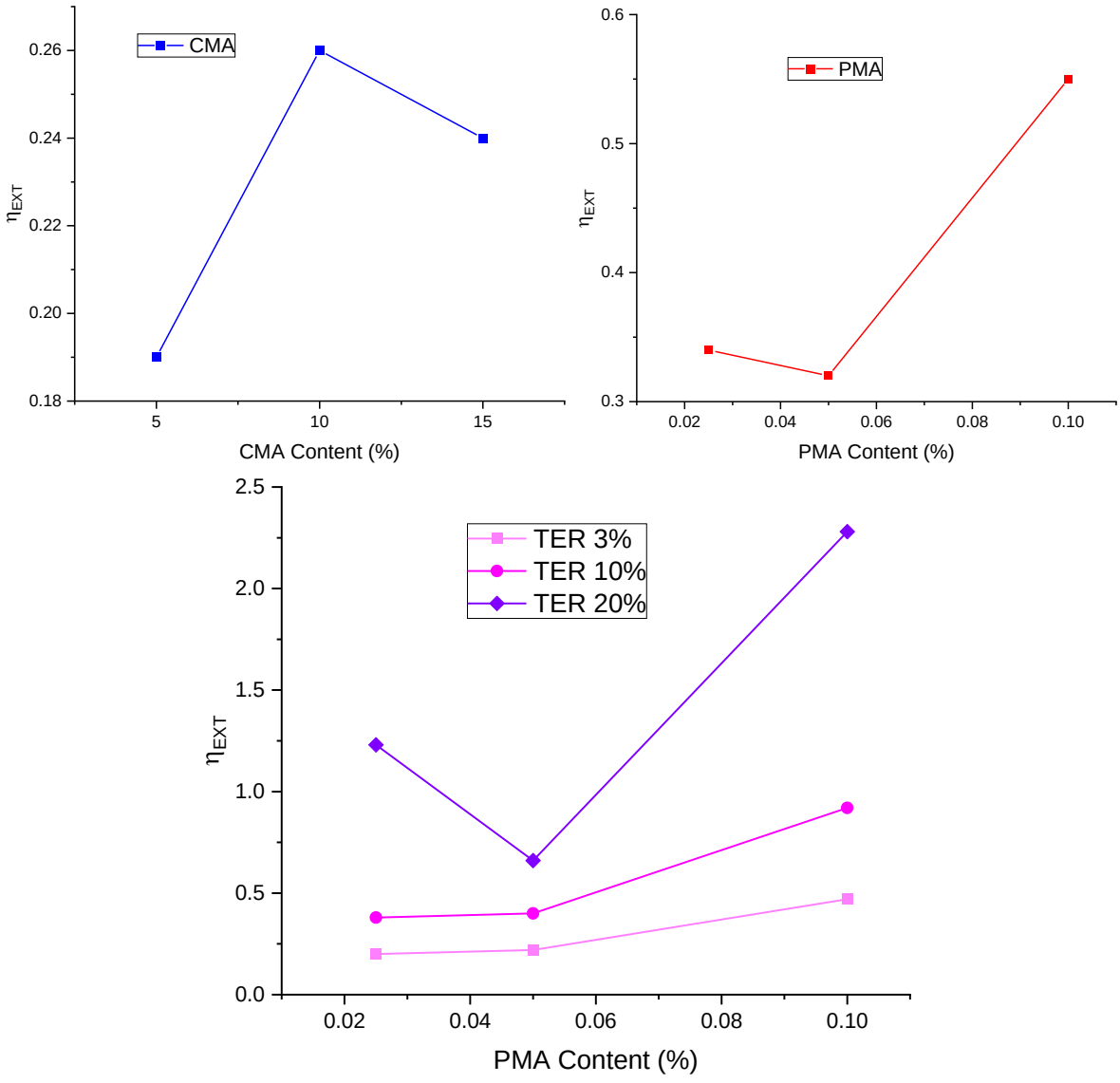

Figure 3.43 – External photon efficiencies of the prepared LSCs.

It can be noticed that the external quantum efficiency of the devices is proportional to the content of luminophore in the polymer, although some of the devices seem to not follow this trend, notably the ones with a PMA content of 0.050%.

Photovoltaic Tests

After measuring the photon efficiencies of the devices, PV tests were performed using a multimeter connected to four IXYS KXOB25-12X1L solar cells in series, covering two opposing edges of the LSC devices. The devices were then placed under a solar simulator lamp while running the I-V tests.

The photovoltaic efficiency of the device was calculated using the following formula:

$$PCE_{LSC} = \frac{FF \cdot I_{SC} \cdot V_{OC}}{P_{OPT}^{IN} \cdot A_{LSC}}$$

Tests were performed in two different configurations: in the first one, the cells are coupled with the glass slabs using EVA glue strips and the device is placed directly under the solar simulator, as shown in Figure 3.44.

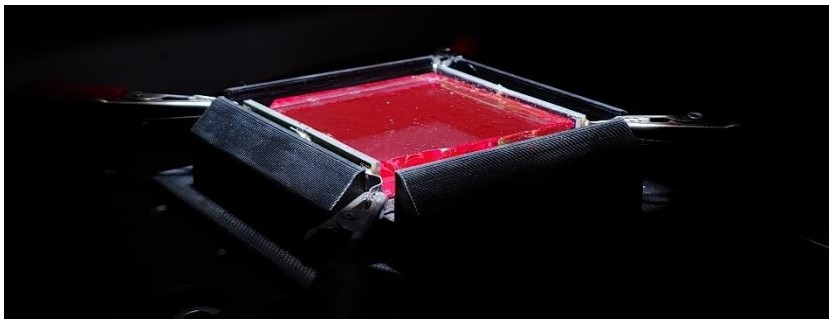

Figure 3.44 – No mask configuration for PV tests in LSC devices.

The second configuration, labelled as "MASK", is obtained by covering the upper edges of the solar cells with a black mask, in order to avoid direct irradiation of the cells and overestimation of the efficiency of the devices. The results of the tests are reported in Table 3.13.

Table 3.13 – PV efficiencies of the fabricated LSC devices.

Batch Name	**V_{OC} (V)**	**I_{SC} (mA)**	**PCE_{LSC}**
CMA5	2.24	5.93	0.464%
CMA5 MASK	1.57	0.55	0.026%
CMA10	2.24	5.88	0.444%
CMA10 MASK	1.60	0.65	0.029%
CMA15	2.23	5.78	0.438%
CMA15 MASK	1.70	0.75	0.041%
PMA0.025	2.22	5.10	0.384%

PMA0.025 MASK	1.46	0.35	0.015%
PMA0.050	2.25	4.84	0.400%
PMA0.050 MASK	1.64	0.61	0.031%
PMA0.100	2.25	5.70	0.437%
PMA0.100 MASK	1.88	0.99	0.069%
CMA10 PMA0.025 MMA89.975 3%	2.15	5.49	0.329%
CMA10 PMA0.025 MMA89.975 3% MASK	1.78	0.38	0.022%
CMA10 PMA0.050 MMA89.950 3%	2.16	5.71	0.388%
CMA10 PMA0.050 MMA89.950 3% MASK	1.56	0.44	0.019%
CMA10 PMA0.100 MMA89.900 3%	2.17	5.51	0.406%
CMA10 PMA0.100 MMA89.900 3% MASK	1.78	0.93	0.054%
CMA10 PMA0.025 MMA89.975 10%	2.19	5.05	0.380%
CMA10 PMA0.025 MMA89.975 10% MASK	1.64	0.80	0.034%
CMA10 PMA0.050 MMA89.950 10%	2.12	4.81	0.337%
CMA10 PMA0.050 MMA89.950 10% MASK	1.57	0.71	0.032%
CMA10 PMA0.100 MMA89.900 10%	2.21	5.90	0.452%
CMA10 PMA0.100 MMA89.900 10% MASK	1.91	2.11	0.132%
CMA10 PMA0.025 MMA89.975 20%	2.32	9.13	0.740%
CMA10 PMA0.025 MMA89.975 20% MASK	2.02	2.42	0.154%
CMA10 PMA0.050 MMA89.950 20%	2.22	6.86	0.518%
CMA10 PMA0.050 MMA89.950 20% MASK	1.69	0.98	0.050%
CMA10 PMA0.100 MMA89.900 20%	2.24	7.85	0.592%
CMA10 PMA0.100 MMA89.900 20% MASK	2.07	2.38	0.158%

It is clear that the PV performance of the devices is significantly enhanced in the first configuration without the mask, since a lot of photons coming from the lamp are directly absorbed by the cell without entering the LSC. Both configurations are described since the works in literature frequently use the first configuration, but the second one reports more accurate results.

Overall, the values of the PV efficiencies are quite low, but it is to be noted from Table 3.12 that the average η_{ABS} of the devices is also quite low. This means that the results of the PV efficiencies are to be put in perspective with the low concentration of the dyes in the devices, especially PMA if compared to values found in the literature, and their consequent low values of absorbance.

The I-V graphs resulting from the tests are reported in Figure 3.45.

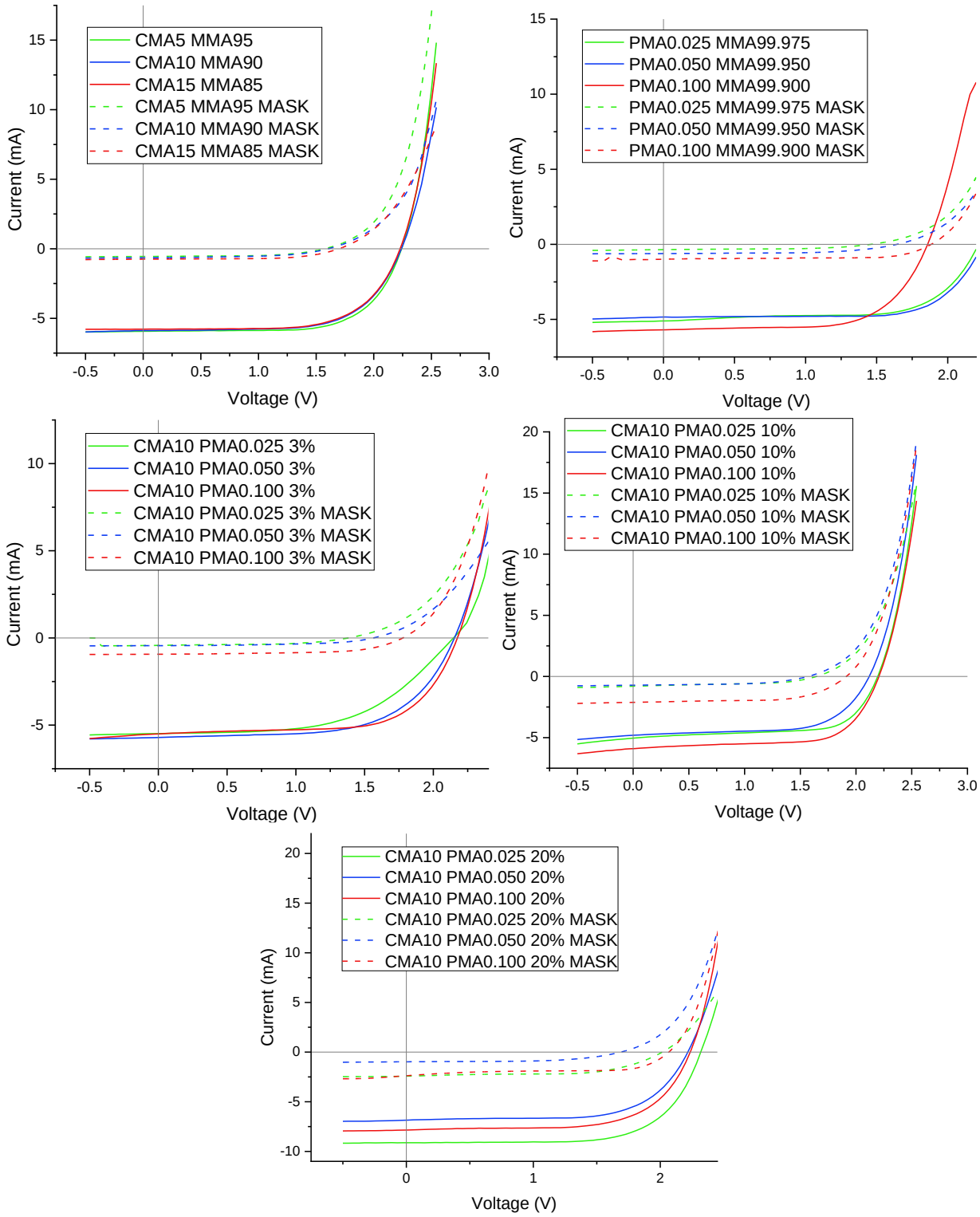

Figure 3.45 – I-V curves resulting from PV tests on LSC devices.

As it can be noticed, the efficiencies of the devices measured with the mask on the LSCs are way lower than their counterpart without a mask. Nonetheless, the results obtained in tests with a mask will be used to compare the PV efficiencies of the devices in Figure 3.46, since they are far more accurate.

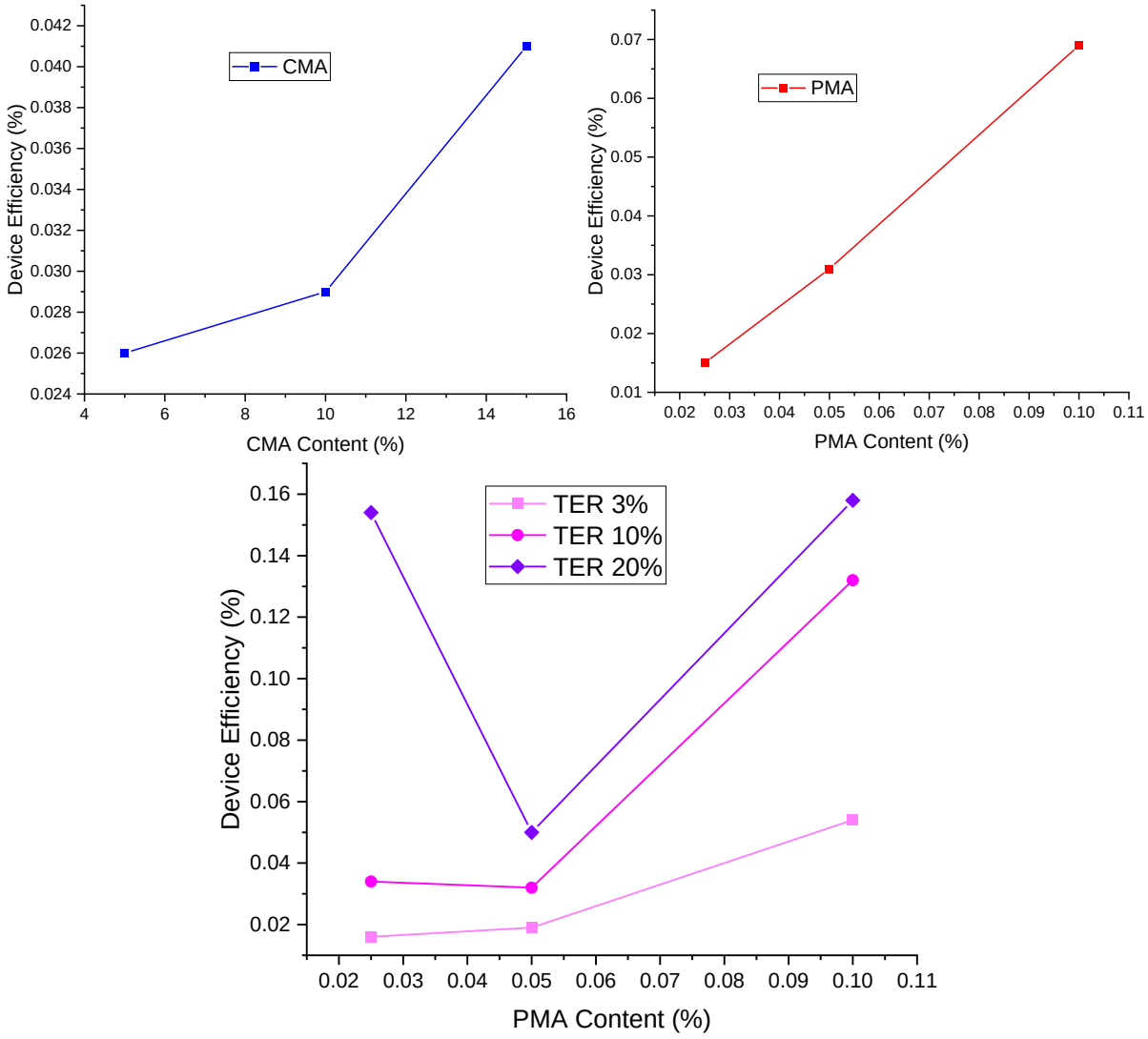

Figure 3.46 – Comparison between PV efficiencies of the LSC devices.

In all devices, an increase in the amount of luminophore leads to higher device efficiency, with the only exception of CMA10 PMA0.050 MMA99.950: the reason why its efficiency is lower than its counterpart with a lower amount of PMA could be related to the results of the NMR analyses on the polymer, which suggest that the amount of perylene in the sample is not proportional to the amount of perylene methacrylate like in the case of the other two synthesized terpolymers.

Finally, the devices with CMA10 MMA90, PMA0.100 MMA99.900 and CMA10 PMA0.100 MMA89.900 are compared with each other to evaluate the effect of the FRET process on the efficiency of the devices.

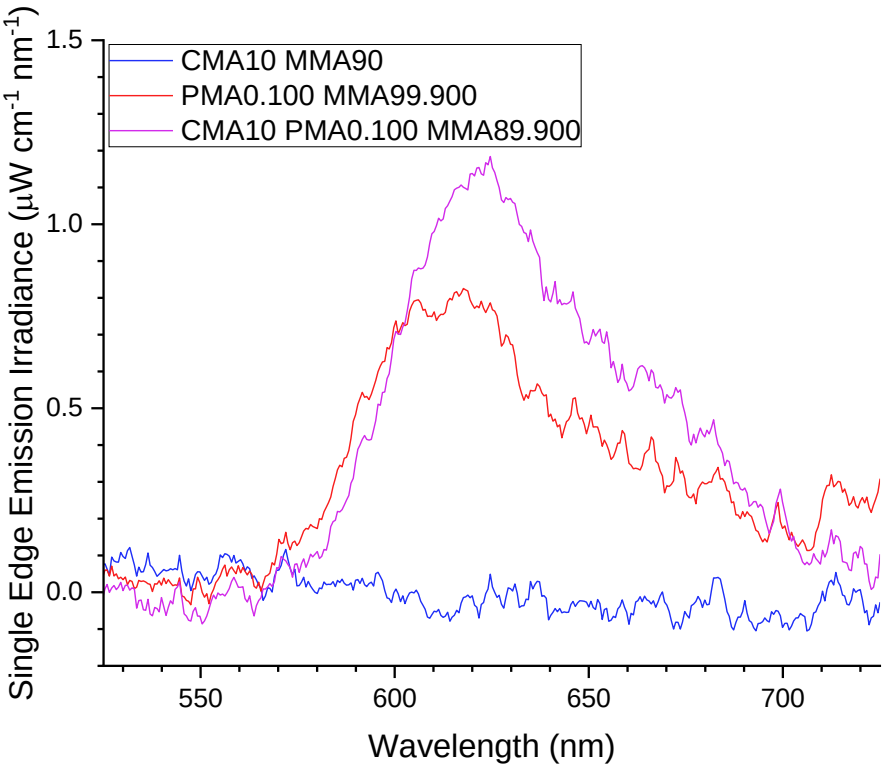

Figure 3.47 – Comparison of the emission irradiance of different LSC devices.

As shown in Figure 3.47, the emission irradiance of CMA10 MMA90 is pretty much negligible between 550 and 700 nm. This is of course expected and due to the fact that coumarin does not emit by fluorescence in that wavelength region. The interesting information is that the emission irradiance of the terpolymer is higher than the one of the PMA-MMA copolymer, with the same amount of PMA in the sample. This is a further highlight of the FRET process in the material.

Colorimetry Tests

Using the spectroradiometer, measurements of colorimetry were performed on the LSCs. The devices were placed above the spectroradiometer and they were illuminated using a common table lamp equipped with a warm white light lamp bulb. Its irradiance spectrum is shown in Figure 3.48.

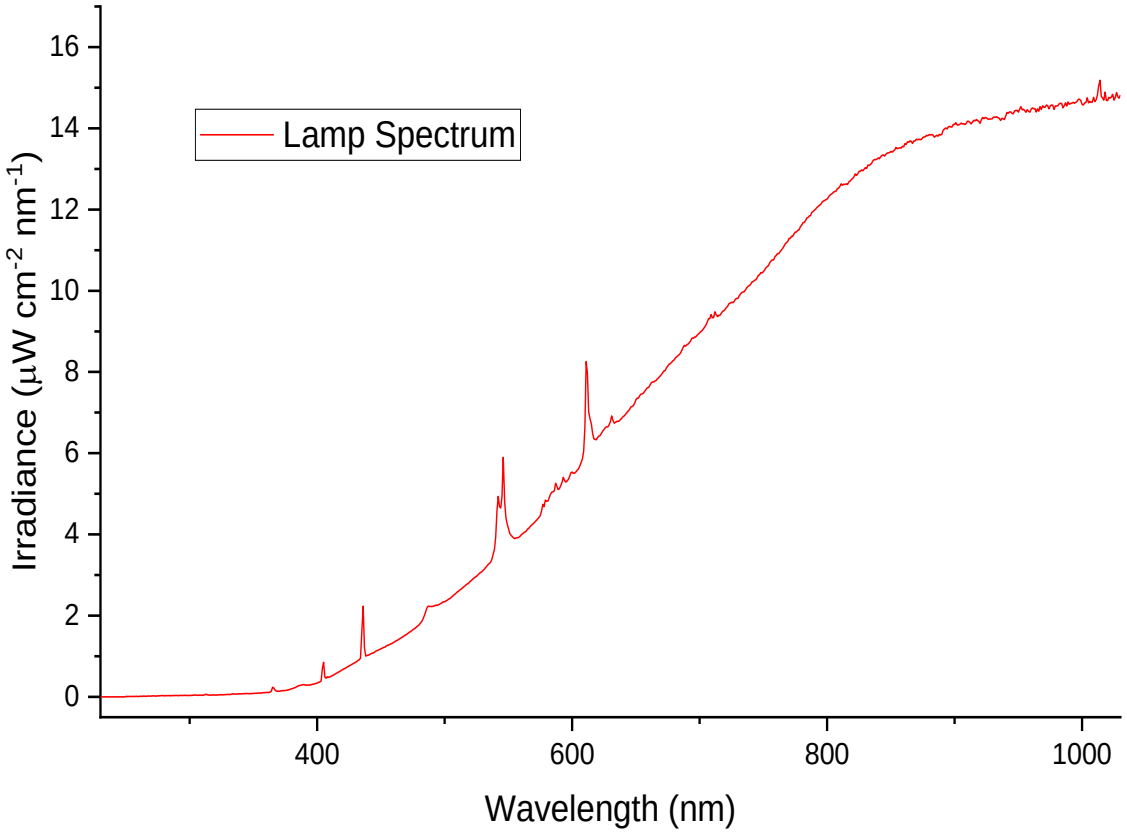

Figure 3.48 – Irradiance spectrum of the warm white light lamp used for colorimetry measurements.

This particular lamp was used because, although the standard method is to use a solar simulator, the intensity was found to be too high, saturating the spectroradiometer and preventing the measurements. Moreover, it was selected in view of the application of the here proposed LSC devices as windows or building elements able to efficaciously perform also in diffuse light conditions. The measured chromaticity values are a quantitative indication of the ability of a light source to reveal the colours of objects when compared to a source of natural light. In particular, the R_a, x and y values of the chromaticity are reported in Table 3.14.

Table 3.14 – Chromaticity values of LSC devices.

Batch Name	x	y	R_a
Reference Lamp	0.4775	0.421	97.73
CMA5 (a)	0.4488	0.4134	95.75
CMA10 (b)	0.4487	0.4135	95.79
CMA15 (c)	0.4487	0.4134	95.71
PMA0.025 (d)	0.4489	0.4135	95.78
PMA0.050 (e)	0.4498	0.4124	96.11

PMA0.100 (f)	0.452	0.4102	96.40
CMA10 PMA0.025 MMA89.975 3% (g)	0.4491	0.4131	95.92
CMA10 PMA0.050 MMA89.950 3% (h)	0.4495	0.4129	95.95
CMA10 PMA0.100 MMA89.900 3% (i)	0.4505	0.4115	96.26
CMA10 PMA0.025 MMA89.975 10% (j)	0.4502	0.4121	96.19
CMA10 PMA0.050 MMA89.950 10% (k)	0.4502	0.4115	96.27
CMA10 PMA0.100 MMA89.900 10% (l)	0.4556	0.4038	91.38
CMA10 PMA0.025 MMA89.975 20% (m)	0.4553	0.4078	94.19
CMA10 PMA0.050 MMA89.950 20% (n)	0.4543	0.4083	95.06
CMA10 PMA0.100 MMA89.900 20% (o)	0.4606	0.3978	85.33

In particular, the x and y values of the LSCs were plotted on the CIE 1931 colour space diagram and compared to the chromaticity values of the table lamp. The diagram is shown in Figure 3.49, where the red square represents the light source and the letters represent the devices, following the denomination reported in the table above.

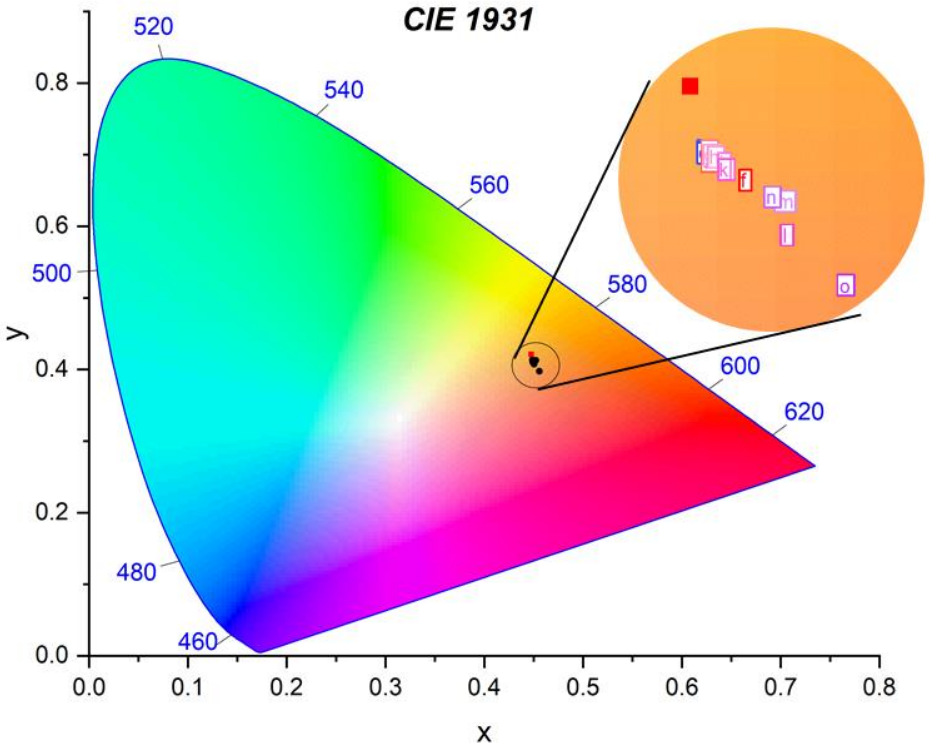

Figure 3.49 – Chromaticity values of the LSCs in the CIE 1931 colour space, where the red square represents the chromaticity value of the lamp used in the measurements.

It can be noted that the points representing the devices are quite close to the one representing the light source. In particular, the device at 10% concentration of the fluorescent terpolymer with 0.100% of PMA and the three devices spin-coated with

20% of fluorescent terpolymer (represented respectively by l, m, n and o) are the furthest from the light source, meaning that they distort the colour of the light passing through the LSC more than the other devices. This is also justified by their R_a values, since these devices are the only ones for which $R_a < 95.5$.

Still, if compared to other high-performance LSCs reported in the literature, the here proposed systems display a minor and quite negligible light distortion, thanks to their high transparency [63]–[65].

To further investigate the optical distortion properties of the devices, AVT measurements were performed.

Average Visible-Light Transmissivity

Finally, calculations were carried out on the LSCs to assess their average visible-light transmissivity (AVT). This figure of merit is particularly useful in describing luminescent solar concentrators, since it evaluates the transmissivity of the devices mediated with the photopic response of the human eye. An LSC with a high AVT is desirable since it means that the device is almost transparent to the human eye under sunlight illumination, an important feature for applications on houses and buildings.

The AVT was calculated with the following formula:

$$AVT\% = \frac{\int T\%(\lambda) \cdot P(\lambda) \cdot S(\lambda)}{\int P(\lambda) \cdot S(\lambda)}$$

where $T\%$ is the transmissivity of the device, measured with a UV-Vis spectrometer, P is the photopic response of the human eye to light, meaning the curve that describes which wavelengths are the cone cells most sensible to, and S is the AM 1.5G solar spectrum expressed as photon flux in $cm^{-2}\ s^{-1}$.

The results of the calculations are reported in Figure 3.50.

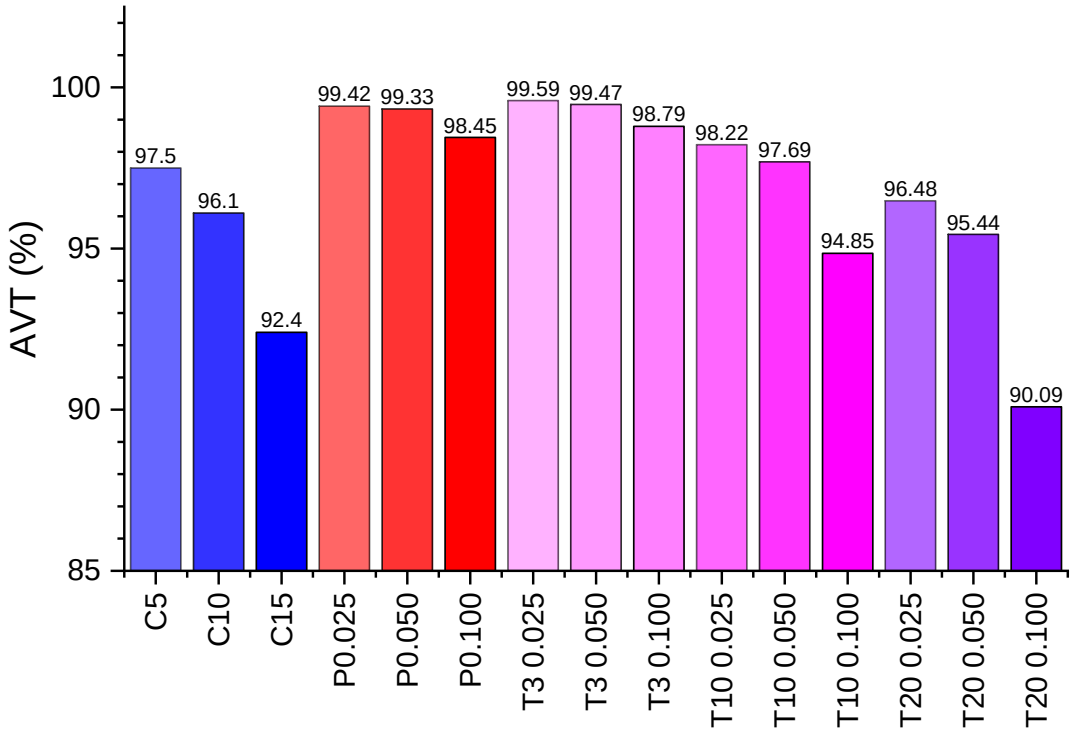

Figure 3.50 – Average Visible-light Transmissivity values of the produced LSCs.

It can be noticed how the values are all above 90%, which are considered very high compared to those found in the literature [66]–[68]. This data is to be considered together with the values of efficiency of the devices. As seen in the literature, lower values of AVT are usually accompanied by higher PCE values, since an LSC with a stronger absorbance usually comes with higher absorbance and photonic efficiencies.

Accordingly, a useful parameter to rationalize the effect of the two metrics is the light utilization efficiency (LUE), defined as the product of AVT and PCE [69]. For instance, for CMA10 PMA0.100 MMA89.900 20%-based LSC devices, tested using a black mask to avoid performance overestimation due to the direct irradiation of PV cells, the LUE value resulted to be equal to 0.14. These values are comparable to those reported in the literature for highly transparent LSCs, which usually range between 0.1 and 1.5 [70]–[72].

In conclusion, the PCE values of the LSCs produced in this work are quite low, but their high AVT and LUE values are very favourable for applications where the transparency of the device is advantageous.

Chapter 4
Conclusions and Future Developments

In this chapter, a small summary of the most significant results of this work is presented.

4.1 Conclusions

This work had the goal of obtaining a novel luminescent terpolymer that could be used as an efficient host matrix for applications in thin-film luminescent solar concentrators. In particular, the luminescent polymer was obtained by the random free-radical polymerization of methyl methacrylate (MMA) and two luminescent methacrylate monomers.

The luminescent monomers were obtained with a urethane bond formation reaction by end-capping a coumarin and a perylene dye with 2-isocyanatoethyl methacrylate. In particular, coumarin methacrylate (CMA) was obtained starting from 4-methylumbelliferone and perylene methacrylate (PMA) was obtained starting from a custom perylene diimide molecule synthesized by the University of Milan.

The two dyes were chosen so to promote and investigate the occurrence of energy transfer between the molecules, in order to broaden the spectral absorption of the LSC device and enhance its efficiency by reducing scattering and reabsorption losses. In fact, the fluorescence spectrum of coumarin overlaps significantly with the absorption spectrum of perylene: the value of the overlap integral was calculated to be $1.47 \cdot 10^{-14}$.

The polymers were synthesized by random free-radical polymerization of MMA with varying concentrations of CMA and PMA. First, copolymers with 5, 10 and 15% molar of CMA with respect to MMA were produced. Various characterization tests and analyses were performed on the polymeric samples to assess their structure and properties: the resulting Tg was around 47 °C and the molecular weight around 40000 g/mol for all three copolymers. Upon investigation of the optical properties of the samples, 10% molar of CMA was found the most advantageous concentration, since its fluorescence spectrum was stronger than the one of the sample with 15% of CMA, albeit its absorption spectrum was lower.

Then, random copolymers with MMA and 0.025, 0.050 and 0.100% of PMA were synthesized. Such low concentrations were utilized due to a lack of precursor PDI dye, but it was determined upon optical analyses that the fluorescence of the luminophore in the polymers was sufficiently strong to obtain a satisfactory energy transfer efficiency. Nevertheless, some difficulties were encountered when analyzing the quantity of incorporated PMA in the polymer via FTIR and NMR spectroscopy analyses, since the signal associated with the perylene was always very weak. The Tg of the copolymers was found to be much higher than that of the CMA copolymers, around 125 °C, as well as the average molecular weight was assessed around 57000 g/mol. A possible explanation for these results is that, albeit PMA is a much bigger molecule compared to CMA, its steric hindrance did not affect the polymerization reaction as much because its content was much lower.

Afterwards, random terpolymers were produced with 10% molar of CMA and 0.025, 0.050 and 0.100% molar of PMA. The average Tg was found to be around 60 °C while the molecular weight was around 45000 g/mol, which are values closer to those obtained with the CMA copolymers. Fluorescence analyses were performed on the polymeric sample to investigate the occurrence of the energy transfer phenomenon via two different techniques. The best sample was found to be the one with the highest concentration of perylene methacrylate, CMA10 PMA0.100 MMA89.900, for which the FRET efficiency was calculated to be 47% with fluorescence measurements and 26% with time-resolved fluorescence measurements.

Finally, all the polymeric samples were utilized to produce LSC devices by dissolving the polymers in chloroform and spin-coating the solutions on soda glass slabs. All the devices were characterized by performing efficiency tests with a spectroradiometer and a multimeter connected to solar cells coupled on the edges of the devices. The best device, obtained by spin-coating a 20% chloroform solution of CMA10 PMA0.100 MMA89.900, was found to have an external photonic efficiency of 2.28%, an absorbance efficiency of 4.44% and a PCE of 0.158%. These values are generally lower than those found in the literature, but it is to be taken into consideration that the quantity of luminophore utilized is much lower than the one typically used. Furthermore, the colorimetry index and the average visible-light transmissivity of the devices were measured: the LSC were found not to distort significantly the colour of the light passing through the device and the AVT was found to be above 90 for all the devices.

In conclusion, the novel luminescent terpolymers produced were found to be suitable candidates as efficient and highly-transparent luminescent host matrices for thin-film luminescent solar concentrators applications. In fact, the LSCs produced with such materials displayed significant transparency to the human eye while having efficiency values compatible with the low quantity of luminophores present in the matrix.

4.2 Luminescent Polymers via Controlled Polymerization

Given the results obtained with luminescent copolymers produced with random free radical polymerization, a possible future path to be explored in research could be represented by the controlled polymerization of luminescent monomers. For example, block copolymers could be synthesized via reversible addition-fragmentation chain-transfer polymerization (RAFT). As described in paragraph 2.2.6, block copolymerization via RAFT is carried out in a series of steps. Initially, a first block is produced by polymerizing a monomer together with the RAFT agent and the initiator. The so obtained macromer is then polymerized again with another monomer in order to obtain a second block in the chain.

In this work, several macromers of methyl methacrylate have been produced in order to find the right ratio between MMA and RAFT agent.

4.2.1 Methyl Methacrylate Macromers

Macromers with an MMA:RAFT agent of 100:4.45, 205:4.45 and 500:4.45 were synthesized. In the following graphs, they are called respectively RAFT100, RAFT205 and RAFT500.

Gel Permeation Chromatography

GPC analyses were performed on the samples to determine their molecular weight. The resulting elution curves are reported in Figure 4.1.

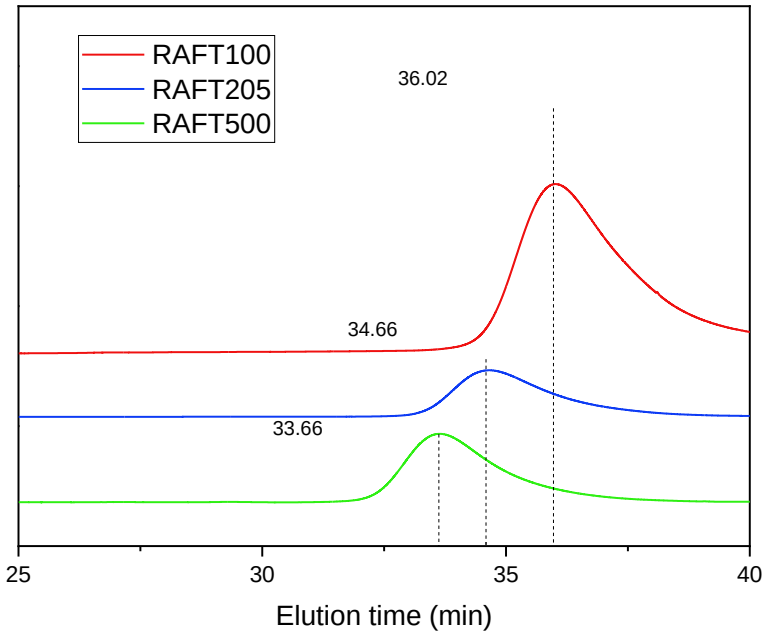

Figure 4.1 – GPC analyses of MMA RAFT macromers.

Reported in Table 4.1 are the main results of GPC analyses on MMA RAFT macromers, showing the number averaged molecular weight, the weight averaged molecular weight and the polydispersity index.

Table 4.1 – Results of GPC analyses on MMA RAFT macromers.

Batch Name	Mn	Mw	PDI
RAFT100	2153	2630	1.22
RAFT205	3772	4580	1.21
RAFT500	6287	7614	1.21

As it can be noticed, the molecular weights of the polymers are quite low, considering that the molecular weight of methyl methacrylate is around 100 g/mol. However, the polydispersity index is also very narrow, meaning that the polymerization is very controlled and the resulting polymer is regular.

Fourier Transform Infrared Spectroscopy

FTIR spectroscopy measurements were performed on the polymers. The resulting graphs are shown in Figure 4.2.

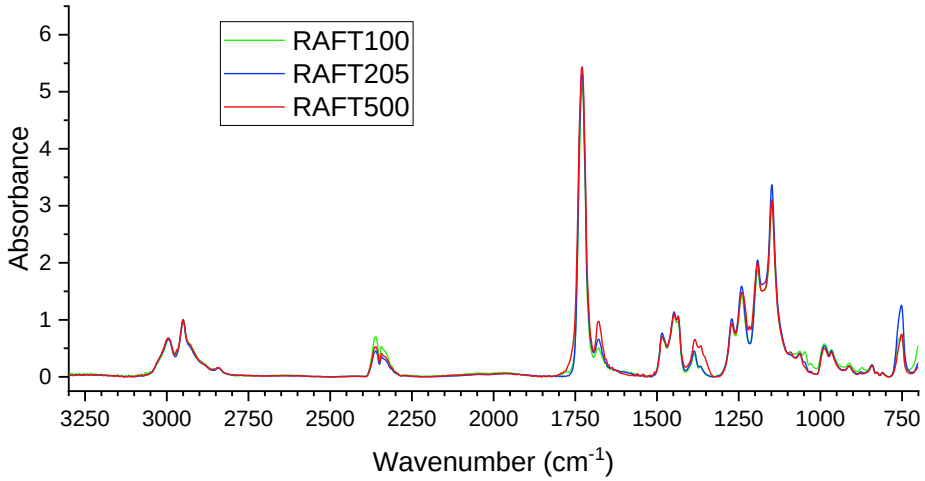

Figure 4.2 – FTIR spectroscopy results on RAFT MMA macromers.

The results show the characteristic peaks of poly methyl methacrylate, indicating that the polymerization reaction was successful.

4.2.2 Coumarin Methacrylate/Methyl Methacrylate Copolymers

After synthesizing the MMA macromers, another block was added in order to obtain a luminescent RAFT copolymer. The first synthesis was carried out to attach a block of coumarin methacrylate, in a ratio of 10:90 CMA:MMA.

Gel Permeation Chromatography

Gel permeation chromatography measurements were performed on the copolymer, in order to compare its characteristic to the macromer. The results are reported in Table 4.2.

Table 4.2 – Results of GPC analyses on the CMA-MMA RAFT copolymer.

Batch Name	Mn	Mw	PDI
RAFT100	2153	2630	1.22
CMA10RAFT100	2519	3136	1.25
CMA10 Random	43116	94156	2.18

From the results, it can be noticed that the molecular weight of the copolymer is greater than the one relative to the RAFT100 monomer. This evidences that the reaction was successful and that the CMA monomer was incorporated in the polymer as a second chain block. Moreover, it is clear how the polydispersity index of the RAFT copolymer is much narrower if compared to the one obtained with random polymerization, although the molecular weight is almost twenty times lower. Still, further studies on the CMA:RA:AIBN molar ratio are required to enhance the length of the CMA block in the polymer chain.

Fourier Transform Infrared Spectroscopy

FTIR analyses were performed on the block copolymer. The results are shown in Figure 4.3.

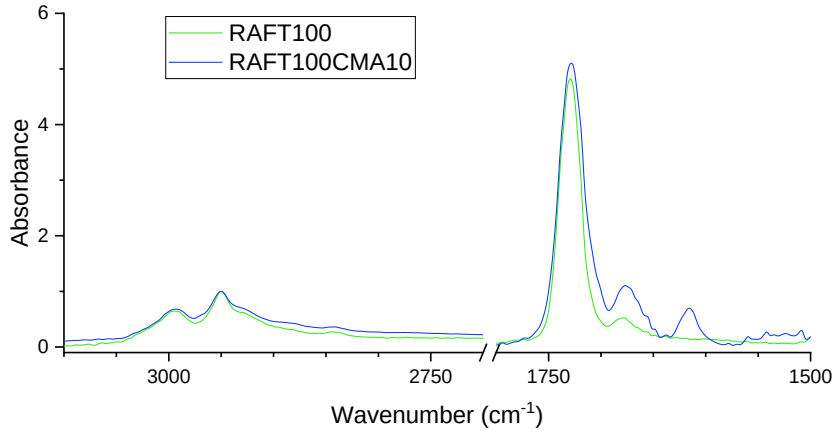

Figure 4.3 – FTIR spectra of CMA-MMA RAFT copolymer.

By comparing the spectrum to the one of the RAFT100 macromer, it is clearly noticeable that the spectrum of the copolymer displays peaks at 1600 and 1650 cm^{-1} attributable to the CMA monomer. This is an indication of the fact that the reaction was successful and the coumarin was incorporated into the polymer.

4.2.3 Perylene Methacrylate/Methyl Methacrylate Copolymers

Another synthesis was carried out in order to attach a block of perylene methacrylate to the RAFT100 macromer. The concentration of monomers was chosen so to synthesize a PMA0.050 MMA99.950 RAFT copolymer.

Gel Permeation Chromatography

GPC analyses were performed on the PMA-MMA RAFT copolymer. The results are reported in Table 4.3.

Table 4.3 – Results of GPC analyses on the PMA-MMA RAFT copolymer.

Batch Name	Mn	Mw	PDI
RAFT100	2153	2630	1.22
PMA0.100RAFT100	2637	3140	1.19
PMA0.100 Random	43534	71462	1.64

The molecular weight of the copolymer is larger than that of the RAFT100 monomer, as can be seen from the data. This indicates that the reaction went well and that the PMA monomer was included as a second chain block in the polymer. Furthermore, the RAFT copolymer's polydispersity index is substantially narrower than that achieved with random polymerization. However, as previously pointed out for the CMA-MMA RAFT copolymer, the increase in molecular weight after the formation of the second block in the polymeric chain is very small, thus further studies must be focused on improving the insertion of PMA monomer.

Fourier Transform Infrared Spectroscopy

FTIR analyses were carried out on the polymeric sample. Results are shown in Figure 4.4.

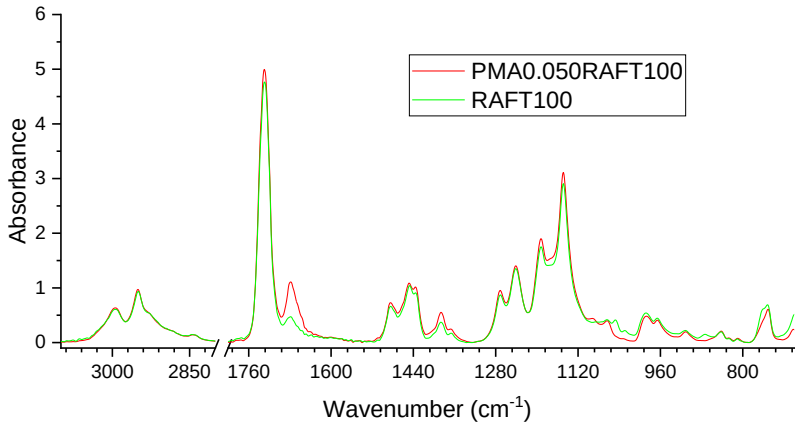

Figure 4.4 – FTIR analyses on PMA-MMA RAFT copolymer.

It can be noticed that the spectra overlap almost perfectly, except for a peak around 1670 cm^{-1} which can be assigned to C=O stretching of diimides groups in the PMA monomer The reason for such a small difference in the spectra could be related to the fact that the molar percentage of PMA in the polymer is very small and could be hardly detected with FTIR spectroscopy.

Summarizing, it can be noted that the polymers produced with RAFT polymerization present a much narrower PDI and more regularity if compared to their counterparts synthesized with random copolymerization, although their molecular weights are much lower.

Figure 4.5 – RAFT copolymers with CMA (left) and PMA (right) displaying bright colours.

The main problem with the fluorescent copolymers produced with RAFT polymerization is that the RAFT agent displays a bright purple colour, that changes during the reaction while the molecular weight of the polymeric chain increases. Thus, the copolymers also display a bright colour, as shown in Figure 4.5, that interferes with the absorption and fluorescence features of the luminophores. A further step in this direction would be represented by the quenching of the RAFT agent in the polymers and their optical characterization to determine their potential usage in LSC devices.

4.3 Other Future Developments

Other than block copolymers produced via RAFT polymerization, other types of controlled polymerization reactions could be exploited to synthesize luminescent polymers with different architectures, in order to study their influence on the efficiency of the energy transfer process and fluorescence phenomena.

Considering the copolymers synthesized in this work, further efforts could be spent in producing luminescent polymers with a higher concentration of luminophore, especially perylene-based.

Furthermore, monomers with chemical functionalities different than methacrylate could be exploited to produce luminescent polymers. For example, polyurethanes could

be synthesized inserting luminophores with two -OH functionalities directly in the polymeric chain as a substitute for polyethylene glycol, as described in paragraph 1.5.1.

Finally, modeling studies and statistical simulations could be performed to better understand the physics of the interactions between photons and LSCs and to find ways to further optimize the devices.

Bibliography

[1] G. Griffini, “Host Matrix Materials for Luminescent Solar Concentrators: Recent Achievements and Forthcoming Challenges,” *Front. Mater.*, vol. 6, p. 29, Mar. 2019, doi: 10.3389/fmats.2019.00029.

[2] I. Papakonstantinou, M. Portnoi, and M. G. Debije, “The Hidden Potential of Luminescent Solar Concentrators,” *Adv. Energy Mater.*, vol. 11, no. 3, p. 2002883, Jan. 2021, doi: 10.1002/aenm.202002883.

[3] N. J. L. K. Davis *et al.*, “Energy transfer in pendant perylene diimide copolymers,” *J. Mater. Chem. C*, vol. 4, no. 35, pp. 8270–8275, 2016, doi: 10.1039/C6TC02555B.

[4] B. Balaban, S. Doshay, M. Osborn, Y. Rodriguez, and S. A. Carter, “The role of FRET in solar concentrator efficiency and color tunability,” *Journal of Luminescence*, vol. 146, pp. 256–262, Feb. 2014, doi: 10.1016/j.jlumin.2013.09.049.

[5] C. Berney and G. Danuser, “FRET or No FRET: A Quantitative Comparison,” *Biophysical Journal*, vol. 84, no. 6, pp. 3992–4010, Jun. 2003, doi: 10.1016/S0006-3495(03)75126-1.

[6] “Energy Technology Perspectives 2020 – Analysis,” *IEA*. https://www.iea.org/reports/energy-technology-perspectives-2020 (accessed Aug. 16, 2021).

[7] “Global Energy Review 2021 – Analysis,” *IEA*. https://www.iea.org/reports/global-energy-review-2021 (accessed Aug. 16, 2021).

[8] “Renewables 2020 – Analysis,” *IEA*. https://www.iea.org/reports/renewables-2020 (accessed Aug. 17, 2021).

[9] E. Kabir, P. Kumar, S. Kumar, A. A. Adelodun, and K.-H. Kim, “Solar energy: Potential and future prospects,” *Renewable and Sustainable Energy Reviews*, vol. 82, pp. 894–900, Feb. 2018, doi: 10.1016/j.rser.2017.09.094.

[10] S. C. Fu *et al.*, “Bio-inspired cooling technologies and the applications in buildings,” *Energy and Buildings*, vol. 225, p. 110313, Oct. 2020, doi: 10.1016/j.enbuild.2020.110313.

[11] C. J. Cleveland and C. Morris, Eds., “Front Matter,” in *Handbook of Energy*, Amsterdam: Elsevier, 2013, p. iii. doi: 10.1016/B978-0-08-046405-3.01001-9.

[12] G. P. Smestad, *Optoelectronics of Solar Cells*. SPIE Press, 2002.

[13] G. K. Singh, “Solar power generation by PV (photovoltaic) technology: A review,” *Energy*, vol. 53, pp. 1–13, May 2013, doi: 10.1016/j.energy.2013.02.057.

[14] “10: Diodes, LEDs and Solar Cells,” *Chemistry LibreTexts*, Sep. 04, 2019. https://chem.libretexts.org/Bookshelves/Inorganic_Chemistry/Book%3A_Introduction_to_Inorganic_Chemistry/10%3A_Electronic_Properties_of_Materials_-

_Superconductors_and_Semiconductors/10.07%3A_Diodes_LEDs_and_Solar_Cells (accessed Aug. 18, 2021).
[15] A. Q. Jakhrani, S. R. Samo, S. A. Kamboh, J. Labadin, and A. R. H. Rigit, "An Improved Mathematical Model for Computing Power Output of Solar Photovoltaic Modules," *International Journal of Photoenergy*, vol. 2014, p. e346704, Mar. 2014, doi: 10.1155/2014/346704.
[16] D. Barlev, R. Vidu, and P. Stroeve, "Innovation in concentrated solar power," *Solar Energy Materials and Solar Cells*, vol. 95, no. 10, pp. 2703–2725, Oct. 2011, doi: 10.1016/j.solmat.2011.05.020.
[17] K. Jo *et al.*, "Soft luminescent solar concentrator film with organic dye and rubbery matrix," *Journal of Polymer Science*, vol. 59, no. 1, pp. 59–69, 2021, doi: 10.1002/pol.20200733.
[18] D. Llères, S. Swift, and A. I. Lamond, "Detecting Protein-Protein Interactions In Vivo with FRET using Multiphoton Fluorescence Lifetime Imaging Microscopy (FLIM)," *Current Protocols in Cytometry*, vol. 42, no. 1, p. 12.10.1-12.10.19, 2007, doi: 10.1002/0471142956.cy1210s42.
[19] J. Roncali, "Luminescent Solar Collectors: Quo Vadis?," *Adv. Energy Mater.*, vol. 10, no. 36, p. 2001907, Sep. 2020, doi: 10.1002/aenm.202001907.
[20] M. G. Debije, R. C. Evans, and G. Griffini, "Laboratory protocols for measuring and reporting the performance of luminescent solar concentrators," *Energy Environ. Sci.*, vol. 14, no. 1, pp. 293–301, 2021, doi: 10.1039/D0EE02967J.
[21] P. Moraitis, R. E. I. Schropp, and W. G. J. H. M. van Sark, "Nanoparticles for Luminescent Solar Concentrators - A review," *Optical Materials*, vol. 84, pp. 636–645, Oct. 2018, doi: 10.1016/j.optmat.2018.07.034.
[22] B. A. Swartz, T. Cole, and A. H. Zewail, "Photon trapping and energy transfer in multiple-dye plastic matrices: an efficient solar-energy concentrator," *Opt. Lett., OL*, vol. 1, no. 2, pp. 73–75, Aug. 1977, doi: 10.1364/OL.1.000073.
[23] C. Tummeltshammer *et al.*, "On the ability of Förster resonance energy transfer to enhance luminescent solar concentrator efficiency," *Nano Energy*, vol. 32, pp. 263–270, Feb. 2017, doi: 10.1016/j.nanoen.2016.11.058.
[24] "Fluorescence Resonance Energy Transfer," *Chemistry LibreTexts*, Oct. 02, 2013. https://chem.libretexts.org/Bookshelves/Physical_and_Theoretical_Chemistry_Textbook_Maps/Supplemental_Modules_(Physical_and_Theoretical_Chemistry)/Fundamentals/Fluorescence_Resonance_Energy_Transfer (accessed Sep. 04, 2021).
[25] R. M. Clegg, "Fluorescence resonance energy transfer," *Current Opinion in Biotechnology*, vol. 6, no. 1, pp. 103–110, Jan. 1995, doi: 10.1016/0958-1669(95)80016-6.
[26] M. de J. Bassi *et al.*, "Non-radiative energy transfer in aqueously dispersed polymeric nanoparticles for photovoltaic applications," *Synthetic Metals*, vol. 275, p. 116740, May 2021, doi: 10.1016/j.synthmet.2021.116740.
[27] J. R. Lakowicz, "Energy Transfer," in *Principles of Fluorescence Spectroscopy*, J. R. Lakowicz, Ed. Boston, MA: Springer US, 1999, pp. 367–394. doi: 10.1007/978-1-4757-3061-6_13.

[28] G. Fortunato, E. Tatsi, F. Corsini, S. Turri, and G. Griffini, "Stimuli-Responsive Luminescent Solar Concentrators Based on Photoreversible Polymeric Systems," *ACS Appl. Polym. Mater.*, vol. 2, no. 9, pp. 3828–3839, Sep. 2020, doi: 10.1021/acsapm.0c00515.
[29] E. Ergin, A. Dogan, M. Parmaksiz, A. E. Elcin, and Y. M. Elcin, "Time-Resolved Fluorescence Resonance Energy Transfer [TR-FRET] Assays for Biochemical Processes," *Current Pharmaceutical Biotechnology*, vol. 17, no. 14, pp. 1222–1230, Nov. 2016.
[30] Q.-H. Xu *et al.*, "The fluorescence resonance energy transfer (FRET) gate: A time-resolved study," *PNAS*, vol. 102, no. 3, pp. 530–535, Jan. 2005, doi: 10.1073/pnas.0408568102.
[31] J. Delgado-Sanchez, I. Lillo-Bravo, and A. Menéndez-Velázquez, "Enhanced luminescent solar concentrator efficiency by Foster resonance energy transfer in a tunable six-dye absorber," *Int J Energy Res*, p. er.6533, Feb. 2021, doi: 10.1002/er.6533.
[32] B. McKenna and R. C. Evans, "Towards Efficient Spectral Converters through Materials Design for Luminescent Solar Devices," *Advanced Materials*, vol. 29, no. 28, p. 1606491, 2017, doi: 10.1002/adma.201606491.
[33] G. Griffini, M. Levi, and S. Turri, "Novel crosslinked host matrices based on fluorinated polymers for long-term durability in thin-film luminescent solar concentrators," *Solar Energy Materials and Solar Cells*, vol. 118, pp. 36–42, Nov. 2013, doi: 10.1016/j.solmat.2013.05.041.
[34] M. Buffa, S. Carturan, M. G. Debije, A. Quaranta, and G. Maggioni, "Dye-doped polysiloxane rubbers for luminescent solar concentrator systems," *Solar Energy Materials and Solar Cells*, vol. 103, pp. 114–118, Aug. 2012, doi: 10.1016/j.solmat.2012.04.019.
[35] "Eu3+-Based Bridged Silsesquioxanes for Transparent Luminescent Solar Concentrators | ACS Applied Materials & Interfaces." https://pubs.acs.org/doi/10.1021/acsami.5b01281 (accessed Sep. 08, 2021).
[36] S. F. H. Correia, P. P. Lima, P. S. André, M. R. S. Ferreira, and L. A. D. Carlos, "High-efficiency luminescent solar concentrators for flexible waveguiding photovoltaics," *Solar Energy Materials and Solar Cells*, vol. 138, pp. 51–57, Jul. 2015, doi: 10.1016/j.solmat.2015.02.032.
[37] D. Pintossi, A. Colombo, M. Levi, C. Dragonetti, S. Turri, and G. Griffini, "UV-curable fluoropolymers crosslinked with functional fluorescent dyes: the way to multifunctional thin-film luminescent solar concentrators," *J. Mater. Chem. A*, vol. 5, no. 19, pp. 9067–9075, May 2017, doi: 10.1039/C7TA01692A.
[38] C. Credi, D. Pintossi, C. L. Bianchi, M. Levi, G. Griffini, and S. Turri, "Combining stereolithography and replica molding: On the way to superhydrophobic polymeric devices for photovoltaics," *Materials & Design*, vol. 133, pp. 143–153, Nov. 2017, doi: 10.1016/j.matdes.2017.07.068.
[39] J. A. H. P. Sol, V. Dehm, R. Hecht, F. Würthner, A. P. H. J. Schenning, and M. G. Debije, "Temperature-Responsive Luminescent Solar Concentrators: Tuning Energy Transfer in a Liquid Crystalline Matrix," *Angewandte Chemie International Edition*, vol. 57, no. 4, pp. 1030–1033, 2018, doi: 10.1002/anie.201710487.

[40] E. Tatsi *et al.*, "Thermoresponsive Host Polymer Matrix for Self-Healing Luminescent Solar Concentrators," *ACS Appl. Energy Mater.*, vol. 3, no. 1, pp. 1152–1160, Jan. 2020, doi: 10.1021/acsaem.9b02196.
[41] T. Wang *et al.*, "Luminescent solar concentrator employing rare earth complex with zero self-absorption loss," *Solar Energy*, vol. 85, no. 11, pp. 2571–2579, Nov. 2011, doi: 10.1016/j.solener.2011.07.014.
[42] U. Resch-Genger, M. Grabolle, S. Cavaliere-Jaricot, R. Nitschke, and T. Nann, "Quantum dots versus organic dyes as fluorescent labels," *Nat Methods*, vol. 5, no. 9, pp. 763–775, Sep. 2008, doi: 10.1038/nmeth.1248.
[43] M. G. Debije and P. P. C. Verbunt, "Thirty Years of Luminescent Solar Concentrator Research: Solar Energy for the Built Environment," *Advanced Energy Materials*, vol. 2, no. 1, pp. 12–35, 2012, doi: 10.1002/aenm.201100554.
[44] W. E. Benjamin *et al.*, "Sterically Engineered Perylene Dyes for High Efficiency Oriented Fluorophore Luminescent Solar Concentrators," *Chem. Mater.*, vol. 26, no. 3, pp. 1291–1293, Feb. 2014, doi: 10.1021/cm403286v.
[45] I. Parola *et al.*, "Fabrication and Characterization of Polymer Optical Fibers Doped with Perylene-Derivatives for Fluorescent Lighting Applications," *Fibers*, vol. 5, no. 3, Art. no. 3, Sep. 2017, doi: 10.3390/fib5030028.
[46] Y. Wang, Y. Zhang, J. Wang, and X.-J. Liang, "Aggregation-induced emission (AIE) fluorophores as imaging tools to trace the biological fate of nano-based drug delivery systems," *Advanced Drug Delivery Reviews*, vol. 143, pp. 161–176, Mar. 2019, doi: 10.1016/j.addr.2018.12.004.
[47] Y. Yu, X. Li, Y. Yuan, and H. Zhang, "A fluorescent alternative copolymer combined energy transfer and charge transfer with large and tunable Pseudo-Stokes shift," *Polymer*, vol. 217, p. 123477, Mar. 2021, doi: 10.1016/j.polymer.2021.123477.
[48] F. Corsini *et al.*, "Highly emissive fluorescent silica-based core/shell nanoparticles for efficient and stable luminescent solar concentrators," *Nano Energy*, vol. 80, p. 105551, Feb. 2021, doi: 10.1016/j.nanoen.2020.105551.
[49] F. Mateen, M. Ali, S. Y. Lee, S. H. Jeong, M. J. Ko, and S.-K. Hong, "Tandem structured luminescent solar concentrator based on inorganic carbon quantum dots and organic dyes," *Solar Energy*, vol. 190, pp. 488–494, Sep. 2019, doi: 10.1016/j.solener.2019.08.045.
[50] M. R. Kulish, V. P. Kostylyov, A. V. Sachenko, I. O. Sokolovskyi, D. V. Khomenko, and A. I. Shkrebtii, "Luminescent converter of solar light into electrical energy. Review," *Semiconductor physics, quantum electronics & optoelectronics*, no. 19, № 3, pp. 229–247, 2016.
[51] P. Ascencio Carvente *et al.*, "Synthesis of linear and branched hydrophobically associating multiblock copolymers via a one-pot process," *J Polym Res*, vol. 27, no. 8, p. 200, Jul. 2020, doi: 10.1007/s10965-020-02182-6.
[52] J. Huang and S. R. Turner, "Recent advances in alternating copolymers: The synthesis, modification, and applications of precision polymers," *Polymer*, vol. 116, pp. 572–586, May 2017, doi: 10.1016/j.polymer.2017.01.020.

[53] B. Gacal, "The Effect of Polymer Modification on Gas Transport Properties and The Synthesis of Poly(ethylene glycol) (PEG) Containing Polymers via Step-Growth Click Coupling Reaction for CO2 Separation," 2015.
[54] K. Matyjaszewski and T. P. Davis, *Handbook of Radical Polymerization*. John Wiley & Sons, 2003.
[55] V. B. Yasarapudi *et al.*, "Optimization of energy transfer in a polymer composite with perylene chromophores," *J. Mater. Chem. C*, vol. 6, no. 27, pp. 7333–7342, 2018, doi: 10.1039/C8TC02457J.
[56] L. Wang *et al.*, "Perylene bisimide-incorporated water-soluble polyurethanes for living cell fluorescence labeling," *Polymer*, vol. 82, pp. 172–180, Jan. 2016, doi: 10.1016/j.polymer.2015.11.037.
[57] C. Barner-Kowollik, *Handbook of RAFT Polymerization*. John Wiley & Sons, 2008.
[58] G. Moad, E. Rizzardo, and S. H. Thang, "RAFT Polymerization and Some of its Applications," *Chemistry – An Asian Journal*, vol. 8, no. 8, pp. 1634–1644, 2013, doi: 10.1002/asia.201300262.
[59] P. Zhao, J. Jiang, B. Leng, and H. Tian, "Polymer Fluoride Sensors Synthesized by RAFT Polymerization," *Macromolecular Rapid Communications*, vol. 30, no. 20, pp. 1715–1718, 2009, doi: 10.1002/marc.200900318.
[60] Y. Liu *et al.*, "Synthesis and biological imaging of fluorescent polymeric nanoparticles with AIE feature via the combination of RAFT polymerization and post-polymerization modification," *Dyes and Pigments*, vol. 158, pp. 79–87, Nov. 2018, doi: 10.1016/j.dyepig.2018.05.032.
[61] Z. Huang *et al.*, "Amphiphilic fluorescent copolymers via one-pot combination of chemoenzymatic transesterification and RAFT polymerization: synthesis, self-assembly and cell imaging," *Polymer Chemistry*, vol. 6, no. 4, pp. 607–612, 2015, doi: 10.1039/C4PY01421A.
[62] J. P. S. Farinha, P. Relógio, M.-T. Charreyre, T. J. V. Prazeres, and J. M. G. Martinho, "Understanding Fluorescence Quenching in Polymers Obtained by RAFT," *Macromolecules*, vol. 40, no. 13, pp. 4680–4690, Jun. 2007, doi: 10.1021/ma070444g.
[63] F. Corsini *et al.*, "Large-Area Semi-Transparent Luminescent Solar Concentrators Based on Large Stokes Shift Aggregation-Induced Fluorinated Emitters Obtained Through a Sustainable Synthetic Approach," *Advanced Optical Materials*, vol. 9, no. 16, p. 2100182, 2021, doi: 10.1002/adom.202100182.
[64] F. Meinardi *et al.*, "Highly efficient large-area colourless luminescent solar concentrators using heavy-metal-free colloidal quantum dots," *Nature Nanotech*, vol. 10, no. 10, pp. 878–885, Oct. 2015, doi: 10.1038/nnano.2015.178.
[65] S. Mattiello *et al.*, "Chemically Sustainable Large Stokes Shift Derivatives for High-Performance Large-Area Transparent Luminescent Solar Concentrators," *Joule*, vol. 4, no. 9, pp. 1988–2003, Sep. 2020, doi: 10.1016/j.joule.2020.08.006.
[66] Y. Gao *et al.*, "A photovoltaic window with sun-tracking shading elements towards maximum power generation and non-glare daylighting," *Applied Energy*, vol. 228, pp. 1454–1472, Oct. 2018, doi: 10.1016/j.apenergy.2018.07.015.
[67] K. Jo, S. Hong, and and H. J. Kim, "Optical Properties of EVA Films Including V570 for Transparent Luminescent Solar Concentrator," *Applied Science and*

Convergence Technology, vol. 29, no. 1, pp. 14–18, Jan. 2020, doi: 10.5757/ASCT.2020.29.1.014.

[68] K. Kim, S. K. Nam, and J. H. Moon, "Dual-Band Luminescent Solar Converter-Coupled Dye-Sensitized Solar Cells for High-Performance Semitransparent Photovoltaic Device," *ACS Appl. Energy Mater.*, vol. 3, no. 6, pp. 5277–5284, Jun. 2020, doi: 10.1021/acsaem.0c00171.

[69] C. J. Traverse, R. Pandey, M. C. Barr, and R. R. Lunt, "Emergence of highly transparent photovoltaics for distributed applications," *Nat Energy*, vol. 2, no. 11, pp. 849–860, Nov. 2017, doi: 10.1038/s41560-017-0016-9.

[70] Y. Gu, X. Yao, H. Geng, G. Guan, M. Hu, and M. Han, "Highly Transparent, Dual-Color Emission, Heterophase Cs3Cu2I5/CsCu2I3 Nanolayer for Transparent Luminescent Solar Concentrators," *ACS Appl. Mater. Interfaces*, vol. 13, no. 34, pp. 40798–40805, Sep. 2021, doi: 10.1021/acsami.1c07686.

[71] C. Yang *et al.*, "Ultraviolet and Near-Infrared Dual-Band Selective-Harvesting Transparent Luminescent Solar Concentrators," *Advanced Energy Materials*, vol. 11, no. 12, p. 2003581, 2021, doi: 10.1002/aenm.202003581.

[72] G. Liu, H. Zhao, F. Diao, Z. Ling, and Y. Wang, "Stable tandem luminescent solar concentrators based on CdSe/CdS quantum dots and carbon dots," *J. Mater. Chem. C*, vol. 6, no. 37, pp. 10059–10066, Sep. 2018, doi: 10.1039/C8TC02532K.